NASA CONTRACTOR REPORT

NASA CR-2

PREDICTION AND VERIFICATION OF CREEP BEHAVIOR IN METALLIC MATERIALS AND COMPONENTS FOR THE SPACE SHUTTLE THERMAL PROTECTION SYSTEM

Summary Report

John W. Davis and Bruce A. Cramer

1. Report No. CR-2685	2. Government Accession No.	3. R		

4. Title and Subtitle	5. Report Date
Prediction and Verification of Creep Behavior in Metallic Materials and Components for the Space Shuttle Thermal Protection System - Summary Report	July 1976
	6. Performing Organization Code

7. Author(s)	8. Performing Organization Report No.
John W. Davis and Bruce A. Cramer	
	10. Work Unit No.

9. Performing Organization Name and Address	
McDonnell Douglas Astronautics Company - EAST St. Louis, Missouri 63166	11. Contract or Grant No. NAS-1-11774
	13. Type of Report and Period Covered

12. Sponsoring Agency Name and Address	Contractor Report
National Aeronautics and Space Administration	14. Sponsoring Agency Code

15. Supplementary Notes

Langley technical monitor: D. R. Rummler

16. Abstract

A method of analysis has been developed for predicting permanent cyclic creep deflections in stiffened panel structures. This method uses creep equations based on cyclic tensile creep tests and a computer program to predict panel deflections as a function of mission cycle. Four materials were investigated – a titanium alloy (Ti-6Al-4V), a cobalt alloy (L605), and two nickel alloys (Rene'41 and TDNiCr).

Steady-State and Cyclic creep response data were obtained by testing tensile specimens fabricated from thin gauge sheet (0.025 and 0.63 cm nominal). Steady-state and cyclic creep equations were developed which describe creep as a function of time, temperature and load/ Tests were also performed on subsize (6.35 x 30.5 cm) rib and corrugation stiffened panels. These tests were used to correlate creep responses between elemental specimens and panels. The panel response was analyzed by use of a specially written computer program. Creep deflection data obtained from the literature for full size panels were also analyzed and a creep design methodology was developed.

17. Key Words (Suggested by Author(s)) Prediction, Cyclic and Steady State Creep, Thermal Protection System, Metallic Panels, Corrugated Panels, Rib Stiffened Panels, Nickel Alloy (Rene 41 & TDNiCr), Creep Testing, Cobalt Alloy (L605), Titanium Alloy (Ti-6Al-4V)	18. Distribution Statement Unclassified – Unlimited Subject Category 26

19. Security Classif. (of this report)	20. Security Classif. (of this page)	21. No. of Pages	22. Price*
Unclassified	Unclassified	90	$4.75

TABLE OF CONTENTS

LIST OF FIGURES (Continued)

LIST OF TABLES

LIST OF SYMBOLS

δ = maximum elastic plus plastic creep deflection at panel midspan

Δ_c = beam midspan creep deflection

Δ_E = beam midspan elastic deflection

ε = literature survey steady-state strain

ε_c = maximum midspan creep strain (extreme fiber)

ε_{cy} = cyclic creep strain

ε_E = maximum midspan elastic strain (extreme fiber)

ε_{ss} = supplemental steady-state creep strains

E = elastic modulus

I = Panel moment of inertia

σ = stress

ϕ = material thickness

θ = test direction, use value of 1 for longitudinal material direction, 0 for transverse material direction.

L = panel load

M = Moment

P = panel load

T = Absolute Temperature

t = time

W = beam pressure load

$\overline{Y}$ = Maximum distance from neutral axis to extreme fiber

PREDICTION AND VERIFICATION OF CREEP BEHAVIOR IN METALLIC MATERIALS

AND COMPONENTS FOR THE SPACE SHUTTLE THERMAL PROTECTION SYSTEM

SUMMARY REPORT

John W. Davis and Bruce A. Cramer

McDonnell Douglas Astronautics Company - EAST

SUMMARY

A method of analysis has been developed for predicting permanent cyclic creep deflections in stiffened panel structures. This method uses a creep equation based on cyclic tensile creep tests and a computer program called TPSC (Thermal Protection System Creep) to predict deflections as a function of mission cycle. Four materials investigated were: the titanium base alloy Ti-6Al-4V, the nickel base alloy Rene' 41, the cobalt base alloy L605, and the dispersion strengthened nickel base alloy TDNiCr.

Steady-state creep response data were obtained by testing tensile specimens fabricated from thin gauge sheet (0.025 and 0.063 cm nominal). Steady-state and cyclic creep equations were developed which described creep as a function of time, temperature and load. Comparison of cyclic and steady-state creep test data indicated no significant difference existed (for the same total time at load).

Subsize panels (6.35 x 30.5 cm) were tested in order to develop a correlation between the elemental tensile tests and panel creep responses. The two types of panels fabricated and tested were rib stiffened and corrugation stiffened. In order to analyze these panels a computer program was developed. This program referred to as TPSC applies either time hardening or strain hardening theories of creep accumulation using iterative techniques to determine structural rotations, creep strains, and stresses as a function of time. Deflections are determined by numerical integration of structural rotations along the panel length. The approach for creep deflection analysis incorporated in the TPSC computer program has been found to yield predicted panel cyclic creep deflections that are generally between half and twice the test deflections. The time hardening theory of creep accumulation was generally found to be better than strain hardening in predicting the cyclic test data.

Data obtained from the literature for full size panels was analyzed using the methods developed. Comparisons of these deflections with predictions met with somewhat less success than for the subsize panels because variations from cycle to cycle which may have occurred, were not documented in the literature and because the full size panels were subjected to environments other than creep, such as high launch phase loading and acoustics, which can account for variations in data. Predictions of creep deflections are sensitive to both stress level and temperature.

At the conclusion of this program a creep design methodology was developed based on the information gained during the study.

INTRODUCTION

This report describes the results of an investigation directed towards the development of an approach to predict creep deflections in metallic thermal protection system (TPS). These deflections can occur during the ascent or entry phases of a vehicle mission and are a result of differential pressure and thermal loading. It is important to be able to predict these deflections since excessive deflections can result in localized aerodynamic heating and increase the necessity for panel refurbishment, thus increasing vehicle cost.

The development of a prediction approach was accomplished through a four-phase investigation which included correlation of tensile creep data with small panel test data. The first phase of this program was designed to investigate the steady-state (constant temperature and load) and cyclic creep response characteristics of tensile specimens. Steady-state creep data was gathered through a literature survey to establish a reference data base for each alloy from which empirical equations were obtained, describing creep as a function of time, temperature, and stress. Steady-state creep tests were conducted on tensile specimens for the purpose of comparing the creep response of sheet used in this program with that of the literature survey data base, and also to supplement the data base.

Tensile cyclic creep tests were conducted to characterize material cyclic creep response under varying loads and temperatures. These data were used to evaluate analytical methods to predict cyclic creep behavior. Basic cyclic tests, using simple constant stress and temperature cycles to represent flight conditions, provided data for comparison with steady-state response and development of empirical equations for cyclic creep. Other tests were conducted using these same cycles but with a varying stress as a function of cycle to simulate the changing stresses present in a creeping beam as a result of stress redistribution. Additional tests were conducted using complex stress and temperature profiles representative of typical Space Shuttle Orbiter trajectories.

In Phase II corrugation and rib stiffened subsize panels were tested. The creep deflections of these panels were compared with calculations using the cyclic tensile creep equation and a computer program especially written for creep analysis.

Phase III involved using methods of analysis developed in Phases I and II to analyze full size heat shield panel creep deformation data developed on other R/D programs.

In Phase IV recommended creep design procedures for the TPS were established. These procedures provide methods for analyzing material creep data, procedures for design of TPS, and rules for inspection and measurement of panel deflections.

This report summarizes the results of this study by Phase. For further information, the reader is directed to the Phase summary reports (References 1-3).

The International System of units (SI) are used in this report. U.S. Customary Units are also generally provided. Applicable conversion factors are presented in Appendix A.

Statistical analysis was performed by Dr. J. F. Brady, Dr. D. C. Ruhmann, Mr. R. K. Linback, and Mr. W. J. Edens. The experimental portions of the program were performed by Mr. R. L. Hillman (steady-state creep testing) and Mr. B. Munsell (cyclic creep testing).

PHASE I - CYCLE MATERIALS CREEP PREDICTIONS

The first phase of this study was concerned with the steady-stage and cyclic creep behavior of tensile specimens made from four materials in sheet form Ti-6Al-4V, Rene' 41, L605, and TDNiCr. At the start of this phase a literature survey was performed.

Steady-State Literature Survey

A search was performed to gather available creep data for thin gage sheet material, in order to establish a reference data base for the four alloys being studied. As part of this survey the following sources were consulted:

(1) NASA Scientific and Technical Information Facility.

(2) Defense Metals Information Center, Battelle Memorial Institute.

(3) McDonnell Douglas Research and Engineering Library.

(4) Material vendors, research laboratories, airframe and jet turbine manufacturers and others believed to be active in creep studies.

Fifty literature sources out of approximately 600 dating from January 1962 to July 1972 were reviewed in detail.

This search revealed that most of the creep data was inadequate for establishing a data base. For example, much of the data was generated for rod and bar mill forms rather than sheet or strip. These data were rejected because the methods for manufacturing bar are different from those used to produce sheet.

There were, however, a few sources that presented enough detailed information, such as lot number, test direction, gage, and plots or tabulation of strains vs time to establish a reasonable data base. This data is presented in the appendices of Reference (1).

The Ti-6Al-4V data base (Reference 1) consisted of creep tests, performed by two laboratories on sheet produced by two manufacturers. One set of data was obtained from sheets 0.160 cm in thickness, manufactured by Mallory Sharon Titanium Company (now Reactive Metals Inc.) and tested by Joliet Metallurgical Laboratories. The second set of data was obtained from sheets 0.102 and 0.160 cm thick, manufactured by Titanium Metals Corporation of America (TIMET), and tested by Metcut Research Associates. These data were for approximately 120 creep tests at temperatures ranging from 589 to 811K.

The heat treatment selected for Rene' 41 is relatively new (solution treat at 1394K and age at 1172K) and as a result the literature surveyed only produced two sources of data, General Electric and McDonnell Douglas (see Reference 1). The General Electric data consisted of 10 creep tests performed on 0.127 cm thick material while the McDonnell Douglas Data contained 24 tests performed on 0.020 cm thick material. The L605 data (Reference 1 and 4) consisted of tests performed on sheet ranging in thickness from 0.013 to 0.203 cm in the temperature range of 922 to 1255K.

TDNiCr had the largest number of sources available to establish a data base for a dispersion strengthened alloy (References 1, 5 and 6). The data base contained data obtained from Marshall Space Flight Center (NASA), Lewis Research Center (NASA), General Electric, and McDonnell Douglas and consisted of tests performed on sheet ranging in thickness from .038 to .152 cm in the temperature range of 1033 to 1477K.

The steady-state data from the literature survey was used along with a stepwise multiple regression analysis computer program (Reference 7) to develop equations for each alloy. These equations were based on the functional relationship suggested in References 8 through 11 and are presented in Table 1.

TABLE 1
CREEP EQUATIONS BASED ON LITERATURE SURVEY

ALLOY DESIGNATION	EQUATION
Ti-6Al-4V	$\ln \epsilon_i = -24.89504 + 21.40095T + 1.15998 \ln \sigma + 0.63357 \ln t$ $+ 0.00615(\ln t)^2 + 6.94 \times 10^{-6} (\sigma)^2 - 0.3314 \left(\frac{(\ln \sigma) \ln t}{T} \right)$
RENE'41	$\ln \epsilon = 3.81577 - 11.08783 (1/T) + 0.57841 \ln \sigma + 0.63366 \ln t$
L605	$\ln \epsilon = 4.84549 + 2.12881 \ln \sigma + 0.48945 \ln t - 0.29601 \ln \Phi - 19.50143 (1/T)$
TDNiCr	$\ln \epsilon = -12.43906 + 0.01930 \sigma + 2.80992T - 0.00022t - 0.389450 \Theta + 22.45187 \Phi$ $+ 0.35175 \ln t - 1.12398 \ln \Phi$

Establishment Of Steady-State Test Conditions

These equations were the basis for establishing a test matrix for the testing of tensile specimens. Initially several experimental designs were examined in an effort to identify combinations of test temperature and stress which would provide the maximum useful data. In this study the L605 literature survey and equation were used as a base to obtain an experimental design. The following requirements were established for this generation of test data.

(1) Test data would be amenable to development of an empirical creep strain equation. Applicability of each design for satisfying this requirement was checked by generating simulated creep strain data using the L605 equation, performing regression analyses, and evaluating the resulting predictive equation.

(2) Test temperatures should cover the ranges of interest for the material being tested.

6

(3) Test temperatures and stress levels should produce creep strains in the range of interest for metallic TPS. Maximum and minimum levels of creep strain considered reasonable for supplemental steady-state tests were .50% in 50 hours and .06% in 200 hours, respectively.

Some test matrix designs considered are presented in Figure 1. These designs include the simple 3 x 3 factorial design and an orthogonal composite design, described in References 12 and 13, and shown in Figures 1(a) and 1(b), respectively. While each of these designs satisfied the first requirement ((1) above), they did not satisfy the second or third requirement. This is evident from the figure since even for the narrow temperature range of 1089 to 1200K and the stress range of 13.8 to 69 MPa, creep strains as low as .022% in 200 hours and as high as .6% in 6 hours (69 MPa at 1200K) result. Therefore, these values are outside of the range of interest.

In addition to these two designs, the design shown in Figure 1(c) was considered because it provided a maximum coverage of the temperature and stress of interest for L605. Analysis of the simulated data using regression techniques, however, demonstrated that the resulting prediction equation based on this design was a function of time only.

A fourth design considered is a compromise between the other three. This design, shown in Figure 1(d) allowed testing over the temperature range of 978K to 1255K, and stress range of 13.8 to 110.3 MPa. Values of temperature and stress were selected to be equally spaced in the variables log stress and 1/T (note form of Equation 3, Table 1). This allowed for spacing of tests through-out strain range of interest as well as the temperature and stress range. Study of this design using simulated data and regression techniques indicated that an empirical equation could be derived from the resulting test data. Therefore, this experimental design was used to establish the steady-state creep tests. These test parameters are shown in Table 2.

Establishment of Cyclic Test Conditions

The test matrix shown in Figure 1(d) was also used to establish the cyclic test matrix. These tests are referred to as the basic cyclic tests because the results of these tests were the basis of the cyclic creep equation.

The profile used for the basic cyclic test is shown in Figure 2 and is representative of a simplified trajectory consisting of a rapid heat-up, hold at temperature for twenty minutes, then rapidly cooling to approximately 422K. After cool-down the same profile was repeated for a 100 cycle test duration. Total time for each cycle was 55 minutes. The cycle time at maximum temperature and load was 20 minutes.

Stress and temperature levels were selected with the goal of obtaining 100 cycle creep strains up to 0.5%. A summary of these basic tests is presented in Table 3.

In addition to performing tests to develop an empirical equation, other tests were required to determine how the simplified trajectory tests would relate to more complex simulated mission tests. To accomplish this, tests were designed to determine the applicability of strain or time hardening theories.

7

8

TABLE 2
SUPPLEMENTAL STEADY-STATE CREEP TESTS – BASIC MATRIX

TEST NO.	TEST[1] DIRECTION Θ	L605 NOMINAL THICKNESS cm	TEMP K	STRESS MPa	Ti-6Al-4V NOMINAL THICKNESS cm	TEMP K	STRESS MPa	RENE '41[3] NOMINAL THICKNESS cm	TEMP K	STRESS MPa	TDNiCr NOMINAL THICKNESS cm	TEMP K	STRESS MPa
1	1	0.024	978	55.2	0.031	616	317.2	0.027	964	69.0	0.024	1089	62.1
2	1	0.024	978	110.3	0.031	616	475.7	0.027	983	121.4	0.024	1089	110.3
3	1	0.024	1053	27.6	0.031	658	165.5	0.027	1061	34.5	0.024	1200	34.5
4	1	0.024	1053	55.2	0.031	658	317.2	0.027	1061	69.0	0.024	1200	62.1
5	1	0.024	1053	110.3	0.031	658	475.7	0.027	1061	137.9	0.024	1200	110.3
6	1	0.024	1144	13.8	0.031	714	48.3	0.027	1111	69.0	0.024	1339	17.2
7	1	0.024	1144	27.6	0.031	714	165.5	0.027	1111	103.4	0.024	1339	34.5
8	1	0.024	1144	55.2	0.031	714	317.2	0.027	1155	39.3	0.024	1339	62.1
9	1	0.024	1255	13.8	0.031	783	48.3	0.027	1155	121.4	0.024	1478	17.2
10	1	0.024	1255	27.6	0.031	783	165.5	0.027	1180	69.0	0.024	1478	34.5
11	1	–	–	–	–	–	–	0.027	1155	55.2	0.024	1478	27.6

[1] TEST DIRECTION(Θ), 1 = LONGITUDINAL; 0 = TRANSVERSE

[2] TESTED WITH HIGH EMITTANCE COATING. IN THIS CASE THE MATERIAL OXIDE WAS THE COATING MATERIAL.

[3] ALL RENE '41 SPECIMENS TESTED HAD OXIDE COATING.
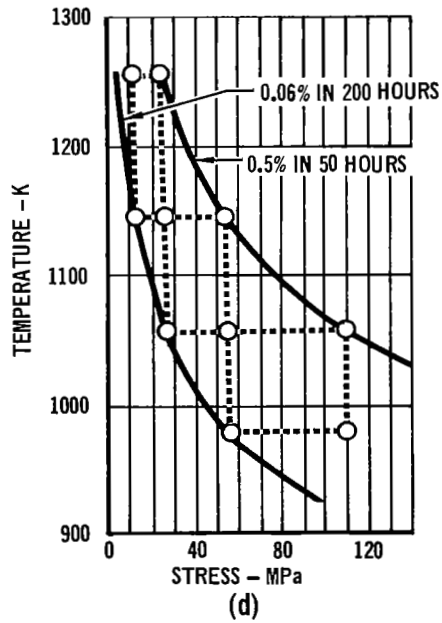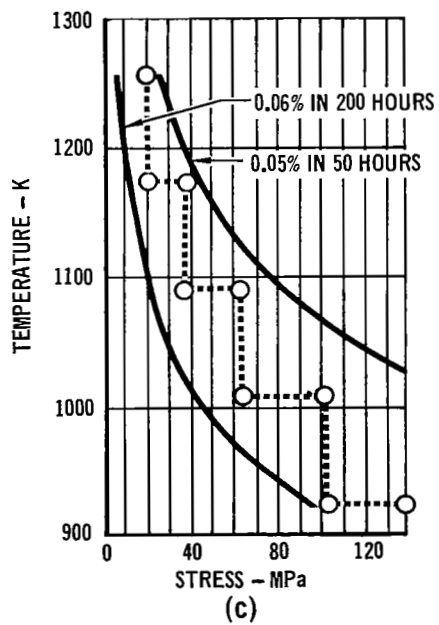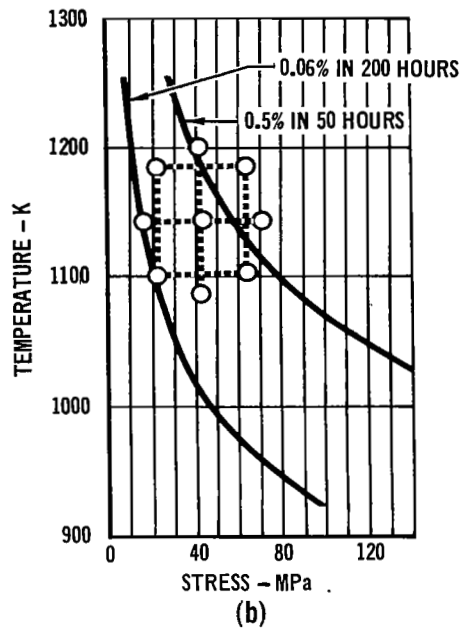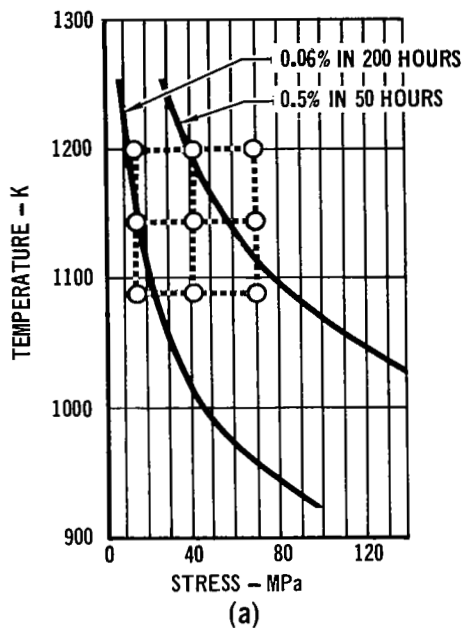
FIGURE 1 SUPPLEMENTAL STEADY-STATE EXPERIMENTAL DESIGNS

STRESS – TEMPERATURE

TEMPERATURE

STRESS

TIME

TIME AT
MAX STRESS
AND TEMP
= 20 MIN

TOTAL
CYCLE TIME
= 55 MIN
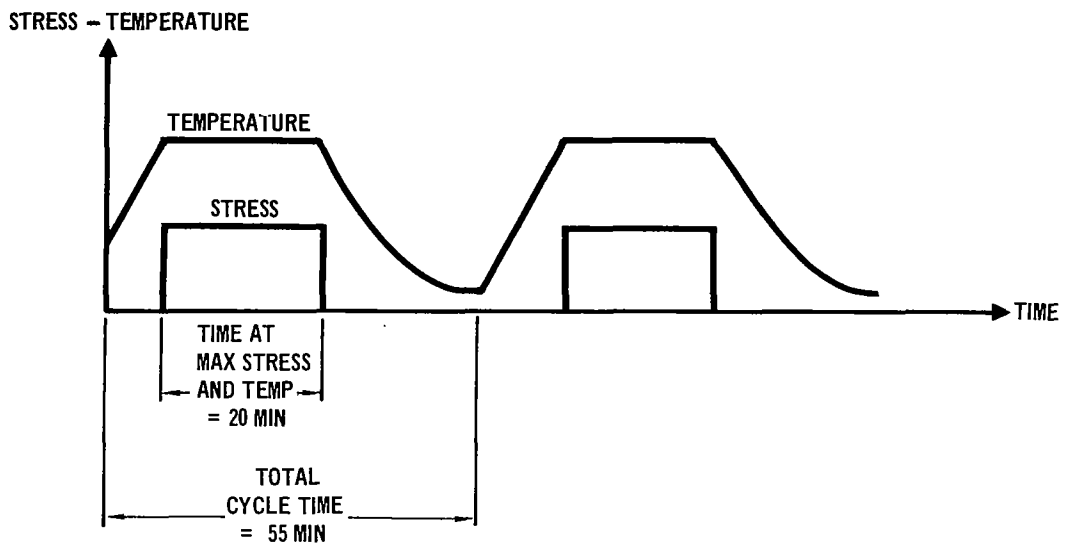
FIGURE 2 STRESS AND TEMPERATURE PROFILES FOR BASIC CYCLIC CREEP TESTS

TABLE 3
BASIC CYCLE TESTS

TEST NO.	ALLOY DESIGNATION							
	L605		RENE'41		Ti–6A1–4V		TDNiCr*	
	TEMP K	STRESS MPa	TEMP K	STRESS MPa	TEMP K	STRESS MPa	TEMP K	STRESS MPa
1	978	128.9 80.7 51.0	1111	104.1 68.7 39.0	658	399.0 299.2 207.0	1089	124.3– 85.7
2	1053	127.6 83.4 52.2	1155	66.5 57.0 46.8	714	295.9 192.0 114.7	1200	108.6– 57.2 9.0
3	1144	73.5 +47.2 29.6	1072	135.1 103.4 68.7	783	129.7 83.6 50.4	1339	60.3– 30.6
4	1255	33.8 20.6 13.2	1033	275.5 207.6 142.0	839	47.2 30.5 19.7	1478	44.3– 16.3

*A TOTAL OF 26 TDNiCr SPECIMENS WERE TESTED TO BASIC CYCLE PROFILES THROUGH THIS RANGE OF STRESS SHOWN.

This was accomplished by performing the basic cyclic profile shown in Figure 2 but increasing the load every 10 cycles up to 100 cycles and decreasing the load every 10 cycles to examine the applicability of hardening rules (See Figure 3). The remaining tests were designed to determine if complex trajectories could be idealized. For ease of analysis, an actual entry trajectory, is idealized by dividing it into time increments for which stress and temperature are considered constant. Verification of the acceptability of idealization was accomplished by performing an actual simulation mission profile test.
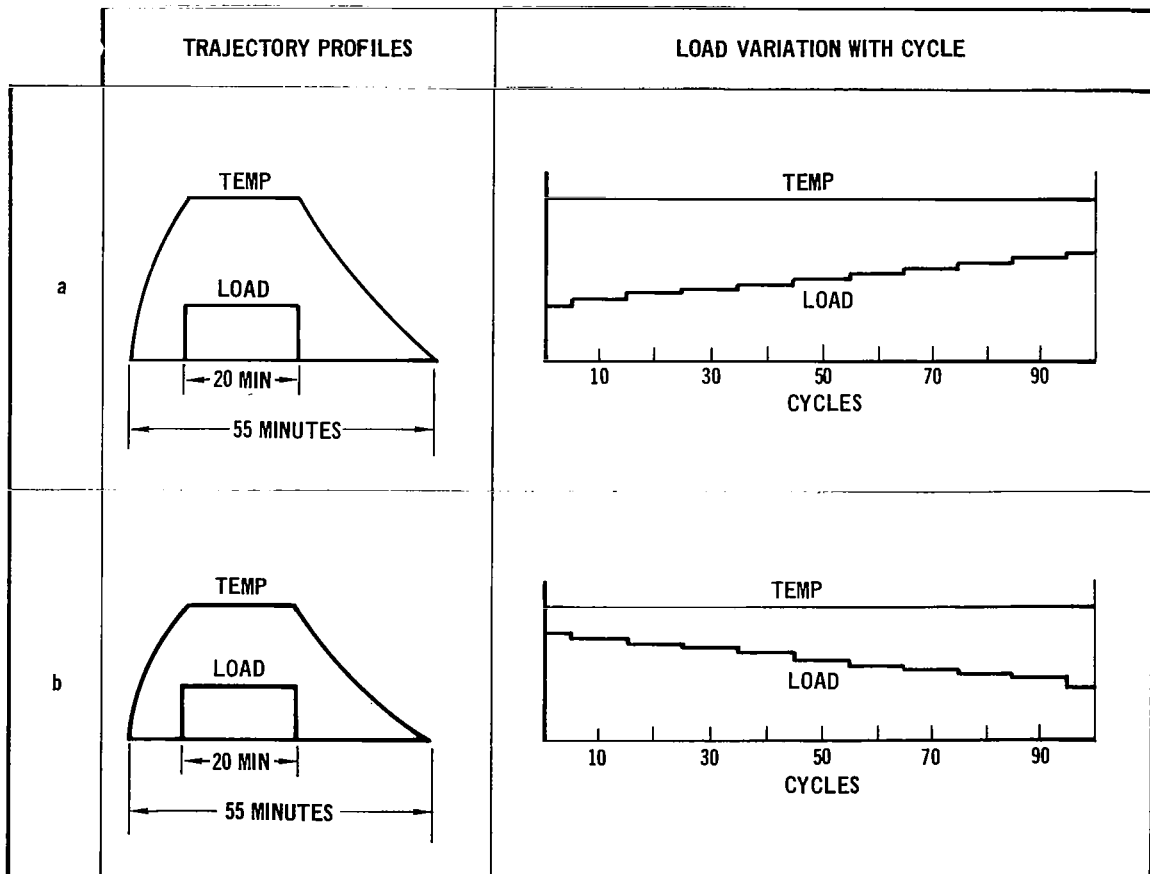
FIGURE 3   TESTS FOR EFFECTS OF VARIATION OF STRESS WITH CYCLE

Experimental Procedure

The same specimen geometry was used for both steady-state and cyclic tests to eliminate any possible variation in creep response due to specimen geometry.

Steady-state creep tests were conducted in resistance heated vertical tube furnaces coupled to filar microscopes. Test loads were provided by weights stacked on platforms attached to the specimens (dead weight loading). Actual strain measurements were accomplished through the use of platinum slide rules spot welded to the specimens. Strains were obtained, in situ, optically by measuring the relative movement of scribe marks on the slide rule over a 5.1 cm (2.0 inch) gauge length. Overall precision of the measurement system for creep strain was considered to be within +0.01% creep strain (e.g., 2% error on a creep strain of 0.5%, 0.490 to 0.510%) based on repeated measurements taken. This error includes variations in readings between different laboratory personnel.

Steady-state strain readings included elastic strains. These elastic strains were recorded at the beginning and at the completion of each test. Temperature measurements were made through the use of potentiometric recorders. The total temperature measurement system (recorder, thermocouple and wire) was calibrated to within 2.8K of the nominal test temperatures. Creep specimen temperatures were determined from chromel alumel thermocouples which were spot welded (at the center and at each end of the slide rule) on nichrome foil strips, which were in turn strapped to the specimen to monitor temperature during testing. For each test the previous thermocouple bead was removed and a new bead and michrome strip were made.

Cyclic creep testing was performed in specially constructed furnaces. The upper part of each furnace contained a stainless steel extension assembly which housed load dynamometers. These dynamometers measure individual loads to each of three specimens in the furnace. Location of the dynamometers inside the furnace system reduced the possibility of load measurement errors which could have been caused by friction at the seal and load rod interface had the dynamometers been outside the furnace. A series of radiation shields were positioned between the dynamometers and the furnace to minimize heat transfer from the furnace. Thermocouples on the dynamometers were monitored during testing to verify that they remained within the calibration temperature range during test. A schematic diagram of the furnace test chamber is presented in Figure 4. The furnace consisted of a muffle tube which was heated by radiation from a resistance heated graphite element.

The specimens were tested in a whiffle tree load fixture designed for use in these furnaces. This fixture is shown in the schematic diagram of Figure 4 The mechanism consisted of two sets of loading pins and clevis fittings which served as load dividers. In this manner the applied load was divided into three separate loads so that three specimens could be tested, at three different load levels, during a single furnace run.

Figure 4 shows the pin and clevis fittings and their relationship to the specimens. By providing several pin fittings with different strap (specimen) attachment locations, several different load ratios could be obtained. Variations in specimen loads due to differential specimen strains were found to be negligible. Loads on each specimen were measured separately by the three load dynamometers provided at the top of the furnace extension assembly.

Data acquisition during the cyclic creep testing was accomplished through the use of a specially designed digital data acquisition system. This system contained 59 channels which were scanned every 50 seconds. The accuracy of
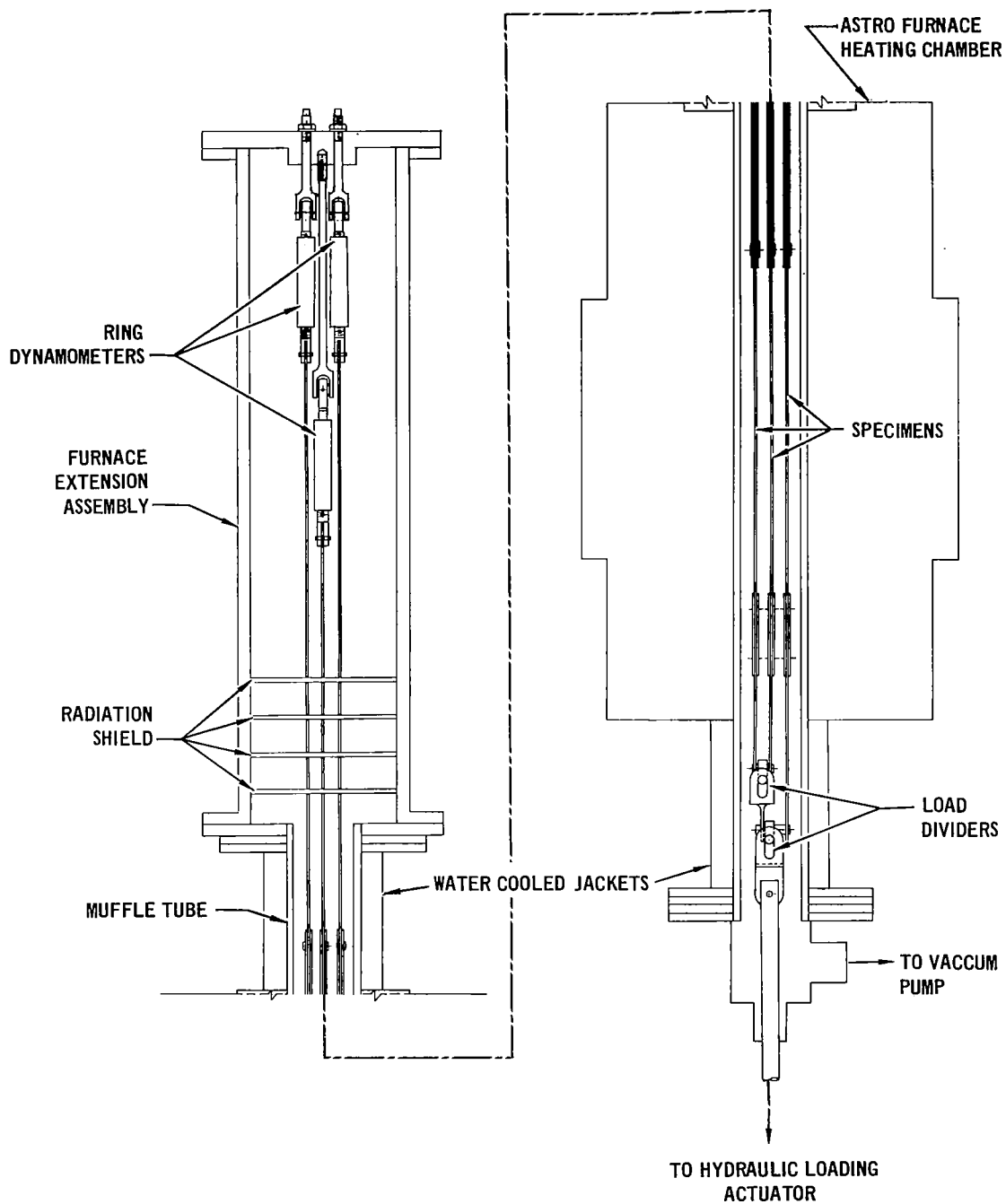
12

FIGURE 4 SCHEMATIC OF FURNACE TEST CHAMBER

this system is ±0.15%. The system recorded the data on tape, and also contained an 8-character digital printer which could be used to check the taped data. During testing the digital acquisition system recorded the output from the ring dynamometers and thermocouple positioned on the dynamometers. The cassette tapes were subsequently analyzed by a computer program which calculated the mean loads and standard deviations. The mean value of load for each cycle was based on recorded loads at 50 second intervals throughout the test profile. An overall mean load and standard deviation were calculated based on the mean values for each cycle. Average stress-time profiles for actual trajectory stress history tests were obtained by data averaging loads at common times in each cycle over the duration of the test. A load of approximately two percent of maximum load was maintained throughout each cycle to prevent slack in the whiffle tree mechanism.

Temperatures during testing were obtained by platinum-platinum-10% rhodium thermocouples which were located within the hot zone of the furnace. Prior to testing, the temperature recording system which included thermocouples, reference junction, and potentiometric strip recorder was calibrated and found to be accurate to within 1.7K. Load and temperature profiles were controlled by an electrostatic curve following system, while pressure within the test chamber was controlled by a regulated leak rate.

The same technique used to measure strains in steady-state creep tests could not be applied to cyclic testing because the furnace did not contain view-ports. Furthermore, the use of platinum slide rules bonded to the specimen can cause problems because when elastic loads are removed and reapplied, slide rule bucking or slippage can result in inaccurate creep strain measurements. Therefore, for this type of testing, the use of scribe marks on the specimen read with a measuring microscope, was judged to provide the most reliable approach.

The distances between the scribe marks on both sides of the specimen were determined by using a measuring microscope. Precision in measurements, based upon multiple measurements by several operators on the same creep specimens, was found to be +.00051 cm.

The cumulative creep strain of each specimen nominally was measured after 1, 5, 15, 25, 75 and 100 cycles. To make the creep strain measurements, specimens were removed from the furnace.

Results and Discussion

Steady-State Creep Tests. - In the experimental portion of this program 69 steady-state creep tests were performed. The steady-state creep tests were designed to not only examine the creep response of the material but also to determine the influence of material thickness (gauge) and grain orientation (longitudinal versus transverse rolling direction) on creep strains. The detailed results of these tests can be found in Reference 1. A portion of the results of these tests for Ti-6Al-4V, Rene' 41, L605, and TDNiCr are presented in Figures 5-11. For clarity, not all of the data points are shown in the figures. Included in these figures are the curves predicted by the equations shown in Table 4. These equations were developed by using data obtained from the hand faired curves shown in Figures 5-10, and a stepwise multiple regression analysis computer program (Reference 14). Comparison of the data

14
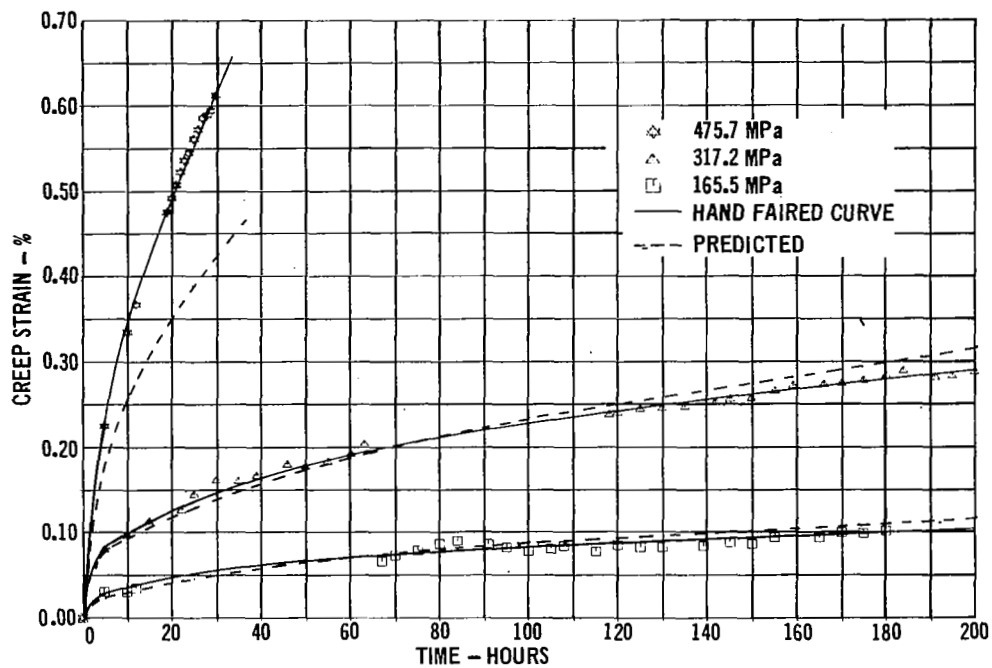
FIGURE 5 Ti–6AI–4V STEADY-STATE CREEP DATA AT 658K
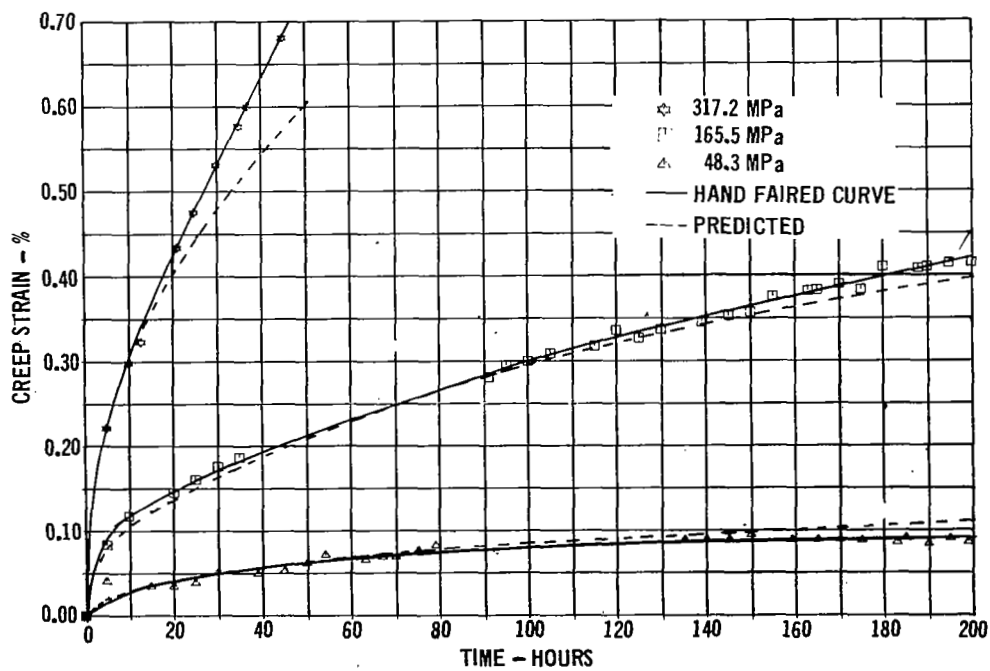
FIGURE 6 Ti–6AI–4V STEADY-STATE CREEP DATA AT 714K

15
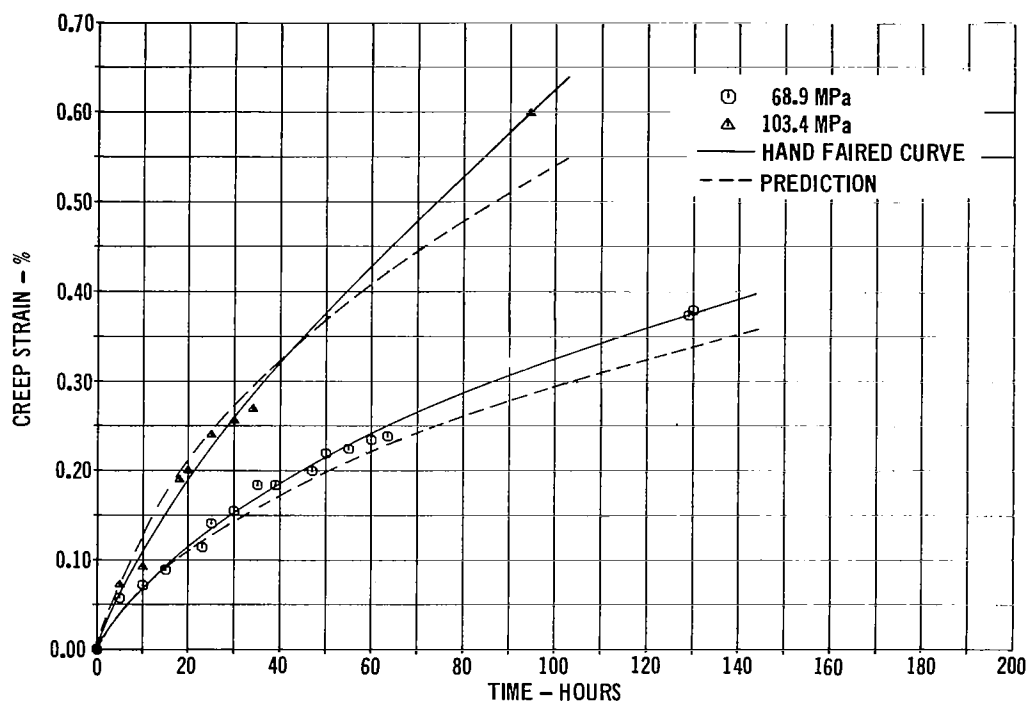
FIGURE 7 RENE'41 STEADY-STATE CREEP DATA AT 1111 K
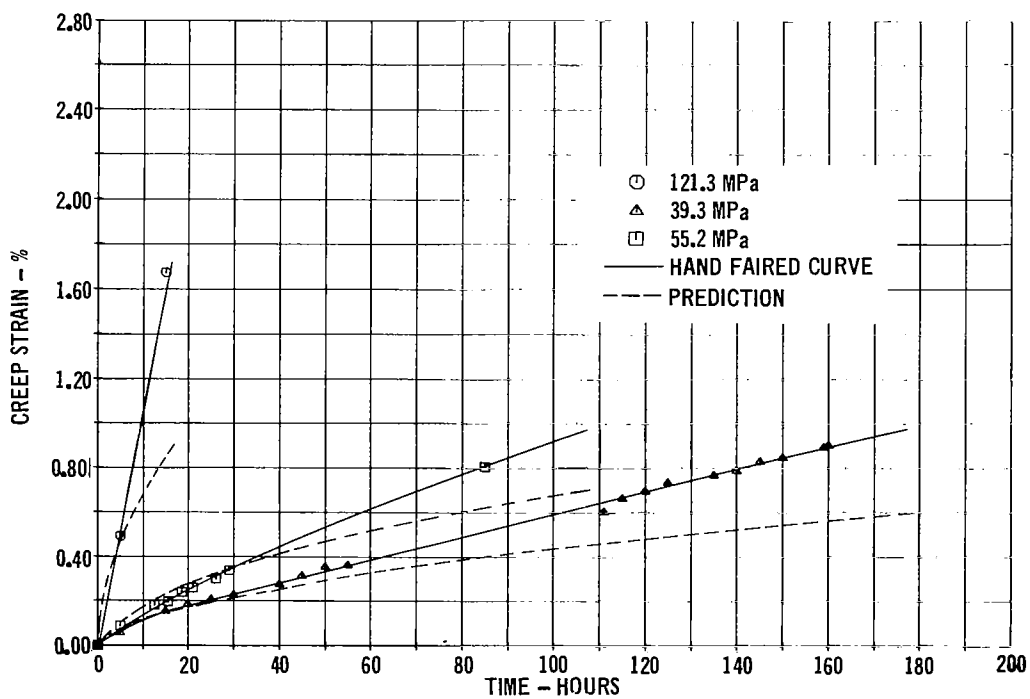
FIGURE 8 RENE'41 STEADY-STATE CREEP DATA AT 1155 K

16
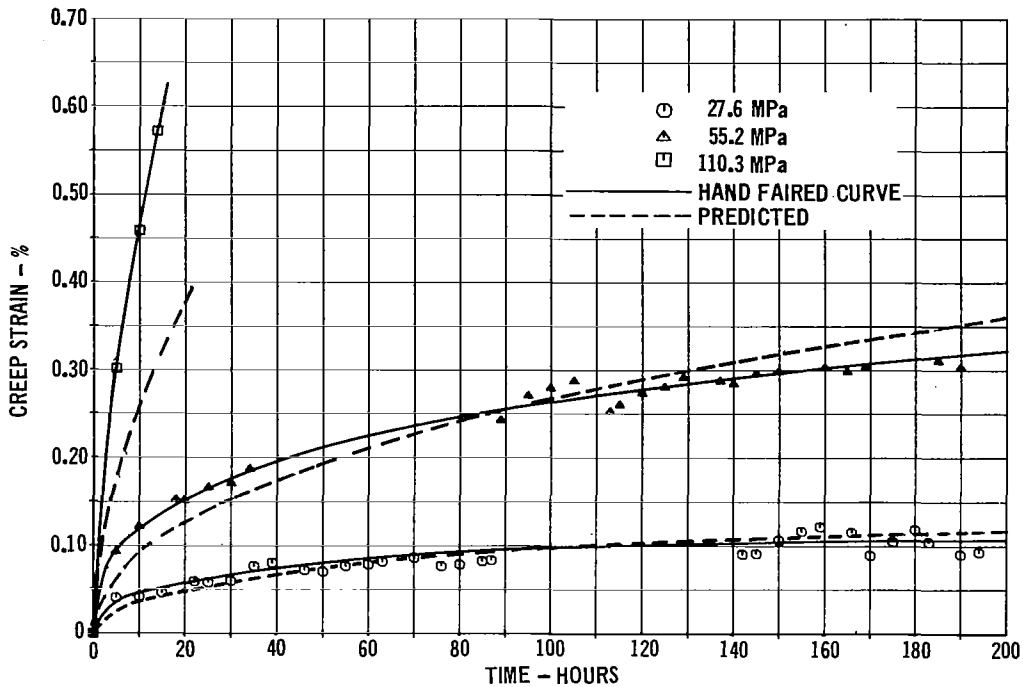
FIGURE 9 L605 STEADY-STATE CREEP DATA AT 1053K
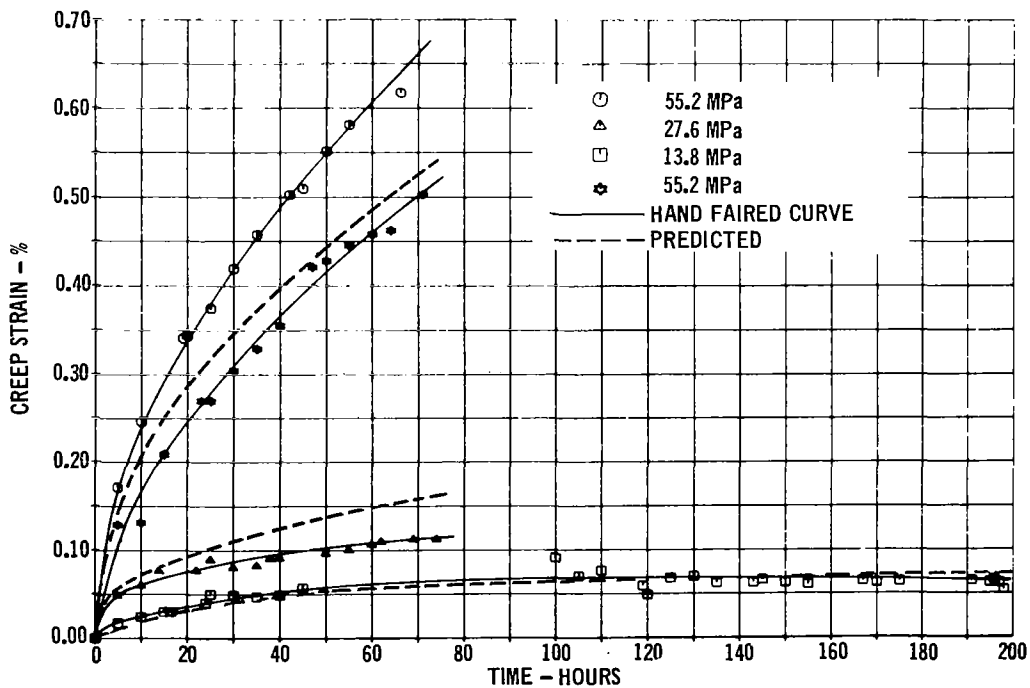
FIGURE 10 L605 STEADY-STATE CREEP DATA AT 1144K
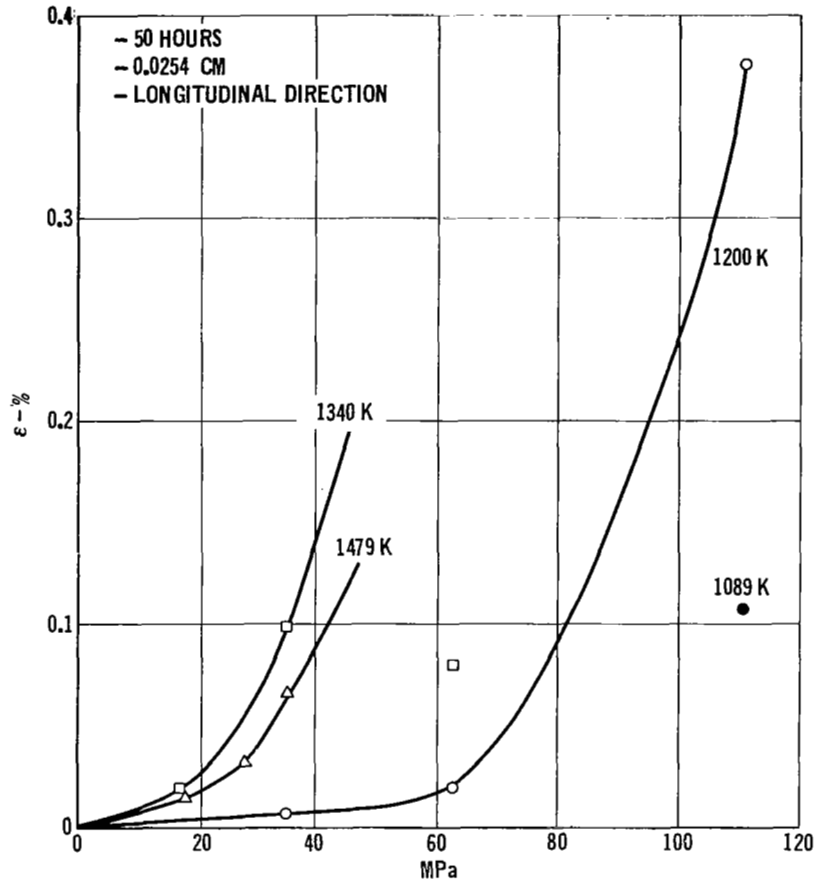
FIGURE 11 TDNiCr STEADY-STATE CREEP DATA AT 50 HOURS

TABLE 4
STEADY-STATE CREEP EQUATIONS

MATERIAL	EQUATION
Ti-6A1-4V	$\ln \epsilon_{ss} = -24.08576 + 22.53736T + 5.89 \times 10^{-6}\, \sigma^2 + 0.90505 \ln\sigma + 0.43365 \ln t$
RENE'41	$\ln \epsilon_{ss} = -35.21304 + 26.34069T + 0.02807 \ln t + 1.03087 \ln\sigma$
L605	$\ln \epsilon_{ss} = -3.92643 - 0.00237\, t + 0.45047\, (\ln\sigma)^3 + 0.55687 \ln t$ $\quad -4.14348\,(1/T) + 0.11052\, \sigma\ln T + 0.0000406\,(T\sigma t)$
TDNiCr	$\ln \epsilon = -12.43906 + 0.01930\,\sigma + 2.80992T - 0.00022t - 0.389450\,\Theta + 22.45187\,\Phi$ $\quad +0.35175 \ln t - 1.12398 \ln\Phi$

18

plots indicates consistency in the data with respect to increasing strain with increasing stress and temperature for all of the materials tested except TDNiCr. A review of the TDNiCr steady-state creep tests revealed some inconsistency in the data. For example, some of the tests at 1340K exhibited greater creep strains than equivalent load tests at 1479K. This inconsistency can be seen in Figure 11 which summarizes the 50-hour creep strains.

In the studies on the influence of specimen orientation (longitudinal vs transverse rolling direction), the results were inconclusive for all of the materials except TDNiCr. In the case of Ti-6Al-4V and L605, in two of the tests, the longitudinal specimens crept faster than the transverse specimens. For Rene' 41, the opposite has occurred, in two of the three tests the transverse specimens crept faster than the longitudinal specimens. For TDNiCr in all three tests, the transverse specimen crept faster than the longitudinal specimens. This trend agreed with the information that was found in the literature survey.

In the studies on the influence of material thickness (gauge), an effect was noted, although in some materials the trend was more pronounced than in others. For Ti-6Al-4V, Rene' 41, and TDNiCr, the thicker material (.060 cm nominal) crept faster than the thinner material (.025 cm nominal). In the case of Ti-6Al-4V the difference, while it existed, was not significant, ($\sim$.48% vs $\sim$.42% for 200 hours at 714K and 165.5 MPa). The reason for the thicker material creeping faster than the thinner was not determined. For the L605, the thinner material crept faster than the thicker material. This trend was also found in the literature (Reference 7) and can be seen in the comparison plots for 30 and 60 hours (See Figure 12). The comparison in the figure is for tests performed at 1144K where close agreement in the literature survey and steady-state creep tests were found. These plots indicate that the data falls into two groups; (1) data for tests conducted on .013 and .025 cm specimens and, (2) data for tests conducted on .064, .102, and .203 cm specimens. Therefore, the gauge effect noted in the literature survey equation, appears to be a step difference attributable to manufacturing processing differences rather than a continuous gauge effect as implied in the literature survey equation.

Data from the steady-state creep tests were used to develop empirical predictive creep equations for all of the materials except TDNiCr. Because of the inconsistency in the TDNiCr data it was decided to use the literature survey equation to represent the data rather than generate a new equation. In developing equations for the other materials, data was obtained from the hand faired creep curves, such as the ones shown in Figure 5-10, for the 10 basic creep tests shown in Table 2. The data consisted of strain values taken at times of 1, 2, 5, 10, and 10 hour increments thereafter to the end of the individual test, from the hand faired curves. This data was used with the stepwise multiple regression analysis computer program and equation formats similar to those used in the literature survey (Table 1) to develop the steady-state creep equations shown in Table 4. Typical comparison of creep strain predictions using the equations shown in Table 4 are presented in Figures 5 - 8 for Ti-6Al-4V and Rene' 41, and in Figures 13-15 for L605 and TDNiCr. From these figures it can be seen that with the exception of Rene' 41 and TDNiCr the equations closely predict the trend of the creep curves. In

the case of TDNiCr the creep strains are generally about one-half of the strains predicted from the literature survey data.
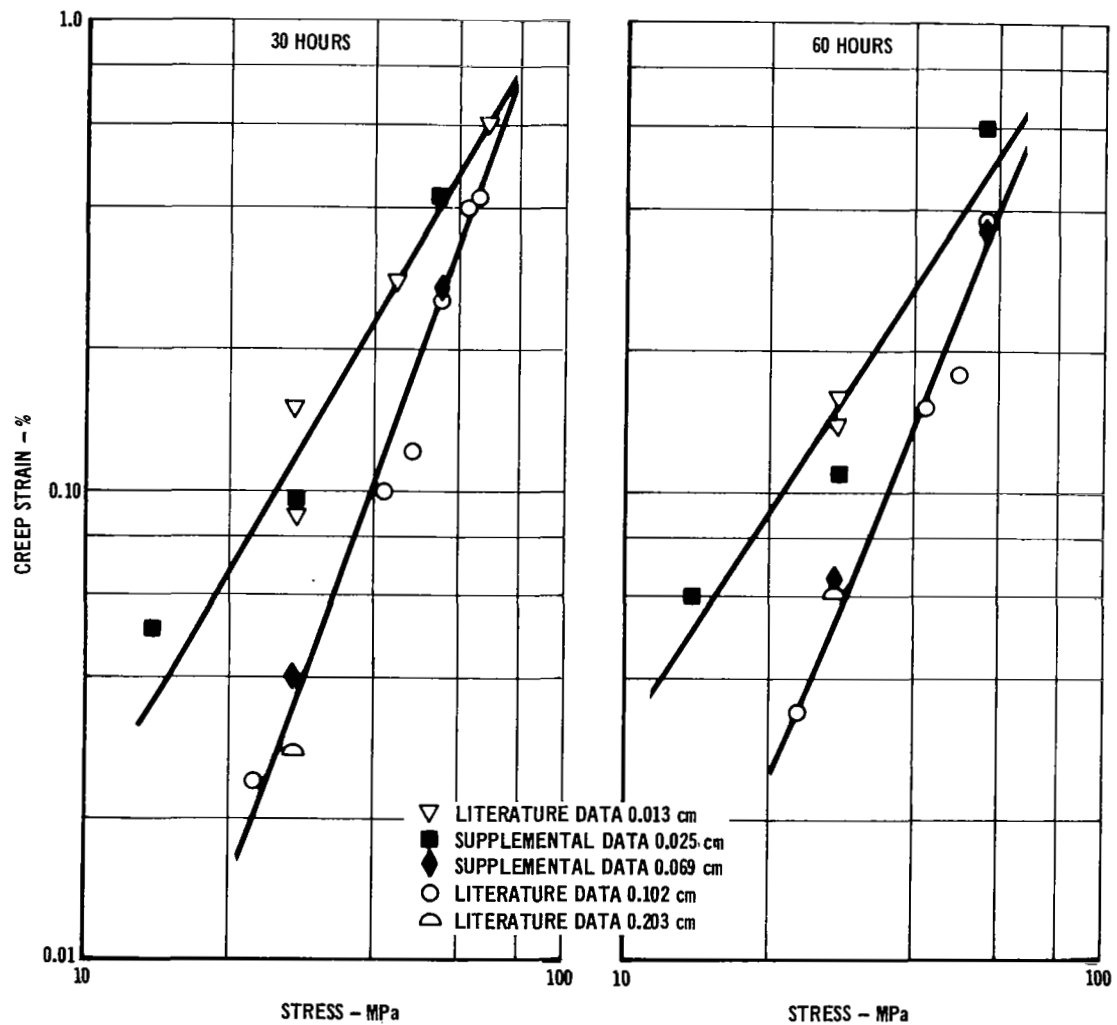
FIGURE 12 COMPARISON OF L605 CREEP DATA AT 1144K FOR THICKNESS
< 0.063 AND > 0.063 cm
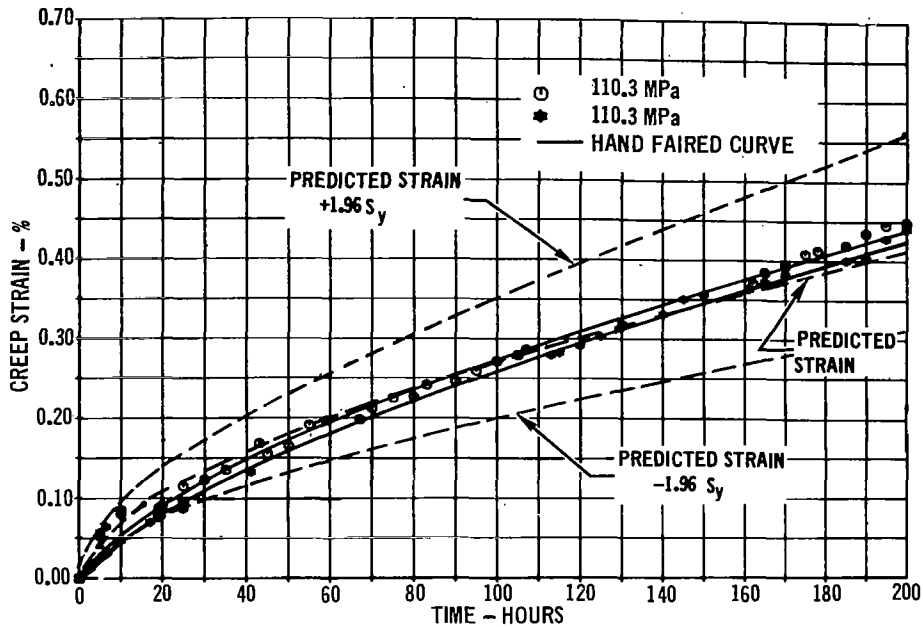
FIGURE 13 COMPARISON OF L605 CREEP STRAIN PREDICTIONS
WITH TEST RESULTS AT 978K AND 110.3 MPa
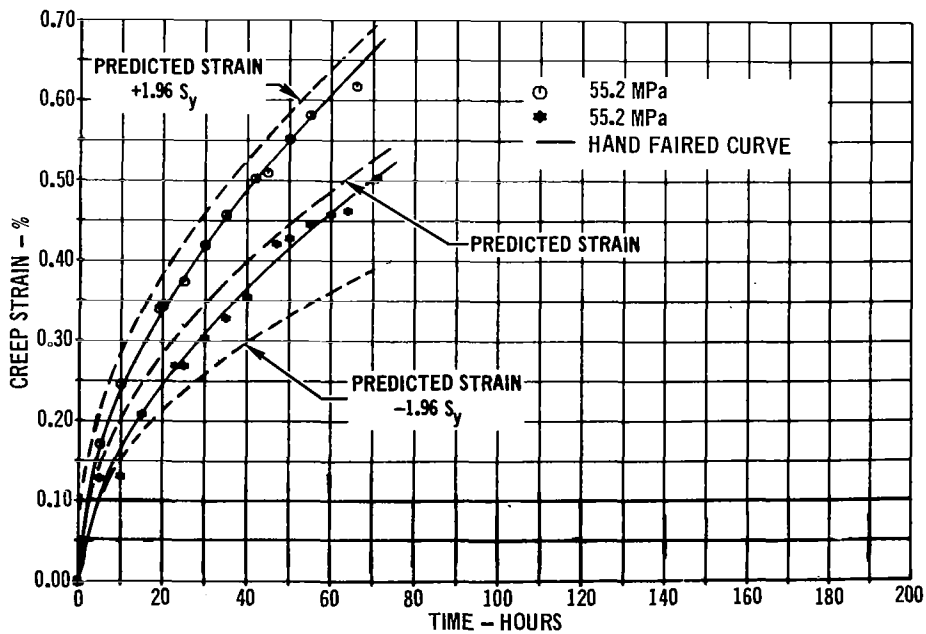
FIGURE 14 COMPARISON OF L605 CREEP STRAIN PREDICTIONS
WITH TEST RESULTS AT 1144K AND 55.2 MPa

21
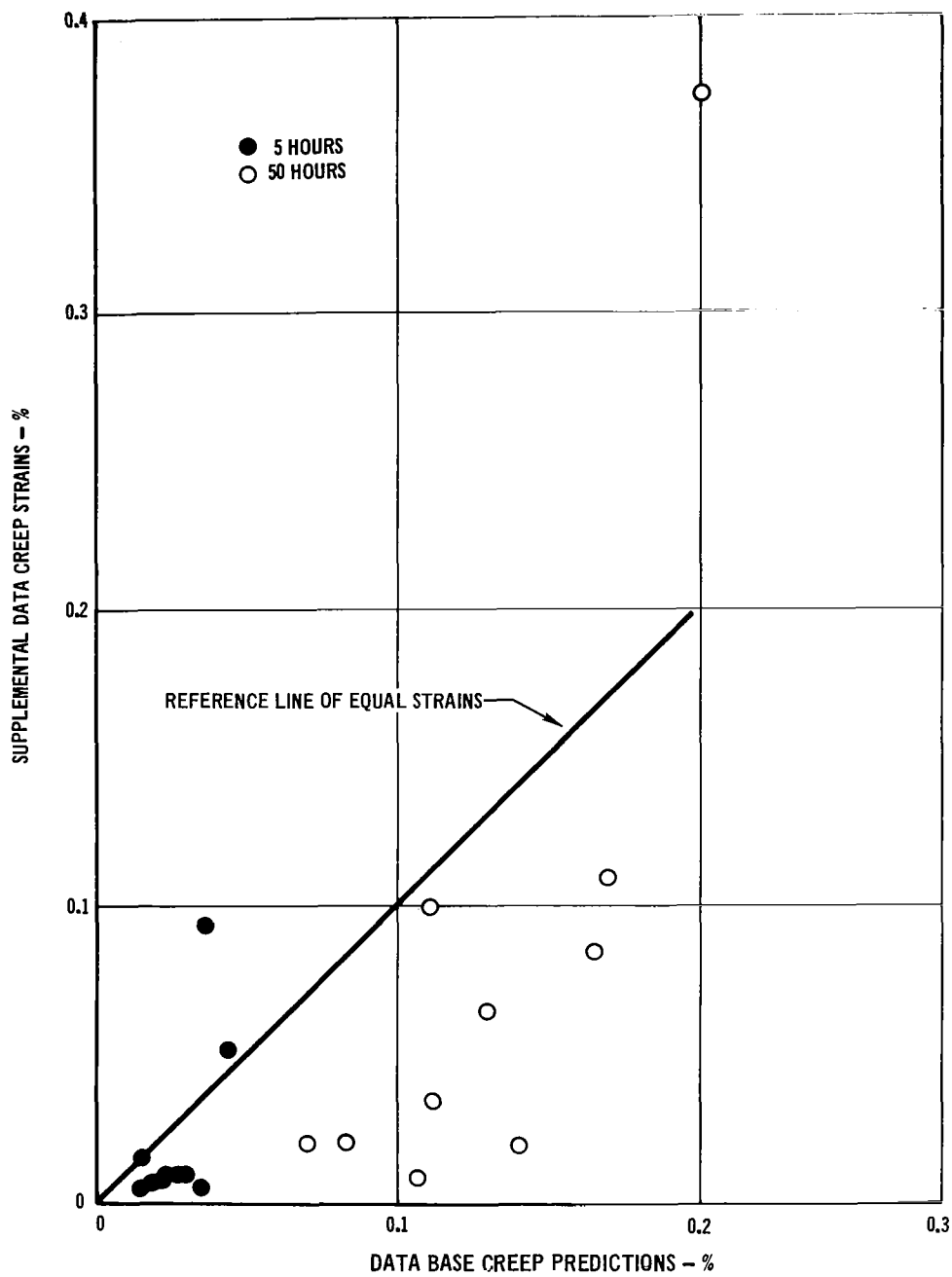
FIGURE 15 COMPARISON OF DATA BASE PREDICTIONS AND
SUPPLEMENTAL TEST RESULTS FOR TDNiCr

Cyclic creep testing. - To determine the cyclic creep response, tests were conducted on 0.025 cm thick specimens in the longitudinal rolling direction for each of the four alloys. The parameters for these tests were presented in Table 3. All of these tests used the basic cycle shown in Figure 2. The detailed results of these tests can be found in Reference 1. A portion of the results of these tests are presented in Figures 16-19. Comparison of these plots, as in the steady-state creep tests revealed consistency in the data with respect to increasing strain with increasing stress. The TDNiCr specimens experienced a large number of failures at all test temperatures. These failures were unexpected (with the exception of the 1478K tests) because the stresses were maintained at lower levels than for the steady-state creep tests. For the 1478K tests the results were consistent with the literature in that the critical stress of 45 MPa (above which stress rupture failures occurred) was verified in the cyclic tests.

Using data obtained from the 5 cycle increments of the hand faired creep curves shown in Figures 16-19, empirical cyclic creep curves were developed. These equations were obtained through the use of a stepwise multiple regression analysis computer program. These equations are presented in Table 5.

For each material, considerable effort was directed toward determining appropriate equation forms, including stress, time, and temperature interaction terms, to provide a "best fit" over the entire range of data resulting in the different equation forms shown. Typical comparisons of the tensile cyclic data and empirical equation predictions for each material are shown in Figures 16 through 19 where time used in the cyclic equations is 20 minutes/cycle.
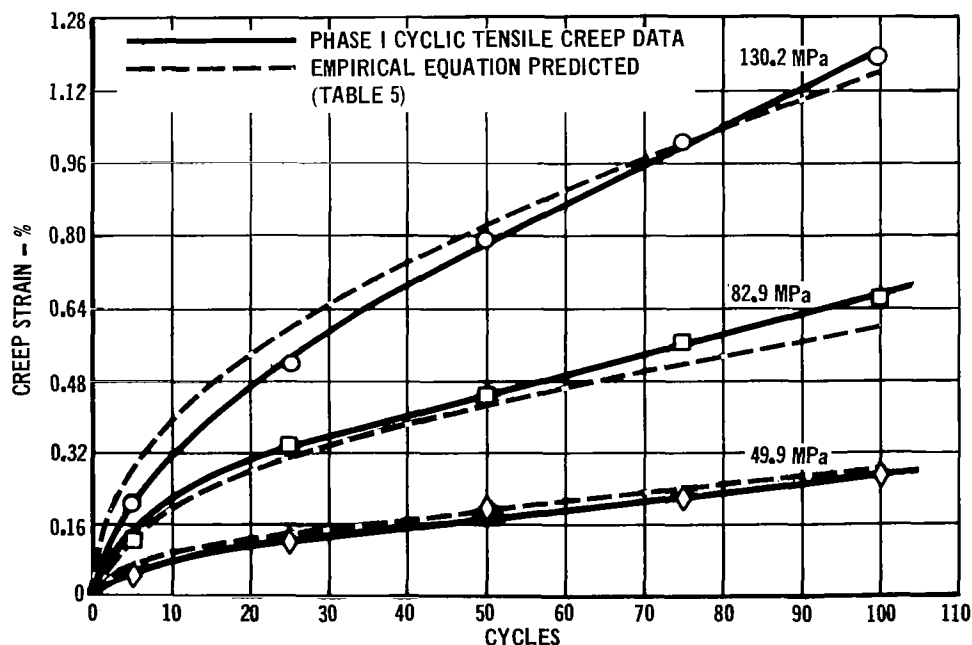
FIGURE 16 COMPARISON OF Ti-6Al-4V PREDICTED AND CYCLIC TEST CREEP STRAINS AT 783 K
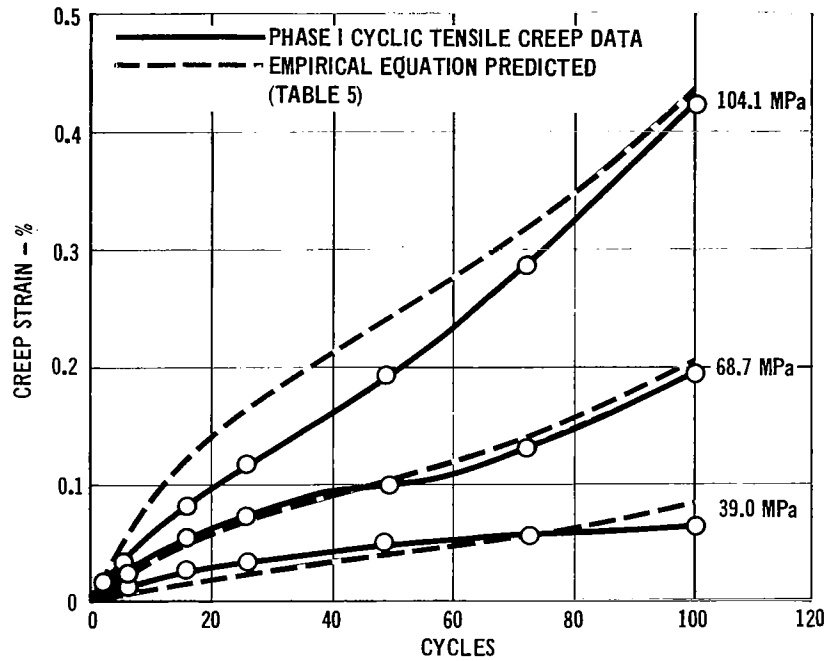
FIGURE 17 COMPARISON OF RENE'41 PREDICTED AND
CYCLIC TEST CREEP STRAINS AT 1111K
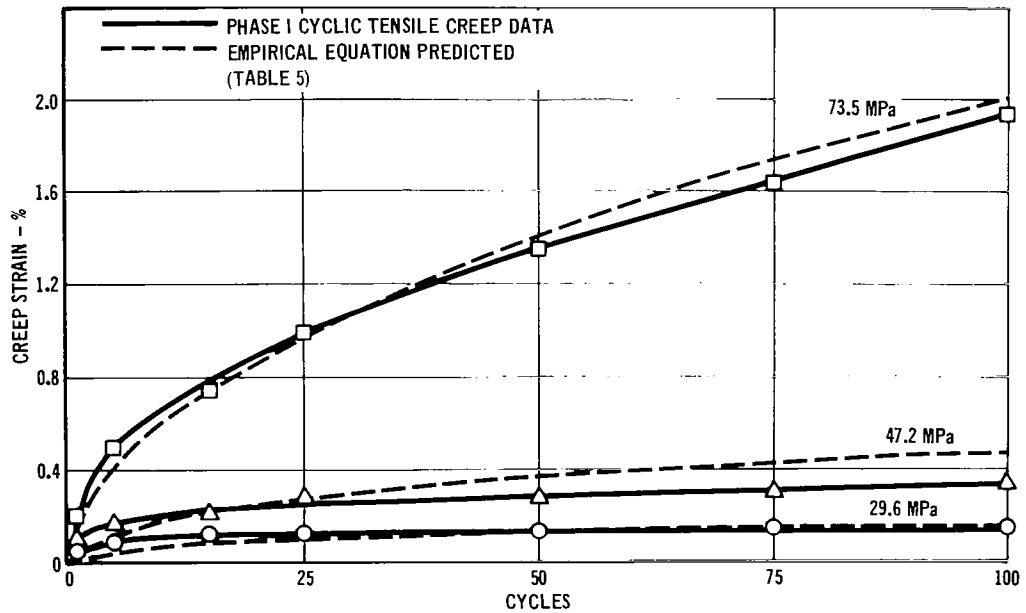
FIGURE 18 COMPARISON OF L605 PREDICTED AND CYCLIC
TEST CREEP STRAINS AT 1144K
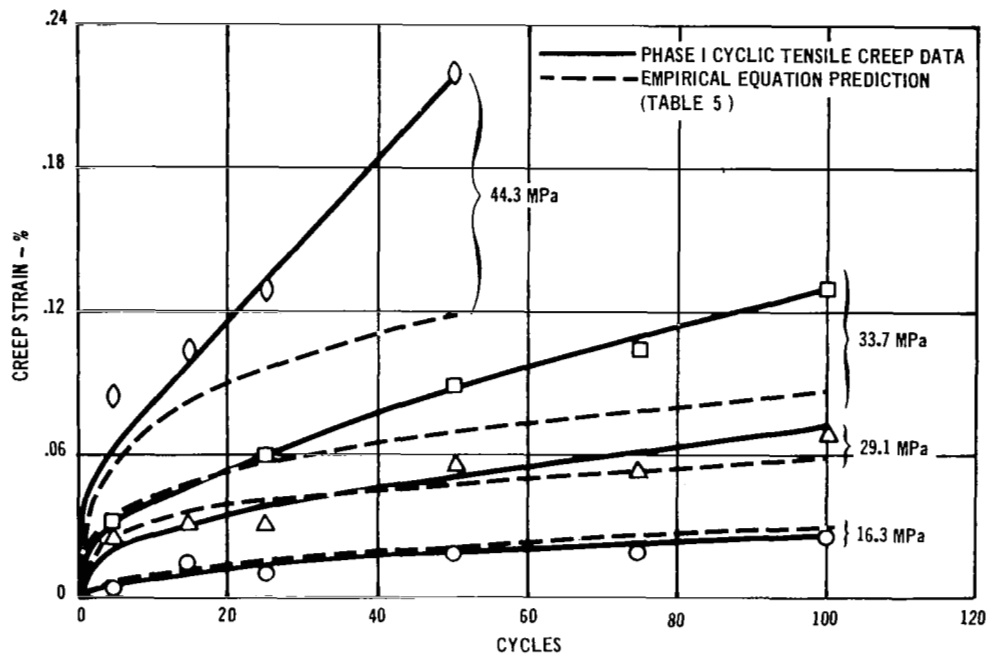
FIGURE 19 COMPARISON OF TDNiCr PREDICTED AND
CYCLIC TEST CREEP STRAINS AT 1478K

TABLE 5

CYCLIC CREEP EQUATIONS DEVELOPED FOR PHASE I TENSILE CREEP DATA

MATERIAL	EQUATION	APPLICABLE TEMPERATURE MAXIMUM
TITANIUM	$\ln \epsilon = -28.94077 + 26.24850\, T + 2.52 \times 10^{-6}\, \sigma^2 + 1.40406\, \ln\sigma + 0.46894\, \ln t$	839 K
RENE'41	$\ln \epsilon = -39.55860 + 29.13646T + 0.71922\, \ln t + 0.92125\,(\ln\sigma - 1.931)$ $-0.000016\sigma^2 + 0.08183\,(\ln\sigma - 1.931)^3 - 0.000125\,(t\sigma T) + 0.0000105 t^3$	1155K
L605	$\ln \epsilon = -2.89413 - 0.01743t + 0.54892\, \ln t + 1.31015\, \ln\sigma - 6.66548\,(1/T)$ $+0.19131\, \sigma \ln T + 0.00021\,(T\sigma t).$	1255 K
TDNiCr	$\ln \epsilon = -3.48443 - 10.37282\left(\dfrac{1}{T}\right) + 0.28314\, \ln t + 2.00118\, \ln\sigma$	1478K

TDNiCr represented a somewhat special case from the other materials tested. Because of the low TDNiCr creep strains obtained, it was judged that further refinement of the equation would not have a significant effect on subsize panel predictions. Therefore, effort was placed on testing at stress levels such that some failures would be obtained at each of the test temperatures. Combination of stress and temperature at which failures occurred are indicated in Figure 20. Also shown are the last measured creep strain before failure and stresses at which tests were completed without failure. No creep strains are available for the 1200K temperature tests, since all failures occurred during the first cycle before measurements could be obtained.

The empirical equations presented were derived from the cyclic tensile test data generated at the temperature and stress profiles shown. These tests were conducted for 100 cycles of twenty minutes per cycle and, therefore, the total time of applicability of each of the equations is 33.3 hours.

Comparison of steady-state and cyclic tests. - Comparisons between steady-state and cyclic creep tests are presented in Figures 21-24. In these comparisons the cyclic time was the accumulated time at maximum load and temperature (i.e., 100 cycles = 33.3 hours). Based on the close agreement between the two forms of data, it is concluded that no significant difference exists between the two types of data, for the 4 alloys studied. Even though the two sets of data appear similar, attempts to develop a single equation to predict both sets of data were unsuccessful. Attempts to predict the cyclic data from the steady-state creep equation using various hardening laws were also unsuccessful. Since one equation to explain both sets of data was not obtained, the cyclic creep equation was used for analysis and prediction of all subsequent cyclic creep data.

Creep analysis of complex trajectories. - The creep analysis of complex flight trajectories could not be accomplished by using a simple equation expressing creep as a function of temperature and stress, but was possible by incorporation of various hardening theories. To accomplish this, a computer program for tensile creep trajectory data analysis (CPCE) was developed. The CPCE computer program provides an approach for accumulating creep strains in axially loaded structures, using the strain hardening and time hardening theories of creep accumulation. This program is capable of allowing rapid analysis of tensile cyclic creep test data where stresses and temperatures are varied both within a cycle and as a function of cycle in a variety of tests. The program calculates strains for time hardening, strain hardening, or a combination (rate dependent approach) based on the results of tests involving continuously increasing or decreasing loads (see Figures 3a and 3b). Results for L605 are shown in Figure 25a. From this figure it can be seen that time hardening provided the best predictions in the case of increasing stress (Figures 3a and 25a) while strain hardening provided the best predictions in the case of decreasing stress (Figures 3b and 25b). Therefore, the rate dependent approach was postulated as a combination of time hardening and strain hardening theories. For this approach the time hardening strain rate is calculated at each analysis time step and compared to the strain rate used in the previous step. Then strain hardening or time hardening is applied, depending on whether the strain rate has decreased or increased respectively. A comparison of the 3 approaches is presented in Figures 25a and 25b.
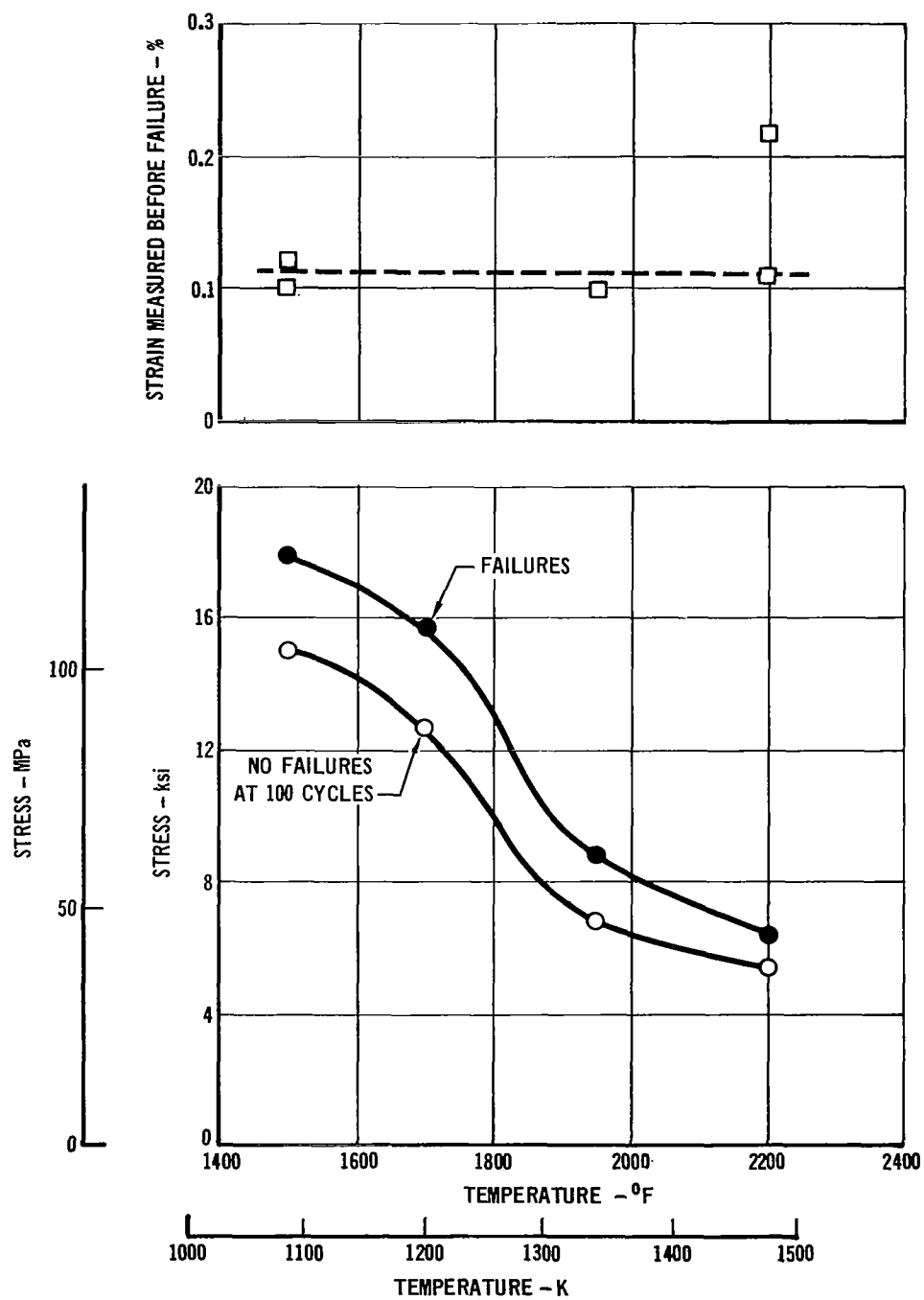
FIGURE 20 TDNiCr CYCLIC TEST DATA

FIGURE 21 COMPARISON Ti-6AI-4V CYCLIC AND SUPPLEMENTAL
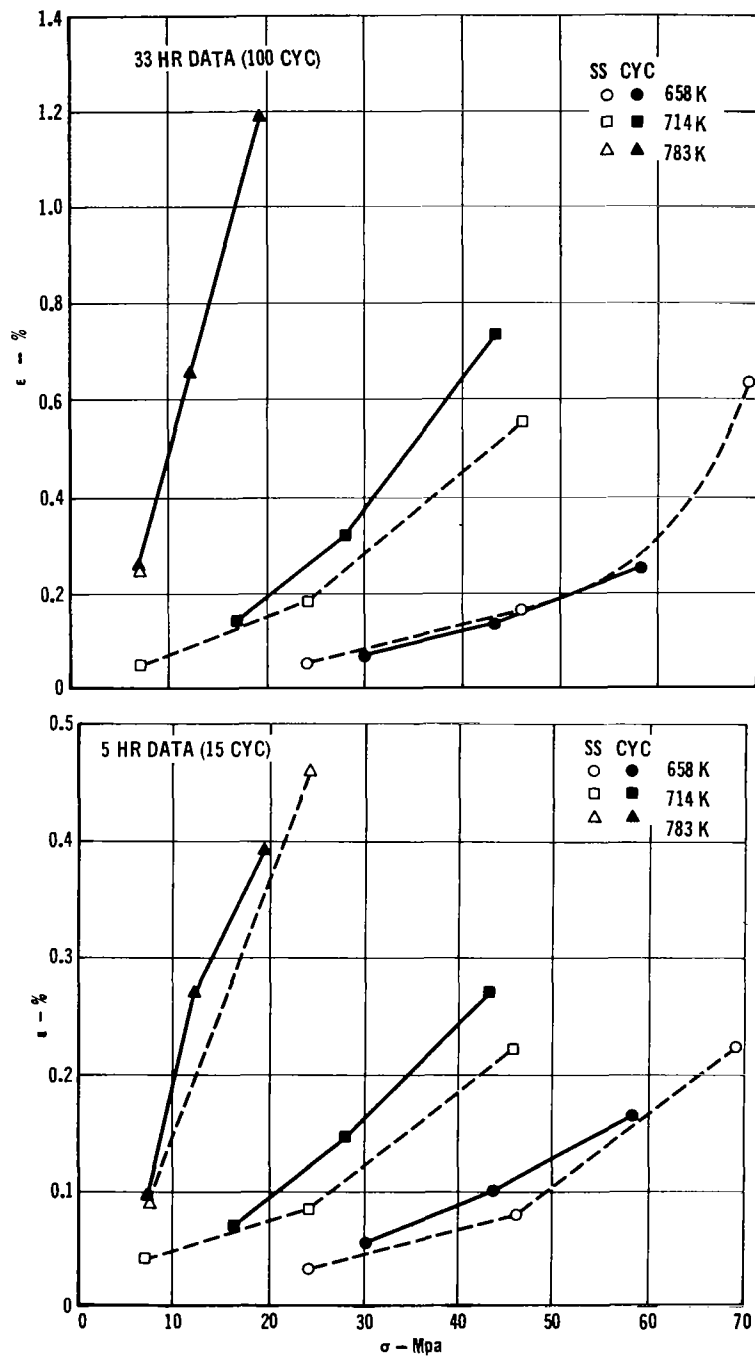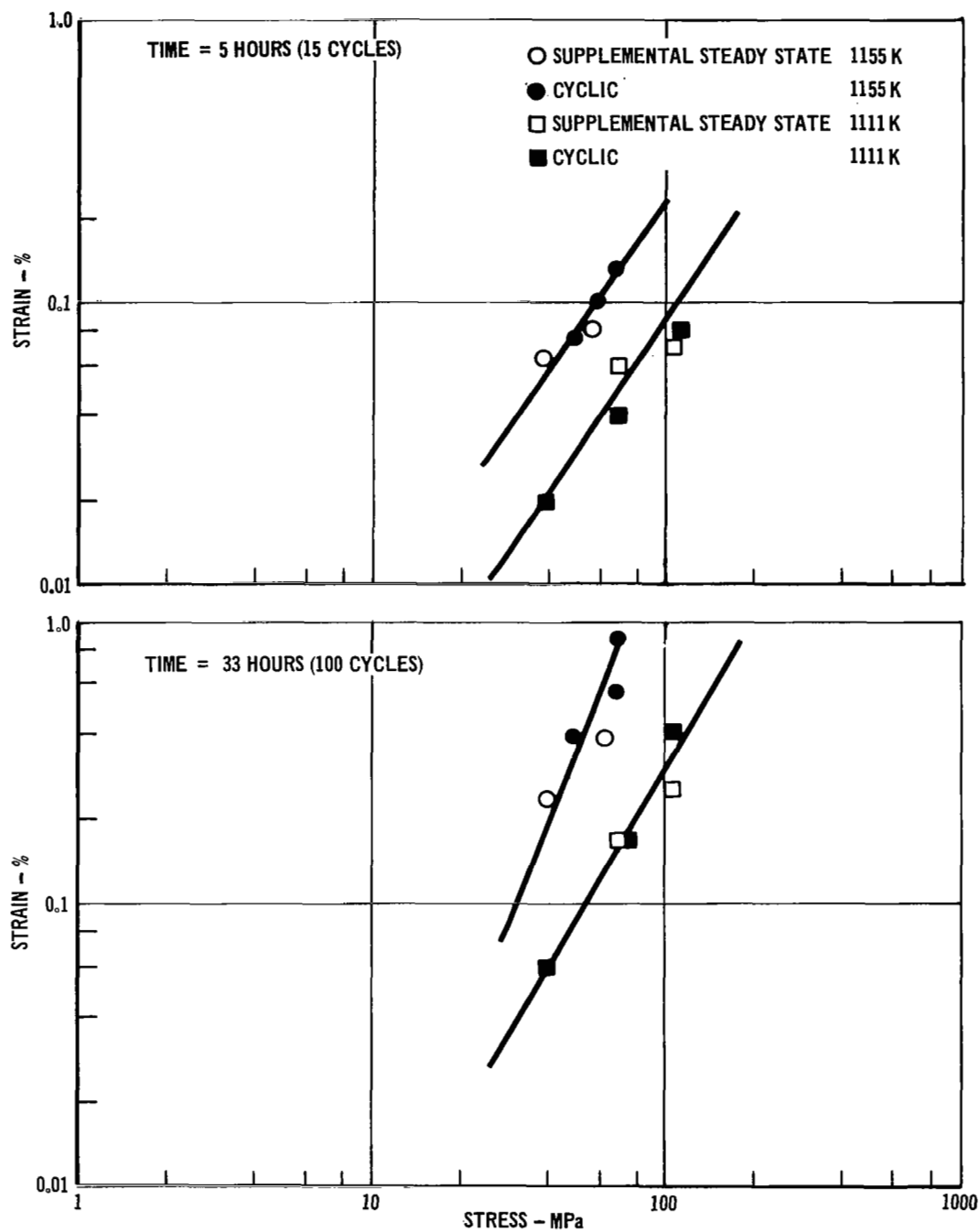STEADY-STATE DATA

FIGURE 22 COMPARISON OF RENE'41 CYCLIC AND SUPPLEMENTAL
STEADY-STATE DATA
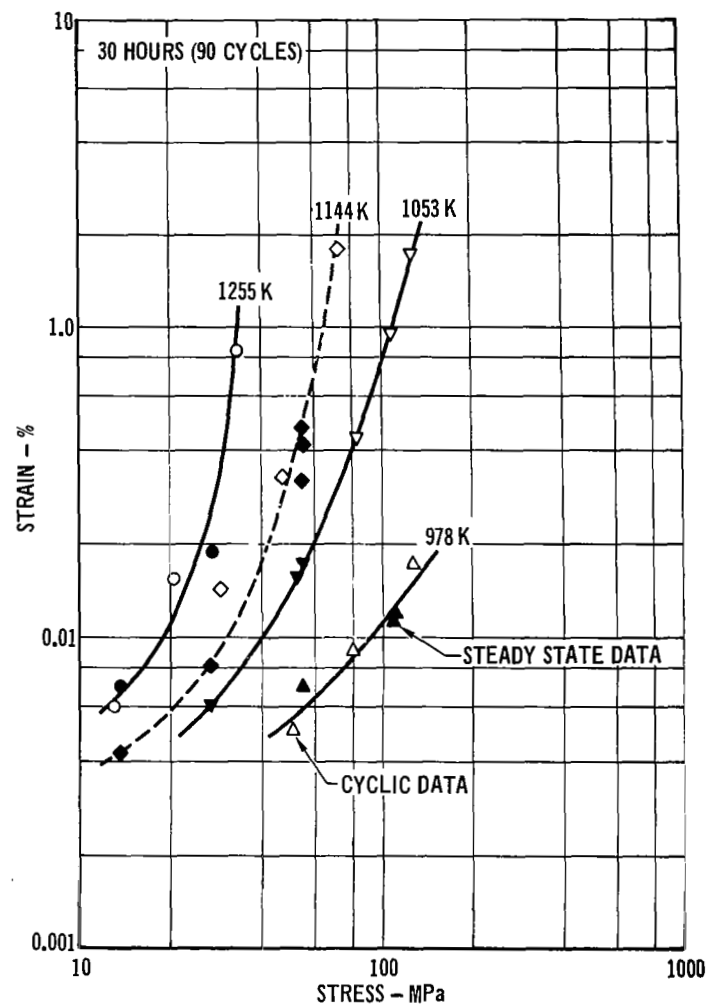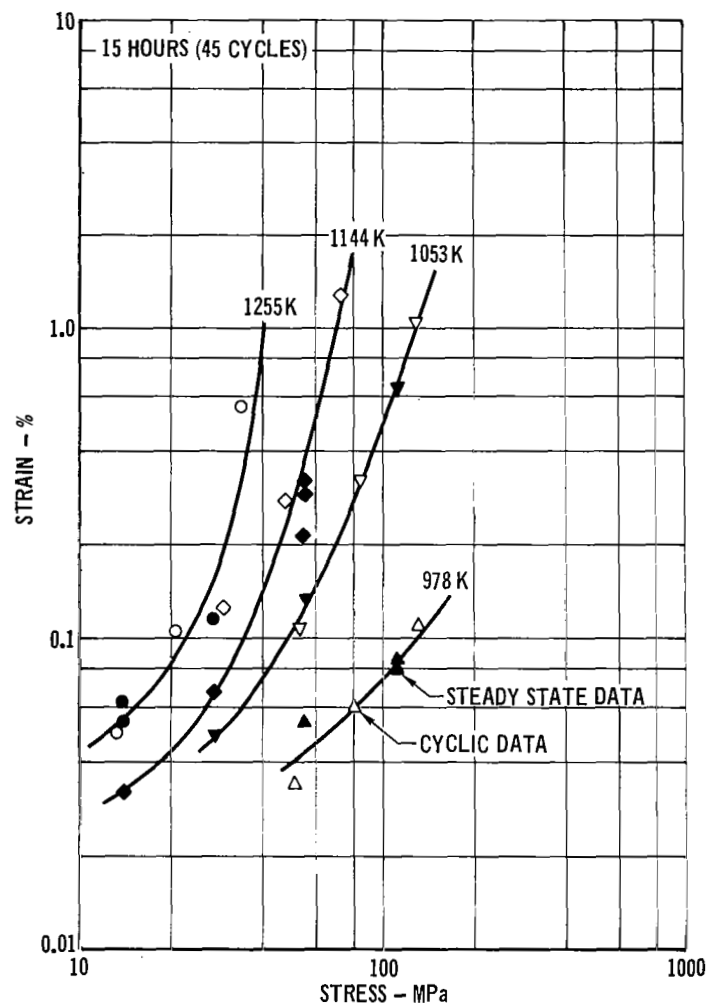
FIGURE 23 COMPARISON OF L605 CYCLIC AND SUPPLEMENTAL STEADY-STATE DATA
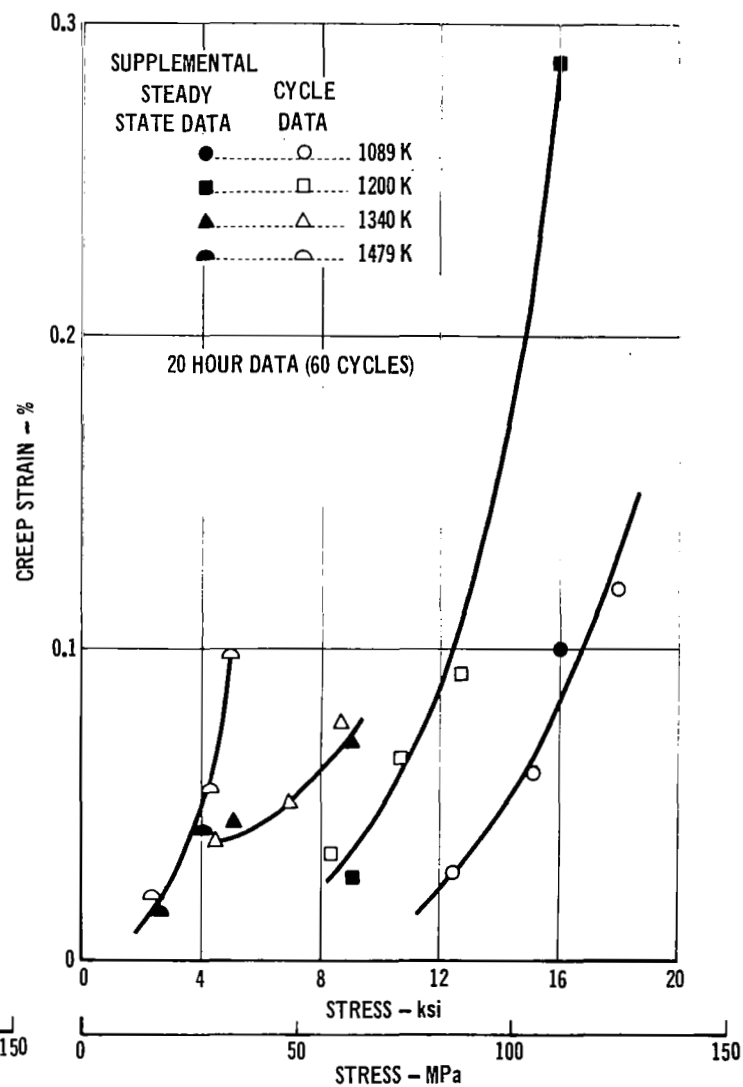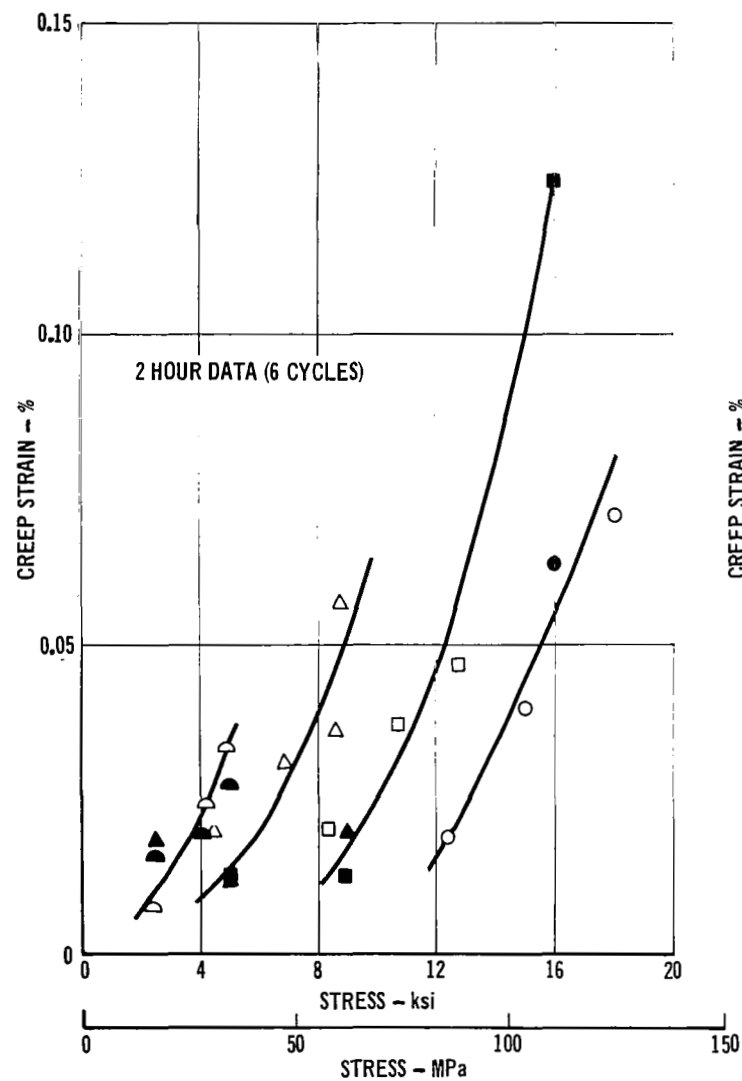
FIGURE 24 COMPARISON OF TD NiCr CYCLIC AND SUPPLEMENTAL STEADY-STATE DATA
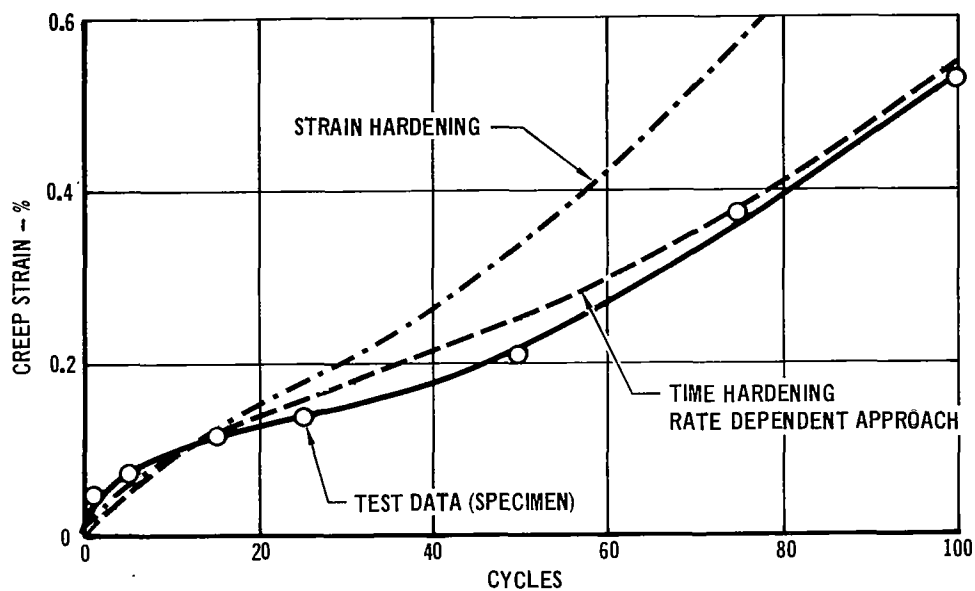
a) Increasing Stress History
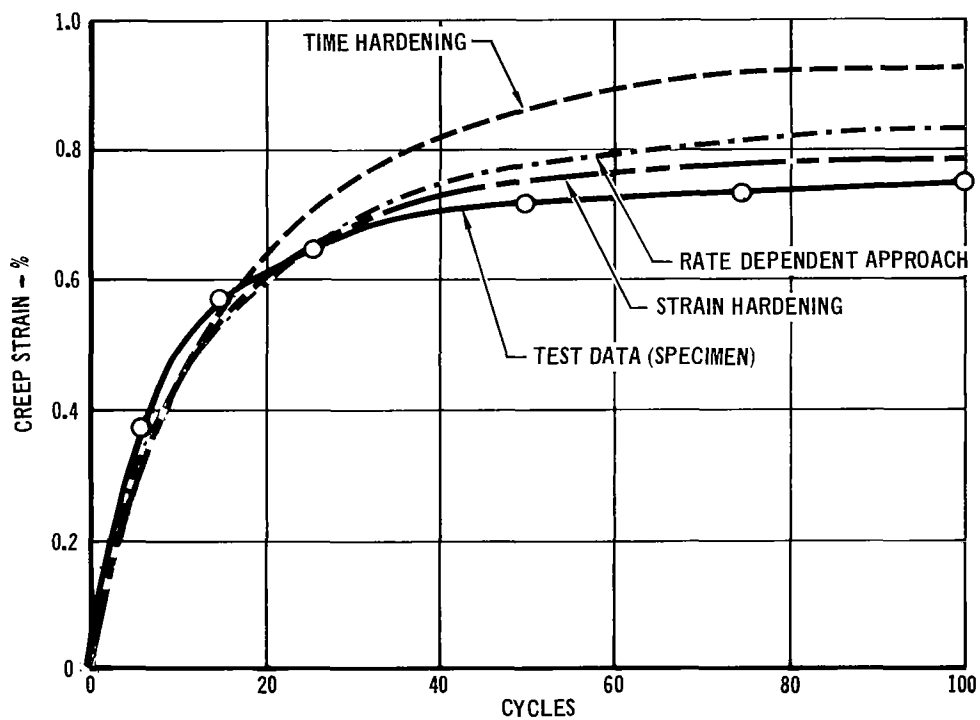
b) Decreasing Stress History

FIGURE 25 COMPARISON OF HARDENING THEORIES USING L605 TEST DATA

One of the objectives of this study was to assess the suitability of idealizing continuously varying stress and temperature profiles into a series of increments of time for which stress and temperature are constant. Since the length of time for these increments will vary with the trajectory, the effect of time at temperature and load had to be evaluated. To determine the magnitude of this effect, a test was performed using a cycle with a maximum time at temperature and stress of 10 minutes. A comparison of the data from this test with the data from a basic cyclic test (Figure 2), which had a maximum time at temperature and load of 20 minutes is presented in Figures 26-29. Each of the data points in this figure represents a total cycle time at load and temperature of 16.67 hours (100 cycles at 10 minutes/cycle for this test and 50 cycles at 20 minutes/cycle for the basic cyclic test). Close agreement between these test data was obtained. The variation noted for the titanium data was the greatest of the four materials. However, even this variation is within the range of expected data scatter. The agreement of these data suggest that the cyclic creep strains are a function of total time at load and temperature only, for cycle times typical of Shuttle entry trajectories. Therefore, application of the cyclic empirical creep strain equation to trajectories appeared warranted. Once this was determined the next step was to determine if the creep strains resulting from an idealized trajectory were similar to those obtained in actual trajectory tests. To accomplish this a simulated mission profile shown in Figure 30 and based on the trajectory shown in Figure 31 was idealized into a series of steps as seen in Figure 30. For the idealized profile it was considered desirable to maintain a constant peak temperature for 20 minutes to be consistent with the basic cyclic tests. Therefore, the temperature profile, shown in the figure, represents an idealization for the entire 20 minute time period. The results of this test along with the 3 methods of prediction are presented in Figure 32 for the L605 alloy. From this figure it can be seen that the rate dependent approach generally provided closer predictions than strain hardening or time hardening theories individually for L605. Although the rate dependent approach provided good predictions for the L605 trajectory tests, it did not improve predictions for the other materials.

For example, in the case of Rene' 41, predictions based on the time hardening theory of creep accumulation were considered best. Predictions based on the strain hardening theory of creep accumulation were found to be approximately the same as for time hardening in predicting strains for testing where the stress was continuously increased as a function of cycle. Both predictions were close to test values. For specimens where stress was continually decreased, the time hardening predictions were up to 30% higher than test strains. However, predictions based on strain hardening were even higher, up to 75% higher than the time hardening predictions.

For titanium cyclic tensile creep tests the strain hardening theory was found to yield the best predictions although predictions resulted in lower creep strain than obtained in testing. The rate dependent approach, used successfully in predicting L605 data, yielded strains comparable to the time hardening predictions for these titanium data. These predictions were approximately 20% below the strain hardening predictions given in Figure 34.
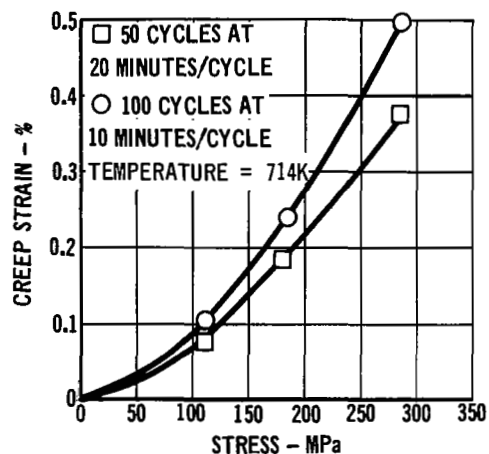
FIGURE 26 Ti-6Al-4V CYCLIC CREEP STRAINS AS A
FUNCTION OF TOTAL TIME AT LOAD
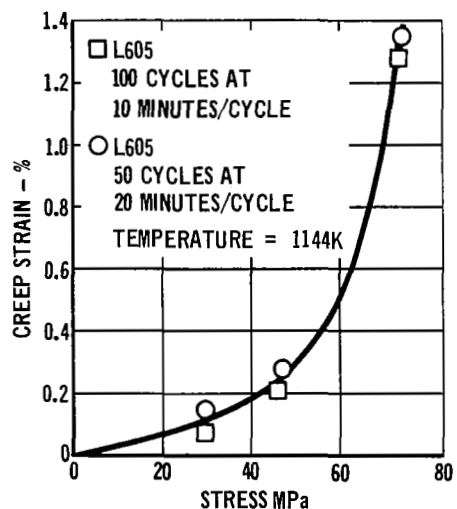
FIGURE 27 L605 CYCLIC CREEP STRAINS AS FUNCTION
OF TOTAL TIME AT LOAD
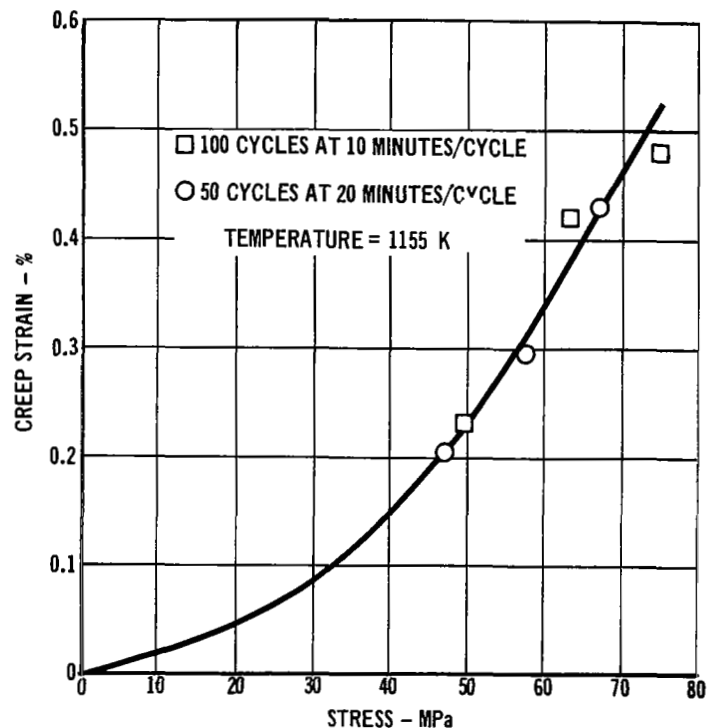
FIGURE 28 RENE '41 CYCLIC CREEP STRAINS AS A
FUNCTION OF TOTAL TIME AT LOAD
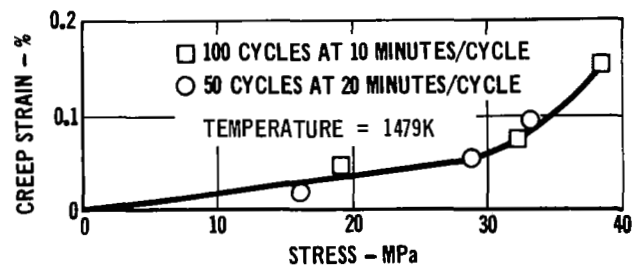
FIGURE 29 TDNiCr CYCLIC CREEP STRAINS AS A
FUNCTION OF TOTAL TIME AT LOAD
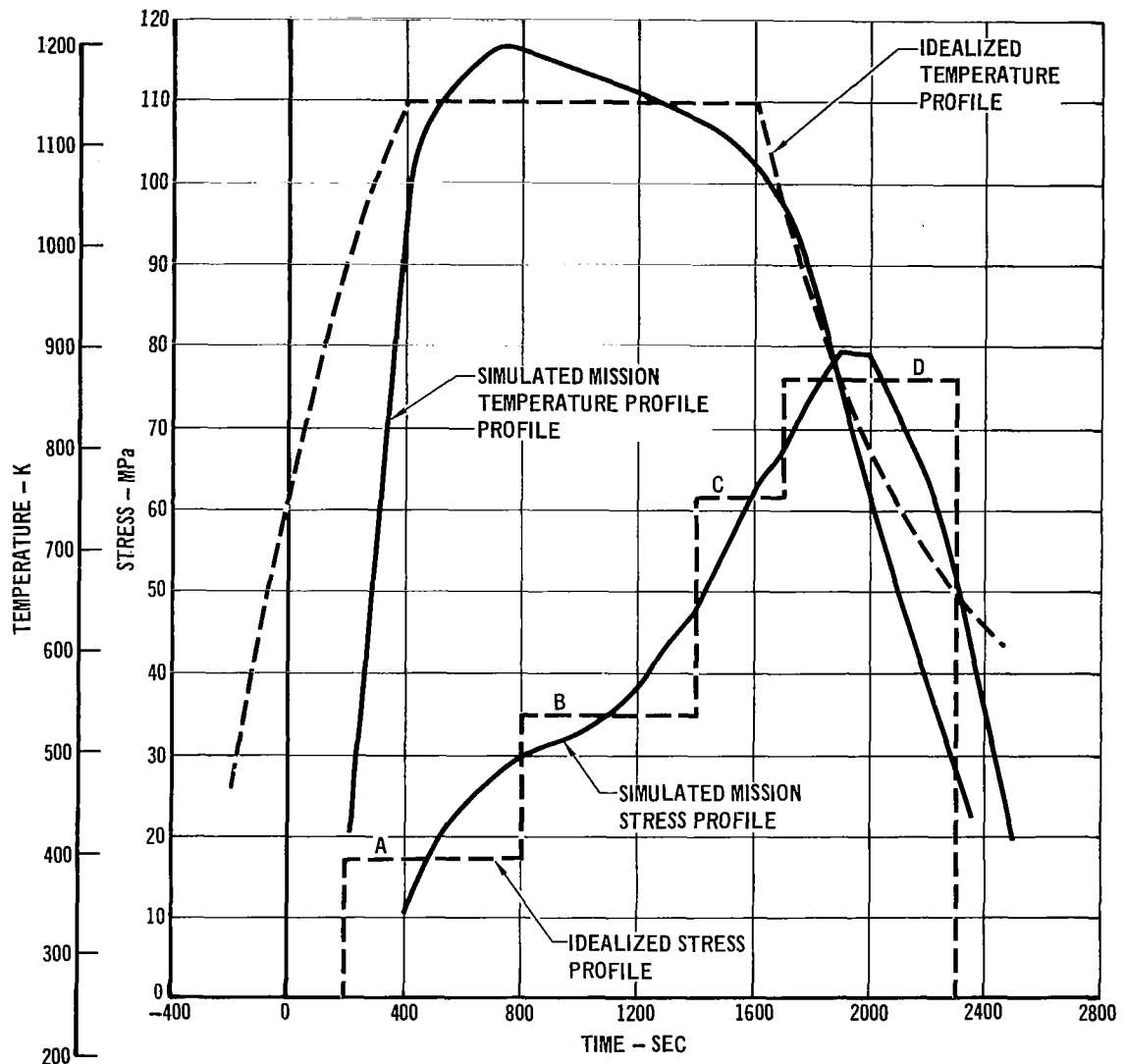
FIGURE 30 SIMULATED MISSION TRAJECTORY AND IDEALIZED PROFILES

Predictions of creep strains for TDNiCr trajectory profile tensile tests using the cyclic creep equation, were found in general to be from 30% to 70% of test strains at 100 cycles. The strain hardening theory of creep accumulation provided the best predictions with time hardening theory yielding lower values.

The conclusion of this phase was to perform a test using a representative shuttle stress, temperature, and pressure profile seen in Figure 30. Comparison of the idealized and simulated mission trajectory creep strain results are shown in Figure 33 for L605. Since there does not appear to be any significant difference between the two tests, it can be suggested that the step stress profile and corresponding flat temperature profile is a good idealization of the actual flight profile.
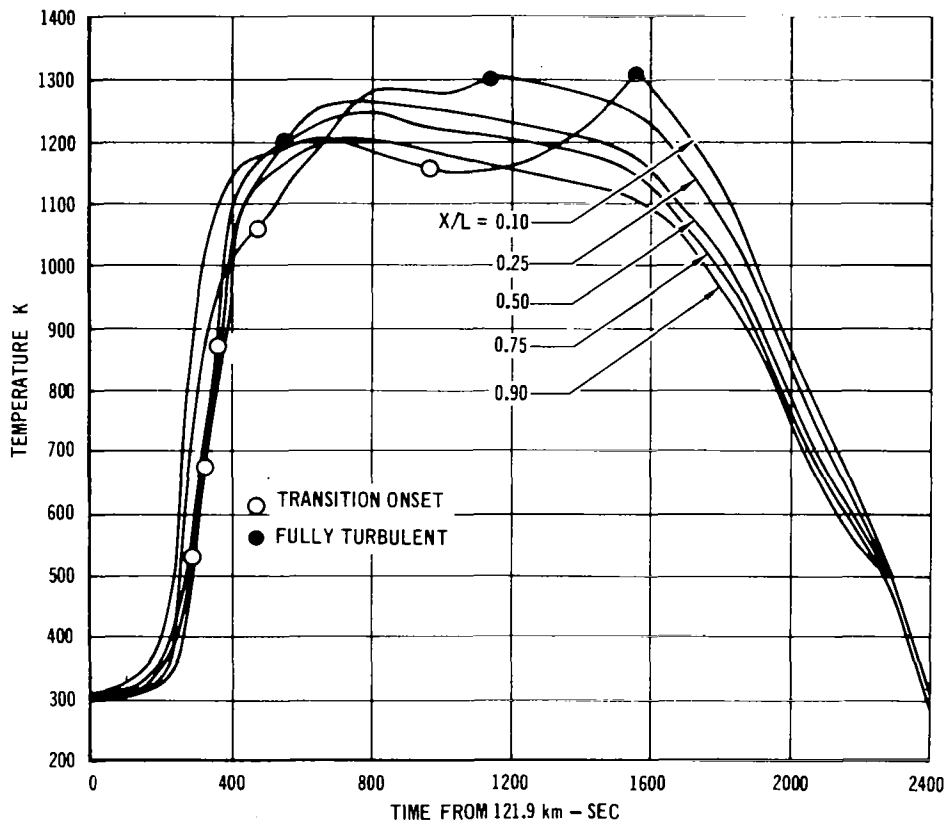
FIGURE 31 REPRESENTATIVE SPACE SHUTTLE ORBITER
BOTTOM CENTERLINE ENTRY TEMPERATURES
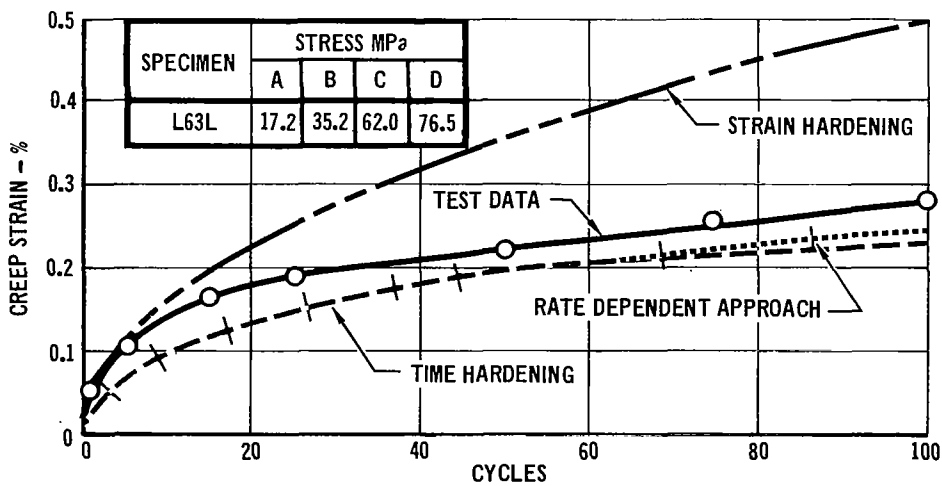
FIGURE 32 L605 CYCLIC — IDEALIZED TRAJECTORY
PROFILES AND RESULTANT CREEP
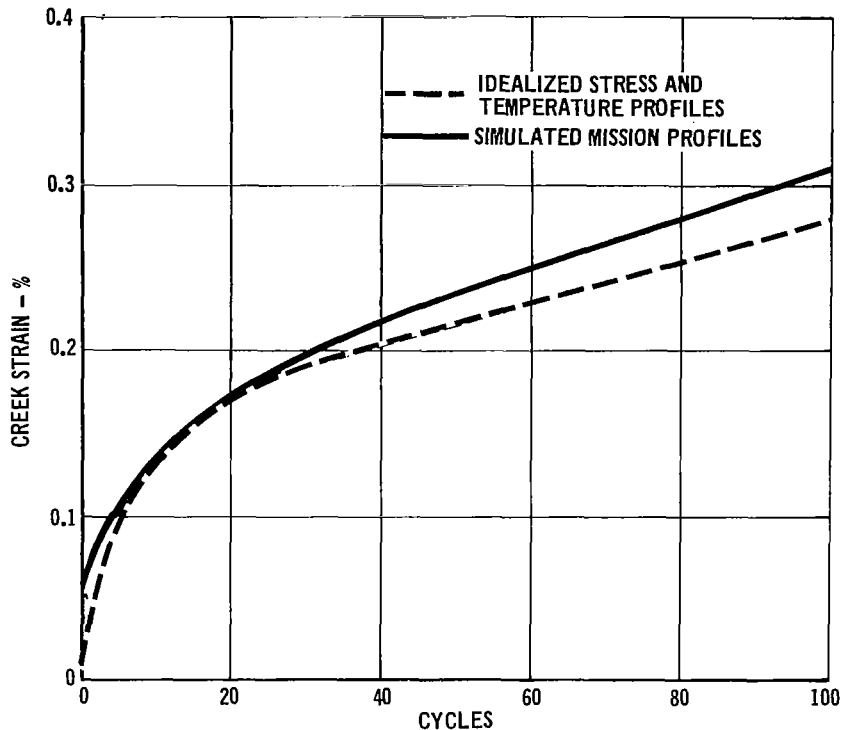
FIGURE 33 COMPARISON OF L605 CYCLIC TENSILE CREEP STRAINS FOR SIMULATED MISSION AND IDEALIZED TRAJECTORIES

To determine our predictive capability for the simulated mission profiles, the stress and temperature profiles were idealized into 10 steps or a total of 1000 steps for the 100 cycle creep accumulation analysis (22 steps were used for L605). The analysis steps used were for 200 second duration (100 sec. for L605). The results of these analyses are shown in Figures 34-37.

The total time of 33.3 hours maximum (100 cycle of 20 minutes/cycle) for which the cyclic creep empirical equation was derived, is exceeded at 55 cycles. Therefore, creep predictions beyond this time are outside equation limits and should not be used. This recommendation is based on the fact that the form of the cyclic equation (Table 5) allows strains to decrease at accumulated times greater than 33 hours. As a result, extrapolation beyond 33 hours can result in incorrect strain predictions. This trend can be seen in Figures 35 and 36 where strain hardening closely approximates the test within the time range (55 cycles), however, outside this range the difference between the two becomes greater with increasing time.
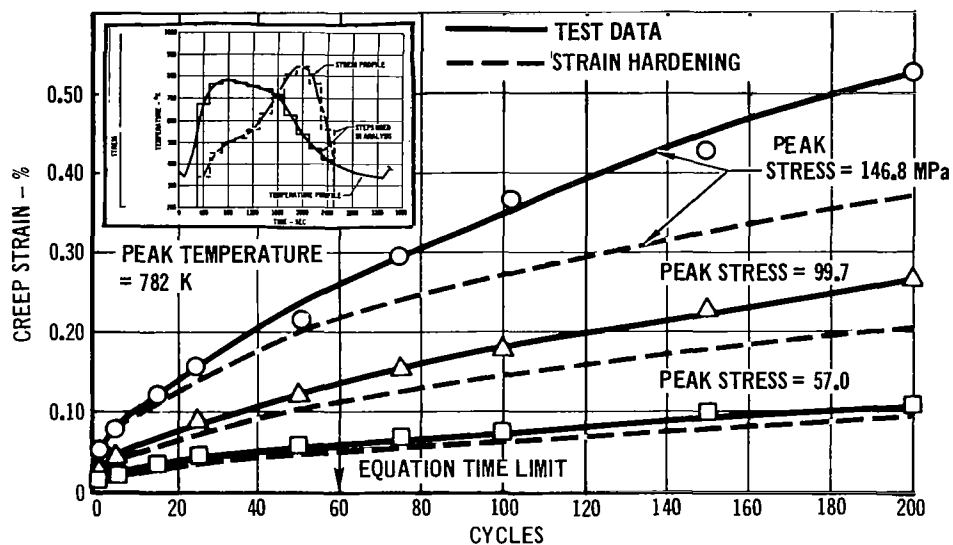
FIGURE 34 PREDICTIONS FOR Ti-6Al-4V MISSION PROFILE TEST
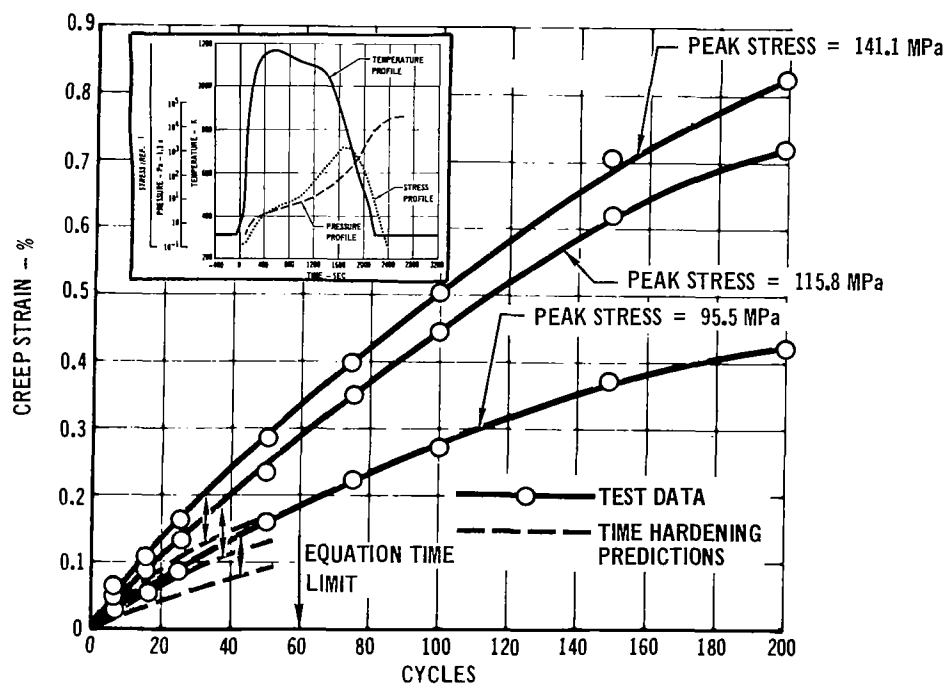
FIGURE 35 PREDICTIONS FOR RENE'41 MISSION PROFILE TEST
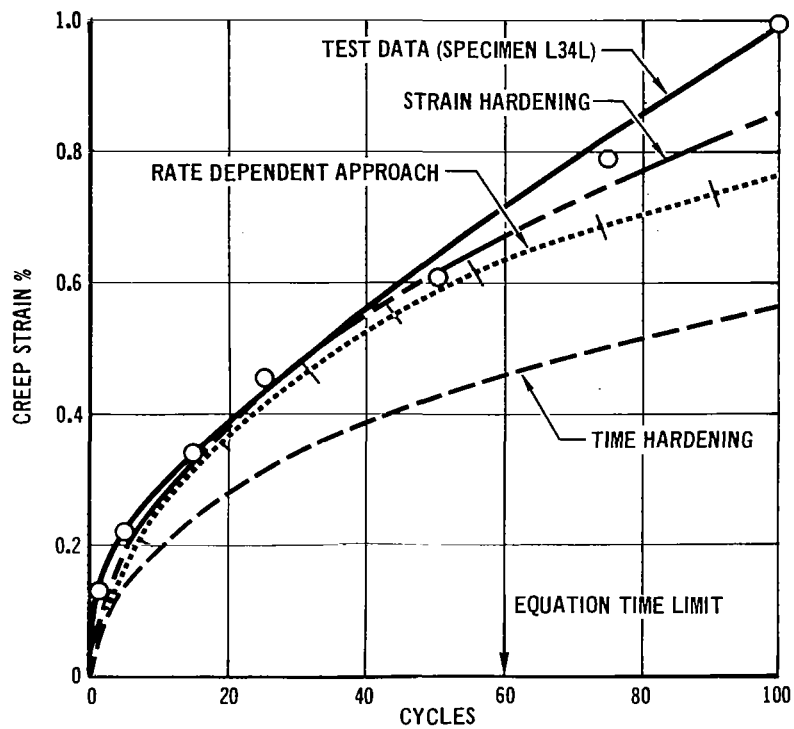
FIGURE 36 PREDICTIONS FOR L605 MISSION PROFILE TEST
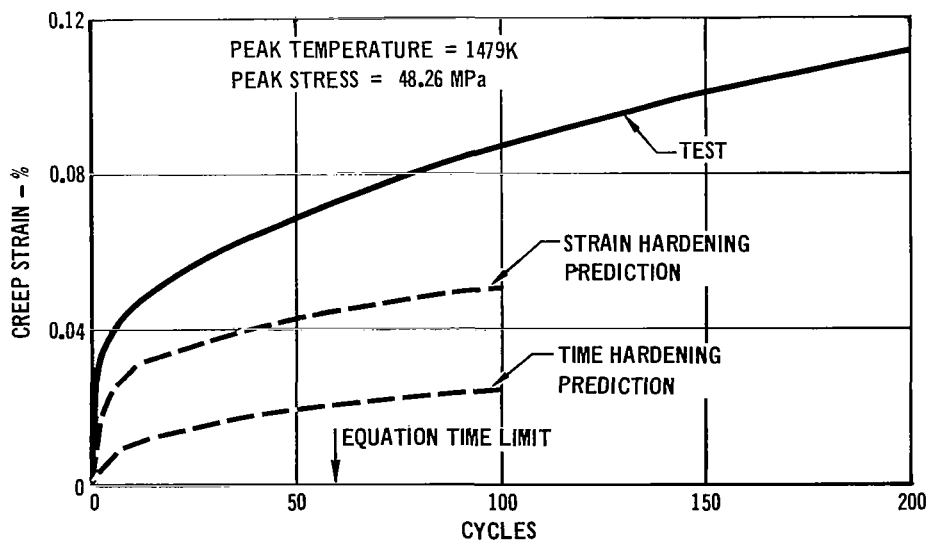
FIGURE 37 PREDICTIONS FOR TDNiCr MISSION PROFILE TEST

Phase I Conclusions

Test results demonstrated that there is no significant difference between the basic cyclic and steady-state creep strains for the four materials studied under the experimental conditions investigated. A single linear equation describing the combined steady-state and cyclic creep data resulted in standard errors of estimate higher than obtained for the individual data sets. Creep strain equations were successfully developed for both steady-state and cyclic creep data using linear least squares analysis techniques.

The prediction of strains that are produced by complex trajectory and simulated mission tests (using equations based on simple cycles) was successfully accomplished. A computer program was specifically written for this analysis. This computer program is based on combined time and strain hardening theories of creep accumulation. The resultant rate dependent approach for accumulating creep strains appears to provide a good prediction for trajectory test data. This approach utilizes a combination of time hardening and strain hardening accumulation theories in conjunction with the cyclic data empirical equation.

PHASE II - SUBSIZE PANEL CYCLIC CREEP PREDICTION

The second phase of this study was directed toward developing and verifying capability for prediction of creep deflection in metallic heat shields subjected to cyclic entry environments. A computer program, Thermal Protection System Creep (TPSC), was developed for predicting panel creep deflections and seventeen subsize panel specimens were tested to cyclic entry environments. Creep deflections were predicted, using the TPSC program in conjunction with material creep equations developed in Phase I, and compared with test results.

Subsize Panel Configuration

Two subsize panel configurations were selected for testing in this phase of the program. These were the single face corrugation and rib stiffened designs shown in Figure 38. Considerations for establishing panel configurations were based on previous MDAC experience in the design of metallic TPS in connection with Shuttle studies and various in-house studies. In addition, ease of fabrication and applicability to Space Shuttle TPS designs were considered. The section geometry designs were closely coordinated with the test mechanism design to assure compatibility. Panel length of 30.5 cm (12.0 inches) was the maximum length which could be tested in conjunction with the furnace test zone capabilities. Load mechanism geometry in conjunction with furnace dimensions constrained panel width to be less than 6.6 cm (2.6 inches) and panel depth to be less than 1.65 cm (.65 inches). Therefore, panel dimensions of 6.35 cm by approximately 1.3 cm were selected, to allow adequate clearance in the test mechanism. End plates, shown in the figure, were included to serve as support pads during testing. Specimens were fabricated in the McDonnell Douglas Advanced Material Fabrication Facility using the thin gage sheet material procured for this program. All specimens were formed with the material's longitudinal rolling direction coinciding with the panel longitudinal direction.

Corrugated stiffened panels were fabricated for each of the four alloys (L605, Rene' 41, Ti-6Al-4V, and TDNiCr) without difficulty, using continuous spot welding techniques to join the skin to the corrugation and the end plate to the corrugation. Corrugations were formed, using available tooling, to the dimensions shown in Figures 39a and 39b.

Corrugated panels are generally critical for positive bending loads (skin in compression) because allowable bending loads in the positive and negative directions are approximately equal while design loads are higher in the positive direction. Typical pitch lengths used for optimum thin gage metallic TPS corrugated panels have been approximately 3.0 ($\sim$1.2 inches). Pitch lengths less than 3.0 cm are desirable in order to minimize possible response to acoustic loadings associated with Shuttle trajectories. Optimum panel depths vary, depending upon design loads and material strength properties, but are usually in the range of 1.0 to 2.5 cm (0.4 to 1.0 inch). Existing tooling was used for forming the subsize test panel corrugations. Therefore, the corrugation panel specimen cross sections were the same for each of the four materials. Panel dimensions, while not optimum, fall within the range of typical TPS panel dimensions.

Rib stiffened subsize panels were fabricated only from Ti-6Al-4V and L605 sheet material because potential welding problems with Rene' 41 and brazing difficulties with TDNiCr would have required a development effort beyond the scope of this program.

41

SPOT WELDS

30.5

1.30

CORRUGATION

SKIN

END
PLATE

2.54

LONGITUDINAL
MATERIAL DIRECTION

30.5

1.14

RIB

6.35

END
PLATE

SKIN

ELECTRON
BEAM WELD

2.54
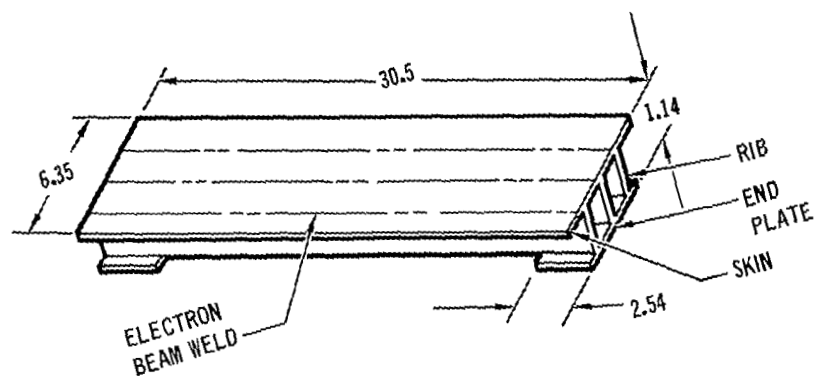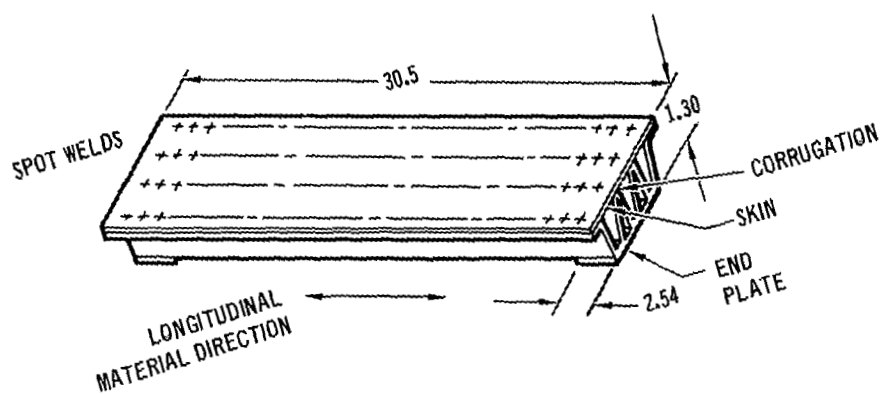
NOTE: ALL DIMENSIONS ARE IN CM

RIB AND CORRUGATION SUBSIZE TEST PANEL CONFIGURATIONS
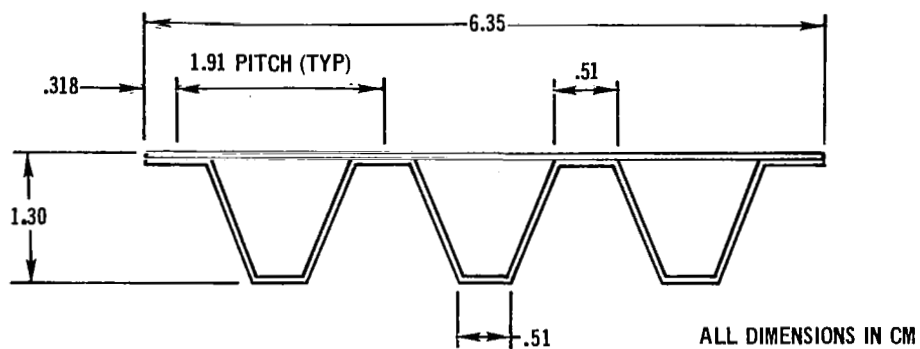
MATERIAL	NOMINAL THICKNESS (CM)	HEAT NUMBER
L605	.024	1860–2–1399
RENE'41	.027	2490–0–8207
Ti–6Al–4V	.031	N–0358
TDNiCr	.024	TC–3875

FIGURE 39 (a) SINGLE FACE CORRUGATION SUBSIZE PANEL DESIGN
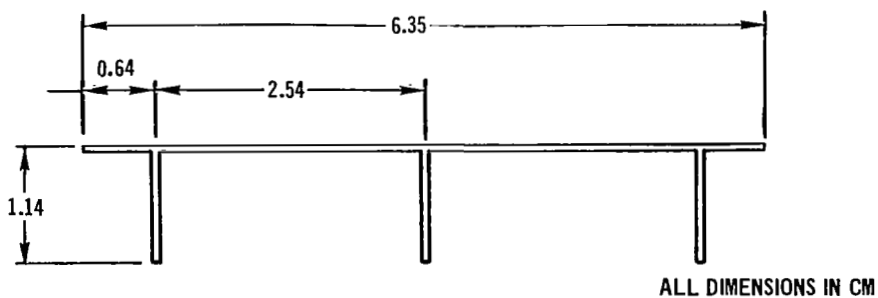
MATERIAL	NOMINAL THICKNESS (CM)	HEAT NUMBER
L605	0.064	1860–2–1396
Ti–6Al–4V	0.051	N–0358

FIGURE 39 (b) RIB STIFFENED SUBSIZE PANEL DESIGN

Cross section geometry, of the rib subsize panel specimens shown in Figure 39b utilizes a rib spacing of 2.54 cm, which is consistent with typical TPS panels and with the panel width allowed for testing. Although a thinner gage skin would be used for an optimum design (Reference 11), it was decided to fabricate the rib stiffened panels using the same skin thickness as the rib to simplify manufacturing. Panel depth of 1.14 cm was established in conjunction with test mechanism loading requirements.

The rib stiffened panel ribs and skins were joined by electron beam welding using the "burn through" technique. Curvature or bowing (midspan deflection of approximately 0.1 cm toward the rib side of the panels) along the length of the rib stiffened panels was evident after fabrication. This was attributed to material shrinkage in the weld zone. The titanium panels were subsequently flattened and stress relieved at 1300°F. Oxide removal by pickling followed the flattening process, resulting in the removal of approximately .001 inch of material. This yielded somewhat thinner gages than previously reported for specimens tested under steady state conditions in Phase I (Reference 1). No attempt was made to flatten the L605 rib panels because the temperatures required produce a microstructure different from that used in the Phase I cyclic tensile tests. Therefore, to keep material in the panel structure consistent with material used in the original cyclic tests, the decision was made to not straighten the L605 panels. L605 rib stiffened panels were tested both in positive bending (skin in compression) and in negative bending (skin in tension) to provide a comparison of creep deflections for determining any detrimental effects of initial curvature on creep deflection results.

Experimental Procedure

Subsize panel creep tests were conducted in a 17.8 cm diameter resistance heated graphite tube furnace, modified by the MDC Materials Laboratory for this type of testing. The furnace and associated controlling equipment are shown in Figure 40. The furnace consists of a ceramic tube sealed at both ends with water-cooled steel plates, and heated by radiation from the resistance-heated graphite element in the furnace. The furnace test zone diameter is 11.4 cm (4.5 inches). This furnace allows simultaneously varying temperature, pressure, and load. All test conditions are automatically programmed and controlled. Temperature measurements and recording accuracies were the same as for the tensile specimen cyclic testing. Based on replicate L605 panel test data the applied loads were found to be reproducible to within 1%.

Creep deflection testing was accomplished using the mechanism shown in Figure 41(a) and (b) to convert axial load, applied by the furnace hydraulic load actuator, to a bending load on the subsize panel. This mechanism was specifically designed to minimize the dependence of applied panel moment on panel deflection. This independence of panel moment and panel deflection was required to maintain applied load accuracies since panel creep deflections continuously changed during testing and were therefore unknown between times at which deflection measurements were recorded.

Loading pin locations for applying load to the subsize panel specimens were established to provide a bending moment distribution which would approximate that for a uniformly distributed pressure load. Those used in the mechanism design (Figure 42) provide a good approximation, as demonstrated in Figure 43.

TEMPERATURE RECORDER

TEMPERATURE CONTROLLER

FURNACE
EXTENSION
ASSEMBLY

PROFILE
SIMULATION
CONTROLLER

LOAD AND PRESSURE RECORDER

FURNACE

PRESSURE SERVO CONTROL SYSTEM
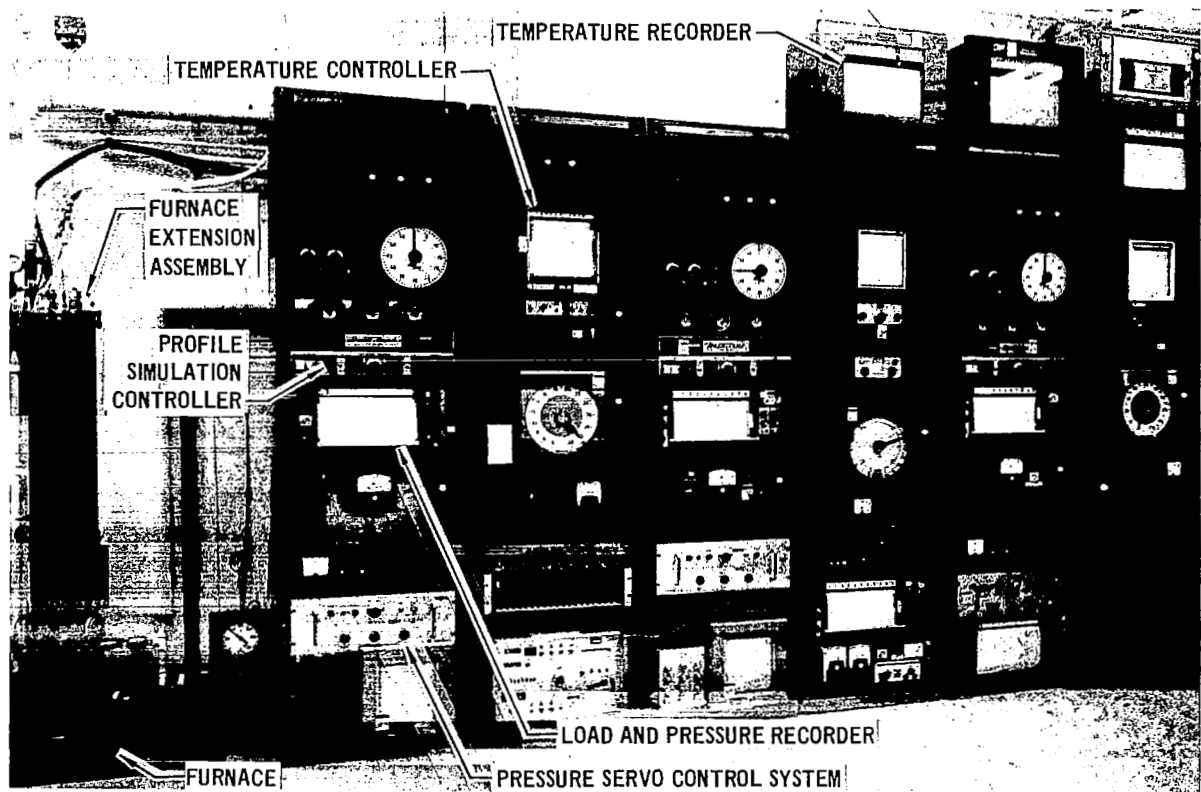
FIGURE 40 ASTRO FURNACE FOR PANEL SPECIMEN CREEP TESTING

45
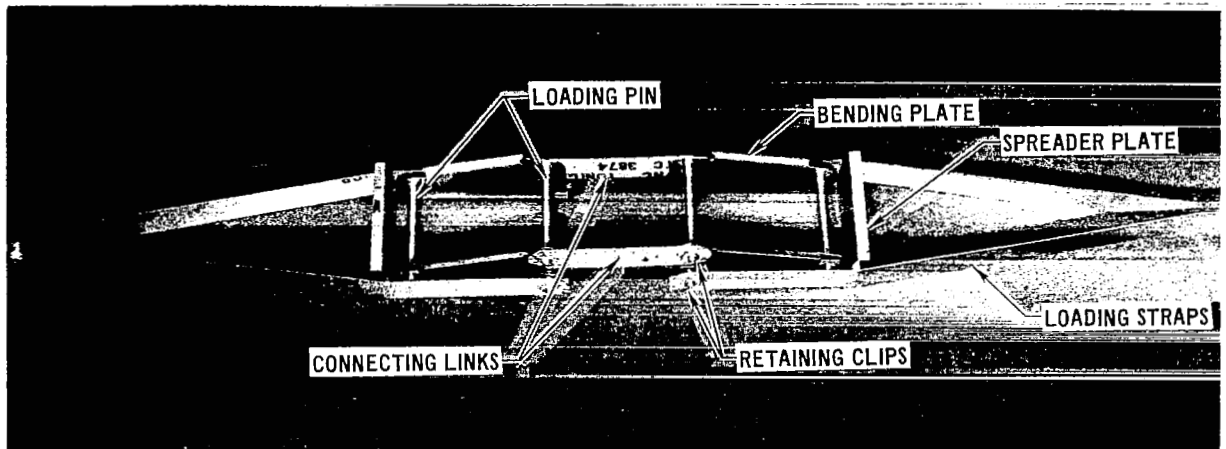
FIGURE 41 (a) LOAD MECHANISM FOR SUBSIZE PANEL TESTING
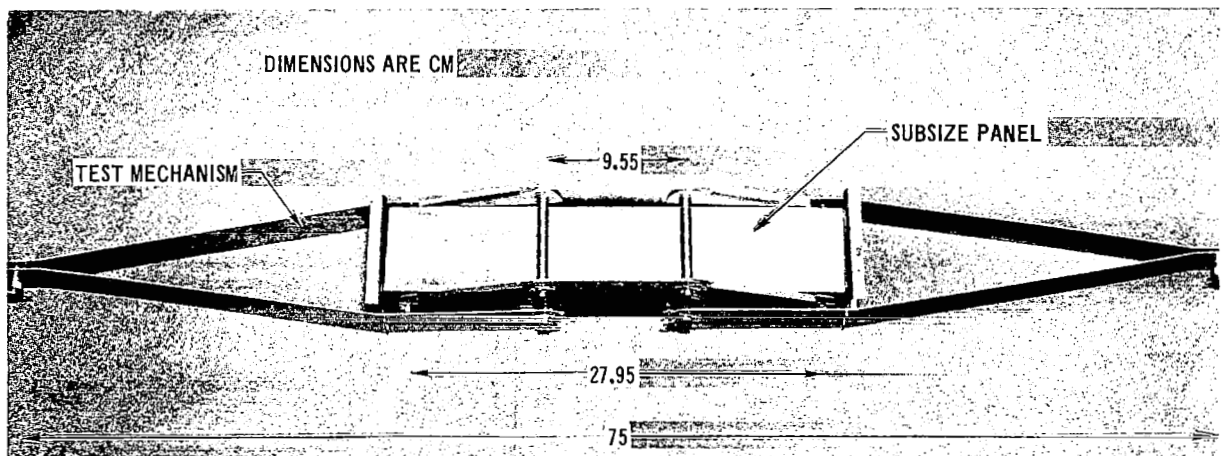
FIGURE 41 (b) LOAD MECHANISM WITH SUBSIZE PANEL INSTALLED
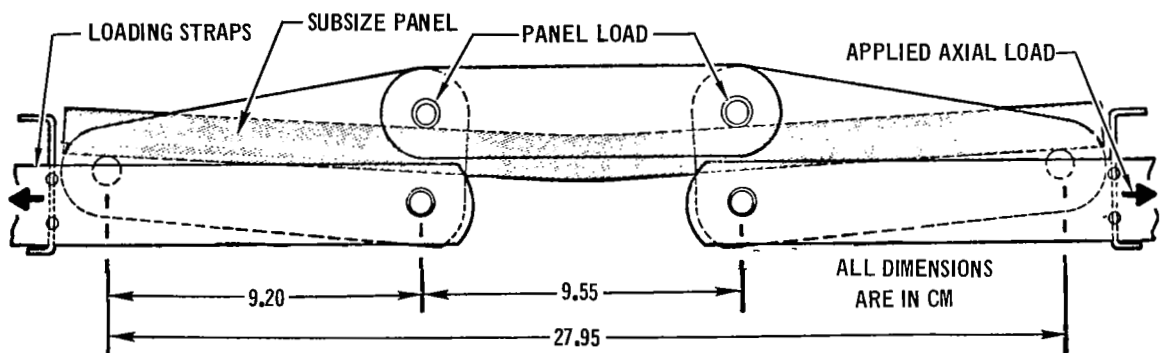
FIGURE 42 MECHANISM CONVERTS AXIAL LOAD TO PANEL BENDING LOAD

ALL DIMENSIONS ARE IN CM
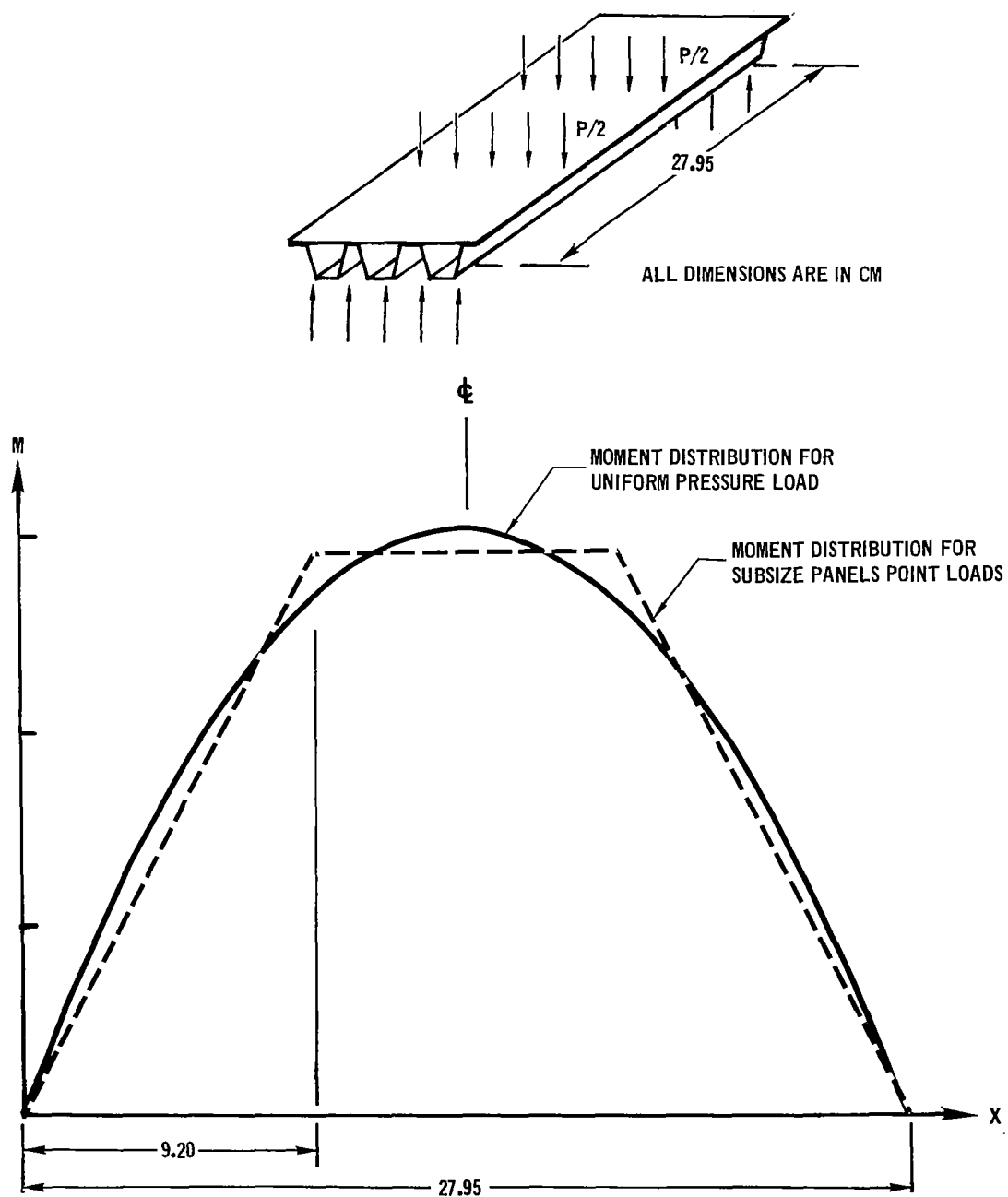
FIGURE 43 SUBSIZE PANEL LOAD AND BENDING MOMENT DISTRIBUTIONS

Two types of profiles were used in subsize panel testing. These profiles were (1) constant stress and temperature for twenty minutes with a constant, low atmospheric pressure as shown in Figure 44(a), and (2) mission profile load, temperature, and atmospheric pressure profiles as shown in Figure 44(b). These were the same profiles used in Phase I tensile creep testing except that an additional five minutes were allowed for cool down for a total cycle time of sixty minutes. During this phase, thirteen corrugation stiffened subsize panels and four rib stiffened subsize panels were tested.

The purpose of subsize panel testing during Phase II was to provide deflection data for verification of prediction capability. In line with this purpose, the primary requirement of panel testing was that, for each material, the creep strains attained were in the range of data obtained in the Phase I tensile creep tests. This was necessary because empirical equations developed in Phase I for cyclic creep response were used in analysis during Phase II. In conjunction with this, it was also desirable to obtain realistic permissible deflections as defined by the criterion established in Reference (14) for TPS deflection based on minimizing local panel heating. This criterion was:

$$\delta = .25 + .01L \text{ (cm)} \tag{1}$$

For typical 2.5 cm deep corrugation and rib stiffened TPS panels, this criterion is consistent with test stress levels and temperature levels designed to yield 100 cycle creep strains of up to approximately 0.5%. The criterion provides for a maximum deflection of .75 cm for a 50.0 cm typical panel length. Using this criteria, the following approach was used to establish test load levels for the mission profiles. For the 30.5 cm (27.9 cm between supports) subsize panels, the allowable creep plus elastic deflection per this criterion is .53 cm. Therefore, a reasonable range of desired creep deflection was from approximately .25 to .50 cm. Load levels required to yield the desired test deflections were obtained based on the assumption that creep deflections obtained in testing would be approximately 50% of those obtained using a linear creep stress-strain assumption. This assumption tended to account for the redistribution of stresses in the beam due to nonlinear creep strain-stress properties. The assumption can be expressed by the following equation:

$$\frac{\Delta_c}{\epsilon_c} = .5 \frac{\Delta_E}{\epsilon_E} \tag{2}$$

Applying this equation and using an elastic deflection based on a uniform pressure loading, the following equation was derived from creep strain at the beam midspan.

$$\epsilon_c = \frac{2\Delta_c}{\Delta_E} \epsilon_E = \frac{2\Delta_c}{\frac{5}{384} \frac{WL^4}{EI}} \frac{WL^2}{8 EI} \overline{Y} = 19.2 \frac{\Delta_c \overline{Y}}{L^2} \tag{3}$$

Calculated creep strains from Equation (3) were entered in plots of creep strain vs stress obtained from Phase I tensile creep tests for the same mission profiles and temperature. The corresponding stress level (σ) was then applied to calculate the required beam bending moment (M):

LOAD – TEMPERATURE

TEMPERATURE (T)

LOAD (P)

ATMOSPHERIC
PRESSURE
= 1.3 Pa

TIME

20 MINUTES
AT LOAD

CYCLE (60 MINUTES)

a) Constant Temperature and Load Profiles

ATMOSPHERIC
PRESSURE

TEMPERATURE

BEAM LOAD (P)

LOAD TEMPERATURE –
ATMOSPHERIC PRESSURE

CYCLE (60 MINUTES)

TIME

0   800   1600   2400   3200

TIME – SEC

b) Mission Temperature and Load Profiles
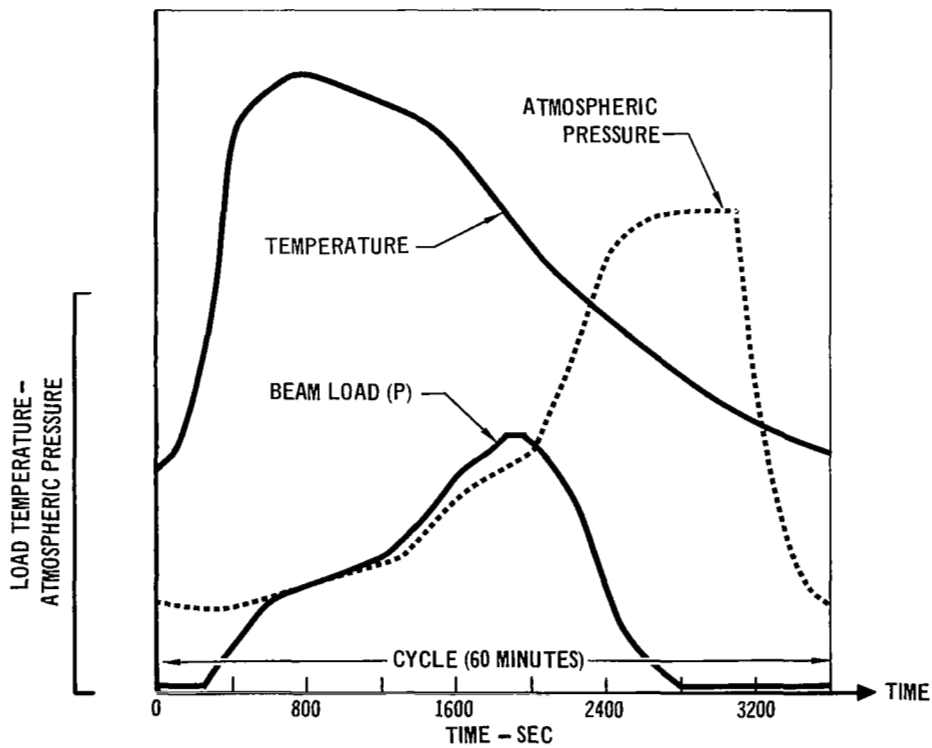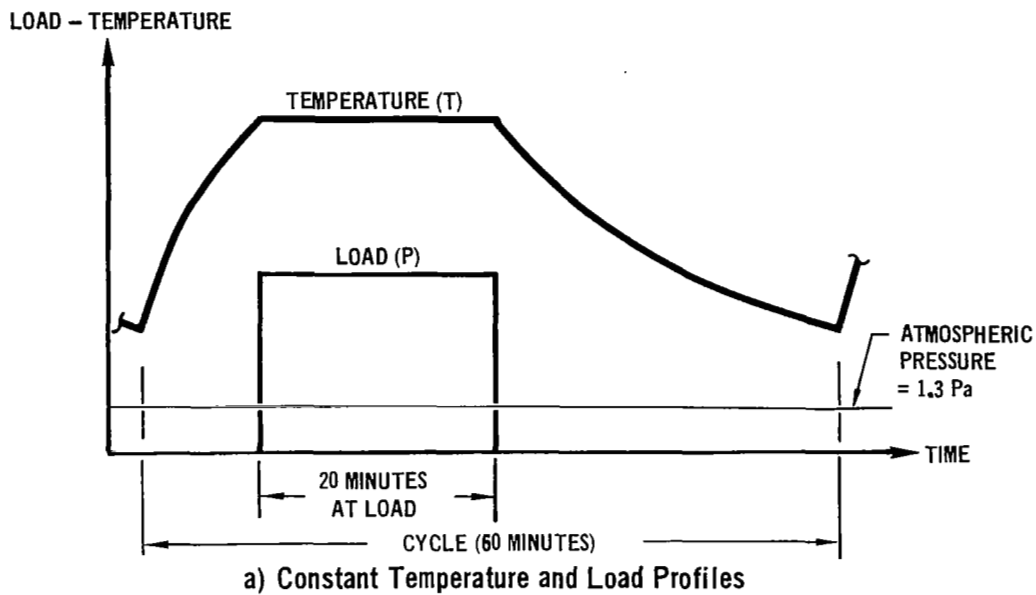
·FIGURE 44 SUBSIZE PANEL TEST PROFILES

It is of interest to note that if this calculation was carried out for a full size 51 cm (20 inch) TPS panel, the creep strain required to attain the same creep deflection is lower because the strain is inversely proportional to the square of beam length.

Therefore, use of the deflection criterion (δ = .25 + .01L) with subsize panels, results in requirements for greater creep strains than would be attained in a full size panel under the same criterion. As long as the cyclic creep test data and corresponding empirical equation developed in Phase I was applicable over the creep range required (as in the case of L605), the criterion was used. That is, subsize panel creep deflections of up to approximately .5 cm were acceptable. However, in the case of Rene' 41 panels, where the Phase I cyclic tensile specimen creep was generally less, lower deflections were used in order to stay within the limits of empirical equation prediction capability.

Cumulative creep strain of each specimen was measured after 1, 5, 15, 25, 50, 75 and 100 cycles (variations from this plan were made in some cases and are shown with the specific test data (Reference 2)). Deflections were recorded at several locations on the panel, selected to allow adequate definition of the deflected shape. Measurement locations across the panel width were selected to coincide very closely with the stiffeners for both the rib stiffened and corrugation stiffened subsize panels. To facilitate measurements, a box was fabricated. This box consisted of a top and bottom plate with panel support points located at 27.94 cm (11.0 inches) spacing to coincide with panel load support points. Deflections were determined at hole locatins in the top plate by using a dial gage to determine distances from the top surface of the plate to the panel skin. Readings were subtracted from reference readings made prior to testing to determine panel deflections. This approach simplified the measurements, provided consistent locations for deflection data, and allowed measurement of either positive or negative deflections.

Analytical Approach

Analysis of the subsize panel tests was accomplished through the use of a computer program developed for creep analysis. This computer program referred to as TPSC (Thermal Protection System Creep), uses iterative techniques and numerical integration to predict creep strains, residual stresses, and permanent deflection, due to creep, in stiffened panel structures subjected to bending loads.

A flexible user oriented input format is used. Input includes geometry and definition of loading and temperature profiles. Panel temperature can be varied both along the panel length and through the depth by either polynominal equation coefficients or tabular input. Temperatures at each panel location are based on these distributions and the input temperature time profile data. Also input equation coefficients to define material creep response. Appropriate creep strain response data are based on temperatures at each location in the panel.

Program output includes a record of geometry input and calculated geometrical data (moment of inertia), trajectory load and temperature data, and creep equation definition. Calculated deflections, creep strains, and residual stresses are output at desired times specified by the program user.

The program was developed specifically for analysis of thermal protection system panels. Therefore, structural definition of leading candidates, such as corrugation stiffened, rib stiffened, and zee stiffened concepts, is incorporated into the TPSC program. Modeling of the specific panel structural concept for analysis is accomplished automatically, based on overall section input definition. An option is provided for including a beaded skin into any of the cross sections since beads are frequently required in thermal protection system panel designs.

Bending moments along the panel length are computed based on a uniform pressure load input or two point load input. In addition, the moments can be calculated as a function of panel edge support stiffness and the ratio of panel stiffness in the longitudinal and transverse directions. This option is based on combining solutions for an isotropic plate with two sides simply supported and two sides elastically supported as offered by Timoshenko (15) and the solution for an orthotropic plate with four sides simply supported as offered by Lekhnitskii (16). This option provides a first order approach to account for Poisson's effects in orthotropic plate structures.

Within the TPSC program, the panel length is divided into stations over which bending moments are assumed constant and the panel depth is divided into elements over which stresses and strains are assumed constant. At each station and analysis time step, the neutral axis and structural rotation are systematically varied to determine the stress distribution which satisfies both force and moment balance requirements. At each point in the panel the creep component of total strain is based on either the time hardening or strain hardening theory of creep accumulation applied in conjunction with input analytical expressions defining material tensile creep response as a function of stress, temperature, and time. Residual stresses are calculated at each time step by subtracting the elastic stress from the total calculated stress. These residual stresses are used at initiation of analysis for the next time step. Analysis proceeds through all the time steps at each designated station along the panel accumulating and storing structural rotations, creep strains, and residual stresses. At the completion of analysis, rotations are numerically integrated to determine creep deflections. The flow diagram for the analysis presented in Figure 45 provides a reference for the analysis description.

Results and Discussion

Test results for the six L605, three Rene' 41, six titanium, and two TDNiCr subsize panels tested in Phase II are presented in Tables 7 through 10. Predictions for each test made, using the approach incorporated into the TPSC program, are also shown in the tables. Two L605, two Rene' 41, three Ti-6Al-4V, and one TDNiCr subsize panels were tested to the profile shown in Figure 39(a). The remainder of the panels (four L605, one Rene' 41, and one TDNiCr, three Ti-6Al-4V) were tested to the mission profile shown in Figure 39(b). All panels were tested in positive bending (skin in compression) with the exception of one negative bending test of a rib stiffened L605 panel. Plots of panel deflected shapes, midspan deflections as a function of cycle and associated predictions will be presented for typical panels in this section. More comprehensive data including photographs, trajectory data, and deflection data are presented in the Phase II Summary Report (Reference 2).
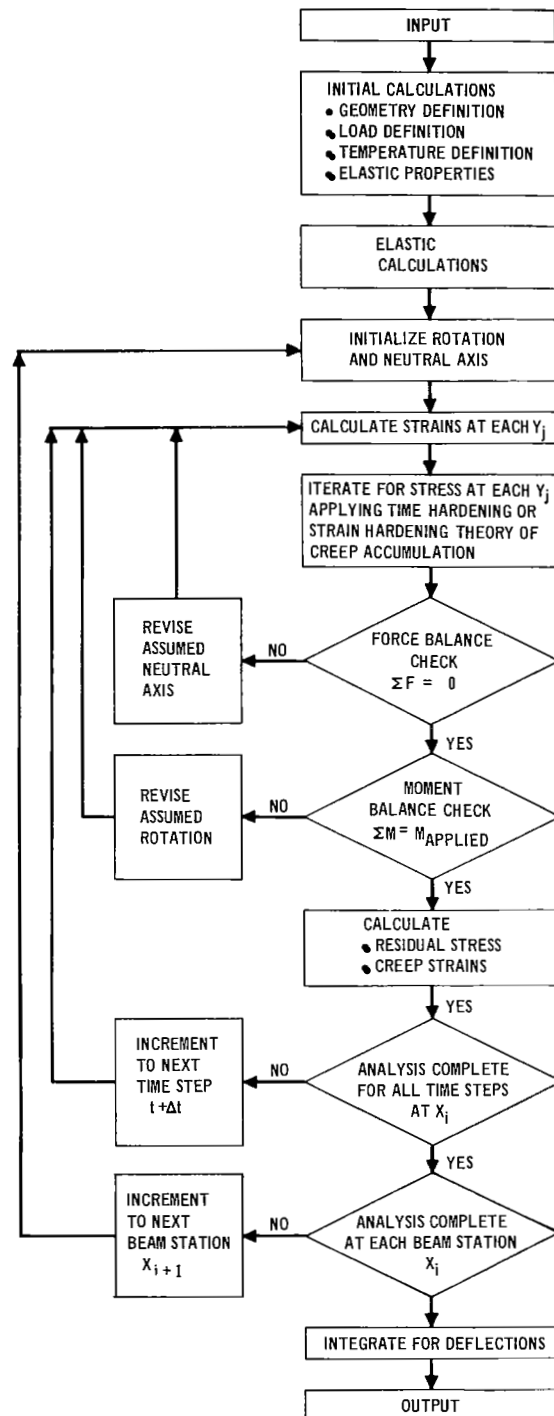
FIGURE 45 ANALYSIS FLOW

It is difficult to determine to what extent each analytical assumption and test parameter influences the predictive capability of the TPSC program. Additionally, during tensile testing (Reference 1) several factors were identified which can affect panel creep deflections. These include the applicability of empirical equations, based on regression analysis of tensile creep data, and the applicability of strain hardening or time hardening theories of creep accumulation. Atmospheric pressure and material recovery phenomena, not accounted for by either the empirical equations or hardening approaches, may also be important. Resulting predictions of cyclic creep deflection have been shown to be sensitive to both stress level and temperature. Such factors as overshoot in temperature for only one cycle or a few cycles could significantly increase the total test deflections.

Review of subsize panel test results and associated predictions revealed two trends. First, for tests to similar cyclic profiles, the thinner gage corrugation stiffened panels exhibited larger deflections, relative to predictions, than the thicker gage rib stiffened panels. Secondly, panels tested applying mission temperature and load profiles exhibited larger deflections, relative to predictions, than similar panels tested applying constant temperature and load cycle profiles. The shape of the predicted deflection-time curves relative to subsize panel test results, in most cases, was found to be similar to the relation between the shape of the predicted tensile strain-time curves (based on the empirical equations derived) and the Phase I tensile creep data. This is indicative that panel deflection predictions can only be as good as the empirical equations (representing the material creep response) upon which the predictions are based.

No relation could be found between stress levels, as a percentage of yield strength or crippling strength, and the prediction capability. A summary of panel stress levels as percentages of the skin crippling stress and as a percentage of material yield strength is provided in Table 6. However, it is reasonable to expect that test deflections for thinner gage panels might be higher than predicted because less section area is effective in carrying the bending load. Therefore, higher stresses, causing greater creep strain, may occur.

L605 Subsize Panel Results

Four single skin corrugation and two rib-stiffened subsize L605 panels were tested as outlined in Table 7. Test temperatures were selected to be the same as those used in testing tensile creep specimens in Phase I of the program.

Predicted deflections, as a function of cycle, for the L605 subsize panels tended to be lower than test values for approximately 15 cycles and then increase to higher than test values by the conclusion of the test. This same trend was noted in the comparison of tensile creep data and empirical equation predictions.

Predicted panel creep deflections obtained using the time hardening theory of creep accumulation were found to generally yield the best predictions. Predictions obtained applying the strain hardening theory of creep accumulation were found to be approximately twice those using time hardening. Predicted variations in deflections due to approximately $\pm 1\%$ ($10°K$ at $1255K$) variation in test temperature are significant.

53

TABLE 6 PANEL TEST STRESS SUMMARY

TEST	PANEL CONCEPT	SECTION GEOMETRY (cm)	TEST TRAJECTORY	SKIN STRESS (COMPRESSION)		% OF SKIN CRIPPLING STRESS		MAX. FIBER STRESS (TENSION)		% OF YIELD STRESS	
				HIGH TEMP. COND.	LOW TEMP. COND.	HIGH TEMP. COND.	LOW TEMP. COND.	HIGH TEMP. COND.	LOW TEMP. COND.	HIGH TEMP. COND.	LOW TEMP. COND.
L605-21 L605-24	Corrugation	Depth = 1.321 Gage = .025 $\bar{Y}$ = .904	Mission Profile	(T = 1200 K) 25.2 MPa	(T = 950 K) 60.3 MPa	32	52	54.8 MPa	131.0 MPa	34	67
L605-22	Corrugation	Depth = 1.321 Gage = .025 $\bar{Y}$ = .904	Constant	(T = 1256 K) 16.1 MPa		24		35.2 MPa		27	
L605-23	Corrugation	Depth = 1.321 Gage = .025 $\bar{Y}$ = .904	Constant	(T = 1053 K) 53.4 MPa		51		115.8 MPa		60	
L605-25 L605-26	Rib	Depth = 1.105 Gage = .064 $\bar{Y}$ = .881	Mission Profile	(T = 1200 K) 17.2 MPa	(T = 950 K) 41.0 MPa	13	20	67.6 MPa	162.0 MPa	42	82
RENE-21	Corrugation	Depth = 1.270 Gage = .028 $\bar{Y}$ = .836	Mission Profile	(T = 1169 K) 32.8 MPa	(T = 940 K) 78.6 MPa	22	24	63.1 MPa	151.0 MPa	20	18
RENE-22	Corrugation	Depth = 1.270 Gage = .028 $\bar{Y}$ = .836	Constant	(T = 1111 K) 95.2 MPa		44		183.4 MPa		36	
RENE-23	Corrugation	Depth = 1.219 Gage = .028 $\bar{Y}$ = .836	Constant	(T = 1111 K) 118.6 MPa		54		228.2 MPa		46	
Ti-22	Corrugation	Depth = 1.321 Gage = .033 $\bar{Y}$ = .859	Constant	(T = 783 K) 52.0 MPa		27		96.5 MPa		21	
Ti-23 Ti-24	Corrugation	Depth = 1.270 Gage = .033 $\bar{Y}$ = .859	Mission Profile	(T = 783 K) 39.6 MPa	(T = 658 K) 94.5 MPa	21	40	73.8 MPa	175.1 MPa	16	31
Ti-25	Rib	Depth = 1.092 Gage = .056 $\bar{Y}$ = .884	Mission Profile	(T = 783 K) 23.1 MPa	(T = 658 K) 55.2 MPa	10	20	97.9 MPa	233.7 MPa	22	42
Ti-26	Rib	Depth = 1.092 Gage = .056 $\bar{Y}$ = .884	Constant	(T = 714 K) 97.2 MPa		36		413.7 MPa		80	
TDNiG-21	Corrugation	Depth = 1.219 Gage = .025 $\bar{Y}$ = .851	Constant	(T = 1478 K) 20.2 MPa		53		42.4 MPa		77	
TDNiG-22	Corrugation	Depth = 1.245 Gage = .025 $\bar{Y}$ = .848	Mission Profile	(T = 1478 K) 10.2 MPa	(T = 1144 K) 24.4 MPa	27	30	21.8 MPa	52.4 MPa	40	38

TABLE 7 L605 SUBSIZE PANEL TEST SUMMARY

| TEST | PANEL SPECIMEN | | PROFILES | PEAK LOAD (P) | | PEAK TEMPERATURE | | CYCLES | FINAL MIDSPAN CREEP DEFLECTION (PREDICTION) | |
| | DESIGNATION | CONFIGURATION | | | | | | | | |
				LBS.	Ka.	°F	K		IN.	CM.
L605–21	L1	CORRUGATION	MISSION (FIG. 44b)	74.3	33.7	1700.	1200.	100	.2259	0.5738 (REF FIG 46)
L605–22	L2	CORRUGATION	CONSTANT (FIG. 44a)	19.8	8.98	1800.	1255.	50	0.9775 (0.10)	0.1969 (0.24)
L605–23	L3	CORRUGATION	CONSTANT (FIG. 44a)	65.7/ 79.6	29.8/ 36.1	1435.	1053.	100	0.1551 (0.23)	0.3940 (0.59)
L605–24	L4	CORRUGATION	MISSION (FIG. 44b)	74.4	33.7	1700.	1200.	50	0.1408 (0.15)	0.3576 (0.39)
L605–25	L6	RIB	MISSION (FIG. 44b)	52.8	24.0	1700.	1200.	50	0.1273 (0.17)	0.3233 (0.42)
L605–26	L7	RIB	MISSION (FIG. 44b)	−52.9	24.0	1700.	1200.	50	−0.1162 (−0.17)	−0.2951 (−0.42)

A uniform green oxide coating was observed on all the L605 panel specimens tested. These coatings ranged from light to dark green, depending on the test temperature and atmospheric pressure. No skin waviness could be detected in the L605 panel specimens.

L605 single skin corrugation stiffened panels L1 and L4 were tested to replicate mission profiles in tests L605-21 and L605-24, respectively. For analysis purposes the beam load profile (P) and temperature load profile (T), shown in Figure 44, were idealized into four steps (Reference 2). These load and temperature steps were applied in sequence in the analysis using the L605 empirical cyclic creep equation (Table 5) in conjunction with the time harden- ing theory of creep accumulation. Shown in Figure 46 are comparisons of mid- span predicted and test creep deflections as a function of cycle and deflec- tions as a function of panel length at 50 cycles.

L605 single skin corrugation stiffened panel L2 was tested to the twenty minute constant panel load (8.98 kg) and constant temperature (1255K) cycle profiles as shown in Figure 47(a). For analysis purposes these twenty-minute load and temperature steps were applied sequentially using the TPSC program. Comparison of predicted deflections at 1255K, with test results, are presented in Figure 47(b) and (c), showing creep deflections along the panel length at 50 cycles and midspan deflections as a function of cycle. Midspan deflections as a function of cycle are also shown as predicted using the strain hardening theory of creep accumulation. As indicated previously, the resulting predic- tions using strain hardening are approximately twice those obtained using time hardening. This result is typical for all the L605 panel tests. Also shown in the figure are the predicted variations in deflections based on the ±1% (10°F @ 1255K) test temperature variations. This result will also be typical for the L605 panel tests.
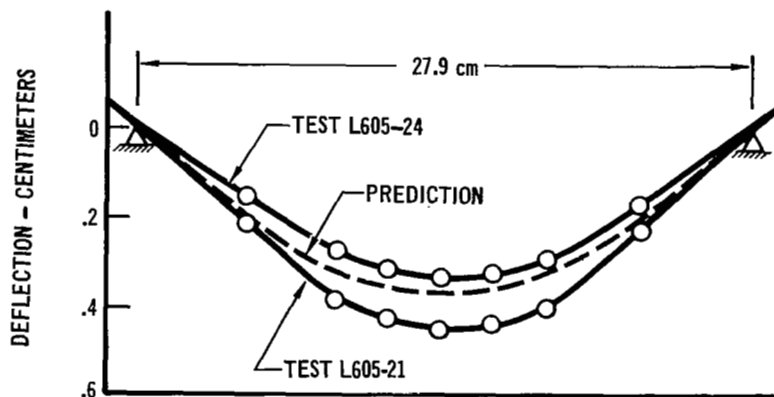
(a) Creep Deflection vs Beam Length at 50 Cycles
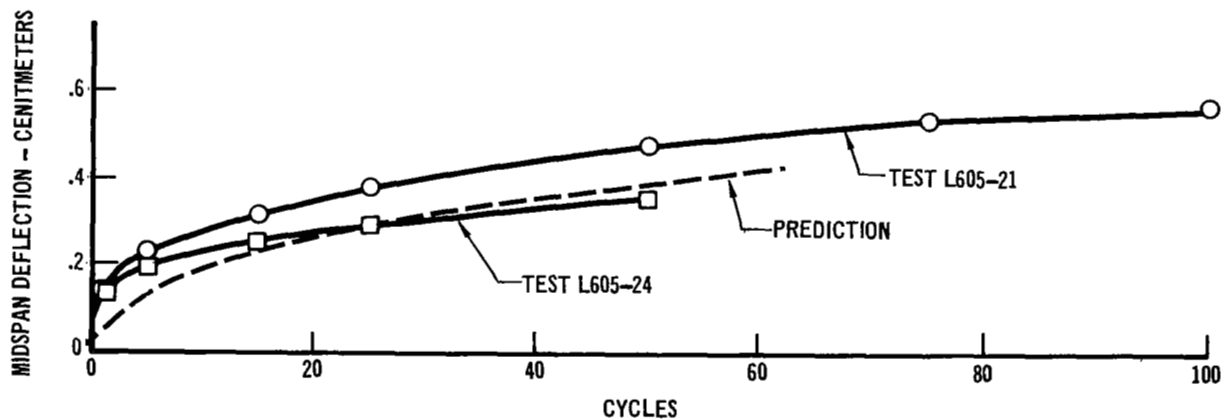
(b) Panel Midspan Creep Deflection

FIGURE 46 COMPARISON OF PREDICTED CREEP DEFLECTIONS WITH RESULTS
OF CORRUGATION PANEL TESTS L605–21 AND L605–24

(a) Test Profiles

(b) Creep Deflection vs Beam Length at 50 Cycles

(c) Panel Midspan Creep Deflection

FIGURE 47   COMPARISON OF PREDICTED CREEP DEFLECTION WITH RESULTS
OF CORRUGATION PANEL TEST L605—22

L605 rib stiffened panels L6 and L7 were tested to 50 replicate mission profiles in tests L605-25 and L605-26, respectively. Comparison of predicted midspan deflections with test values for these two panels is shown in Figure 48. Because the rib panel gage was .064 cm while the equation used in analysis is based on .025 cm gage specimen tests, the material gage effect identified in Phase I was accounted for in the analysis. Therefore, the predicted deflection shown is based on the L605 empirical creep equation, modified to reflect this gage effect. This was accomplished by using the average ratio of .064 cm gage creep strains to .025 cm gage creep strains at 26 hours (50 cycles) from the Phase I tensile test data (Reference 2). This average ratio of .62 changed the constant in the empirical equation (Table 5) from -.3645 to -.8425 for use in the analysis.
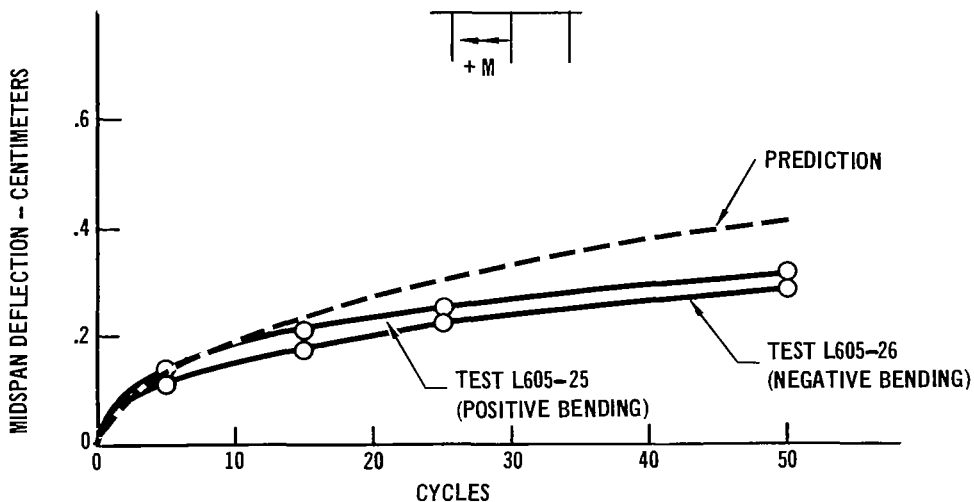
FIGURE 48 COMPARISON OF PREDICTED CREEP DEFLECTIONS WITH
RESULTS OF RIB PANEL TESTS L605-25 AND L605-26

Rene' 41 Subsize Panel Results

Three single skin corrugation subsize Rene' 41 panels were tested as outlined in Table 8.

All panels were tested in positive bending (skin in compression). Test temperatures were selected to be the same as those used in tests of tensile creep specimens in Phase I of the program. Because the 50 cycle creep strains obtained in Phase I at 1111K (1540°F) were only up to approximately .2%, a lower panel deflection of approximately .25 cm (.1 inch) was used to select test load level.

Predicted deflections for the Rene' 41 panels were not as close to test values as had been demonstrated in the case of L605. However, results were generally consistent with Rene' 41 cyclic tensile creep test data obtained in Phase I. As in the case of Phase I analysis results, the time hardening theory of creep accumulation provided the best deflection predictions, although these Predictions were lower than test data for the mission profile and higher than test data for the constant load and temperature profiles. A study conducted

to show the effect of temperature variation on Rene' creep deflections indicated that a temperature variation of approximately 1% (8°K at 1100K). resulted in a creep deflection variation of approximately 25%. Uniform oxide coatings were evident on the specimens and slight waviness of the panel skins occurred.

TABLE 8 RENE'41 SUBSIZE PANEL TEST SUMMARY

TEST	PANEL SPECIMEN		PROFILES	PEAK LOAD (P)		PEAK TEMPERATURE		CYCLES	FINAL MIDSPAN CREEP DEFLECTION (PREDICTION)	
	DESIGNATION	CONFIGURATION								
				LBS.	K_g	°F	K		IN.	CM.
RENE'-21	R1	CORRUGATION	MISSION (FIG 44b)	84.2	37.4	1645.	1169.	100	.1249	.3172 (REF FIG 49)
RENE'-22	R2	CORRUGATION	CONSTANT (FIG. 44a)	99.7	45.2	1540.	1111.	50	.0689 (.16)	.1750 (.40)
RENE'-23	R3	CORRUGATION	CONSTANT (FIG. 44a)	127.7	56.6	1540.	1111.	50	.1729 (.36)	.4392 (.92)

Single skin corrugation stiffened subsize panel R1 was tested to mission temperature and load profiles in test Rene-21. For analysis purposes these profiles were idealized into four steps for application in conjunction with the Rene' 41 empirical cyclic creep equation (Table 5). Presented in Figure 49 are comparisons of predicted and test midspan creep deflections as a function of cycle and deflections as a function of panel length at 50 cycles. Predictions are plotted to 60 cycles in Figure 49(b). This represents approximately the same limit of applicability of the Rene' 41 empirical equation. Beyond this time predictions increase rapidly due to the t^3 term in the equation. Both the time hardening and strain hardening theories of creep accumulation yield comparable deflection predictions with the time hardening theory 27% below the test value and strain hardening theory 35% above the test value at 50 cycles. The effect of temperature distribution and temperature levels on panel deflection predictions will be considered in the analysis of subsize panel test Rene-22.

Rene' 41 single skin corrugation stiffened panels R2 and R3 were tested to constant panel load and temperature profiles in tests Rene-22 and Rene-23, respectively. Applied loads were 45.2 kg (99.7 lbs) and 56.6 kg (127.7 lbs), respectively, for the two panels over the twenty-minute cycle time as shown in Figures 50(a) and 51(a). Temperature in both tests was 1111K (1540°F). Panel outer fiber stress levels obtained in the test were 165 MPa (23.7 ksi) and 224 MPa (32.5 ksi), respectively. Both of these stress levels were above the 104.1 MPa stress level tested to at 1111K in developing the empirical creep equation during Phase I (reference Figure 17). However, these loads were applied to attain reasonable creep deflections. Comparison of predicted midspan creep deflections as a function of cycle are presented in Figure 50(b). Predictions based on the strain hardening theory of creep accumulation were again higher than those based on time hardening, as shown in the figure.
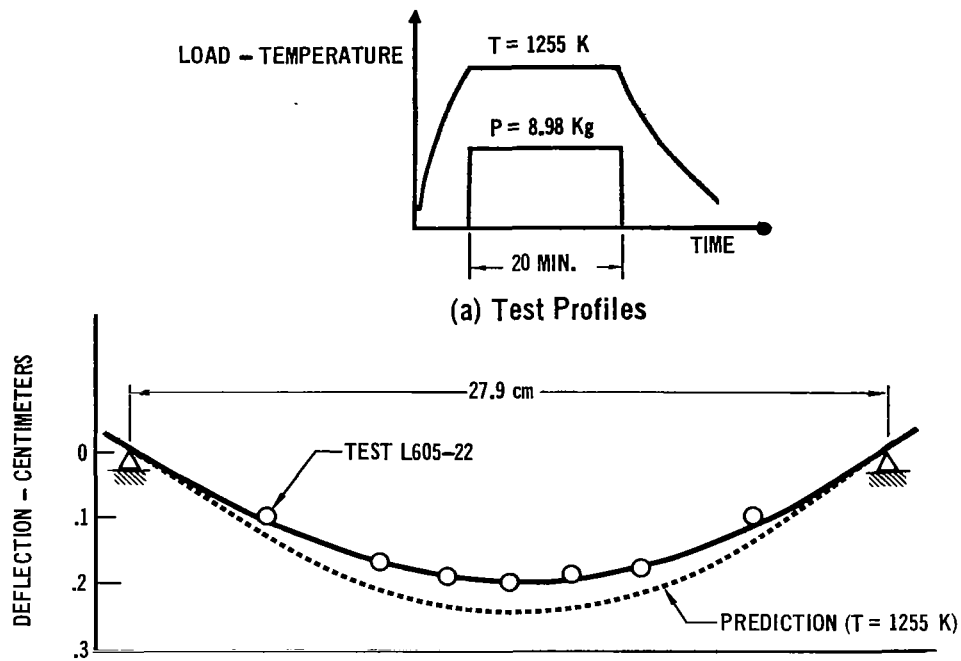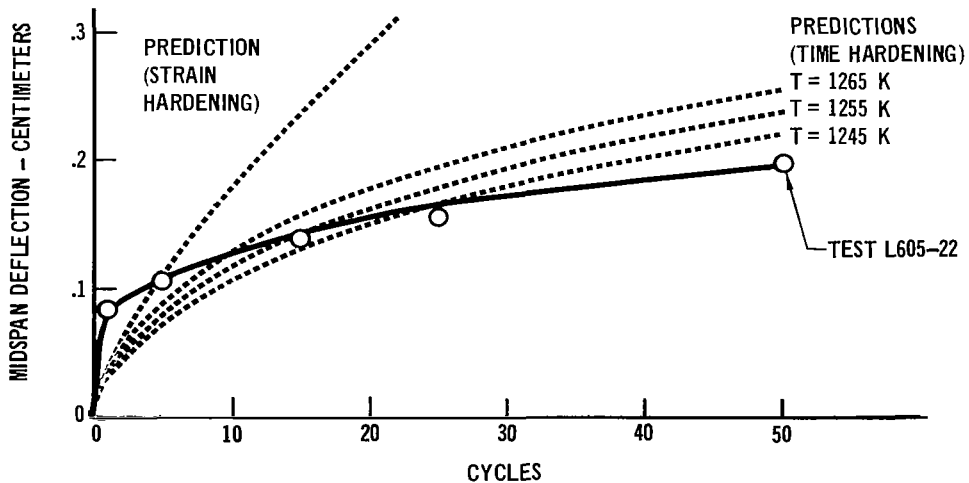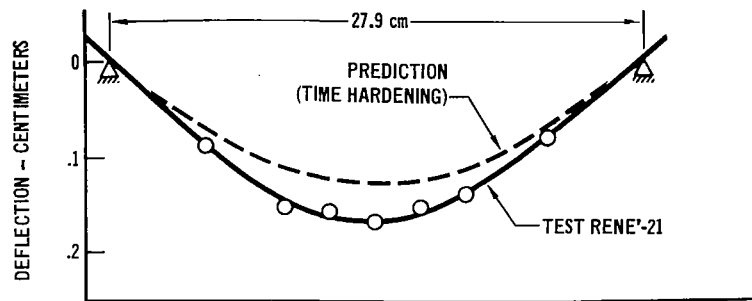
(a) Creep Deflection vs Beam Length at 50 Cycles
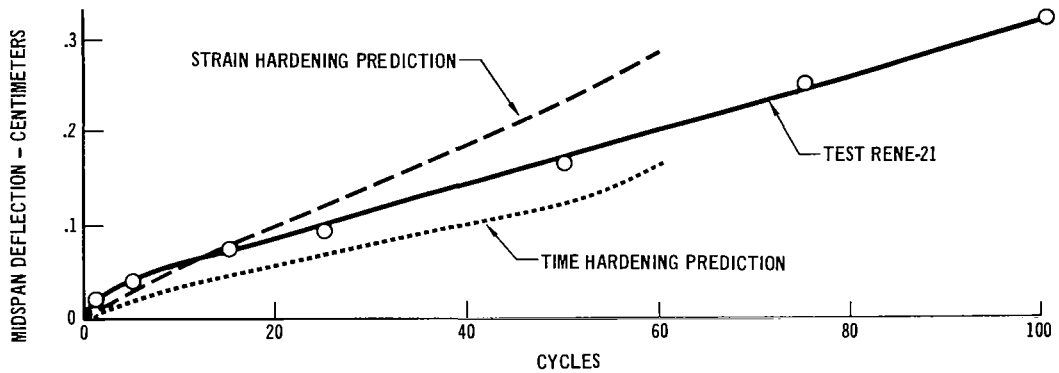
(b) Panel Midspan Creep Deflection

FIGURE 49 COMPARISON OF PREDICTED CREEP DEFLECTIONS WITH
RESULTS OF CORRUGATION STIFFENED PANEL TEST RENE-21

(a) Test Profiles
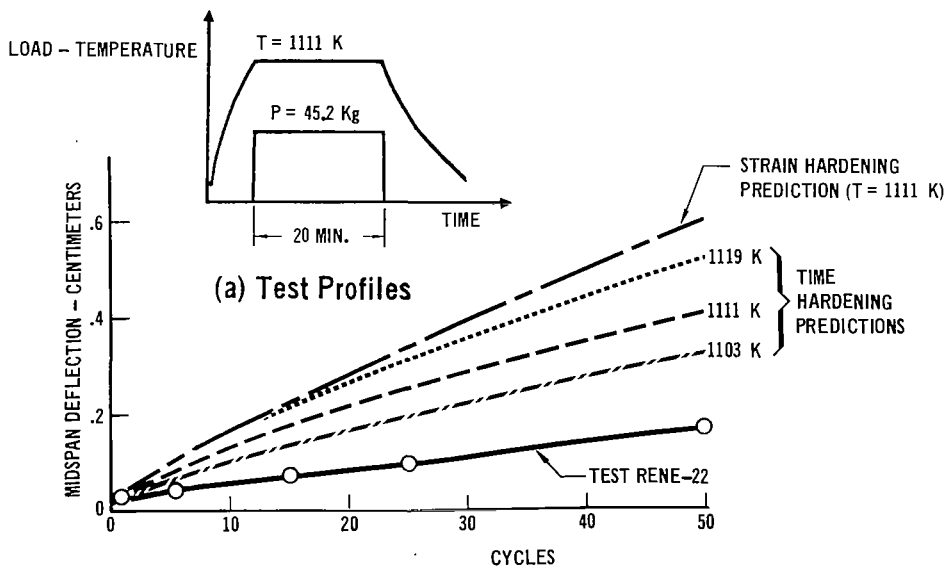
(b) Panel Midspan Creep Reflection

FIGURE 50 COMPARISON OF PREDICTED CREEP DEFLECTIONS WITH
RESULTS OF CORRUGATION STIFFENED PANEL TEST RENE-22.

(a) Test Profiles

(b) Creep Deflection vs Beam Length at 100 Cycles

(c) Midspan Panel Deflections
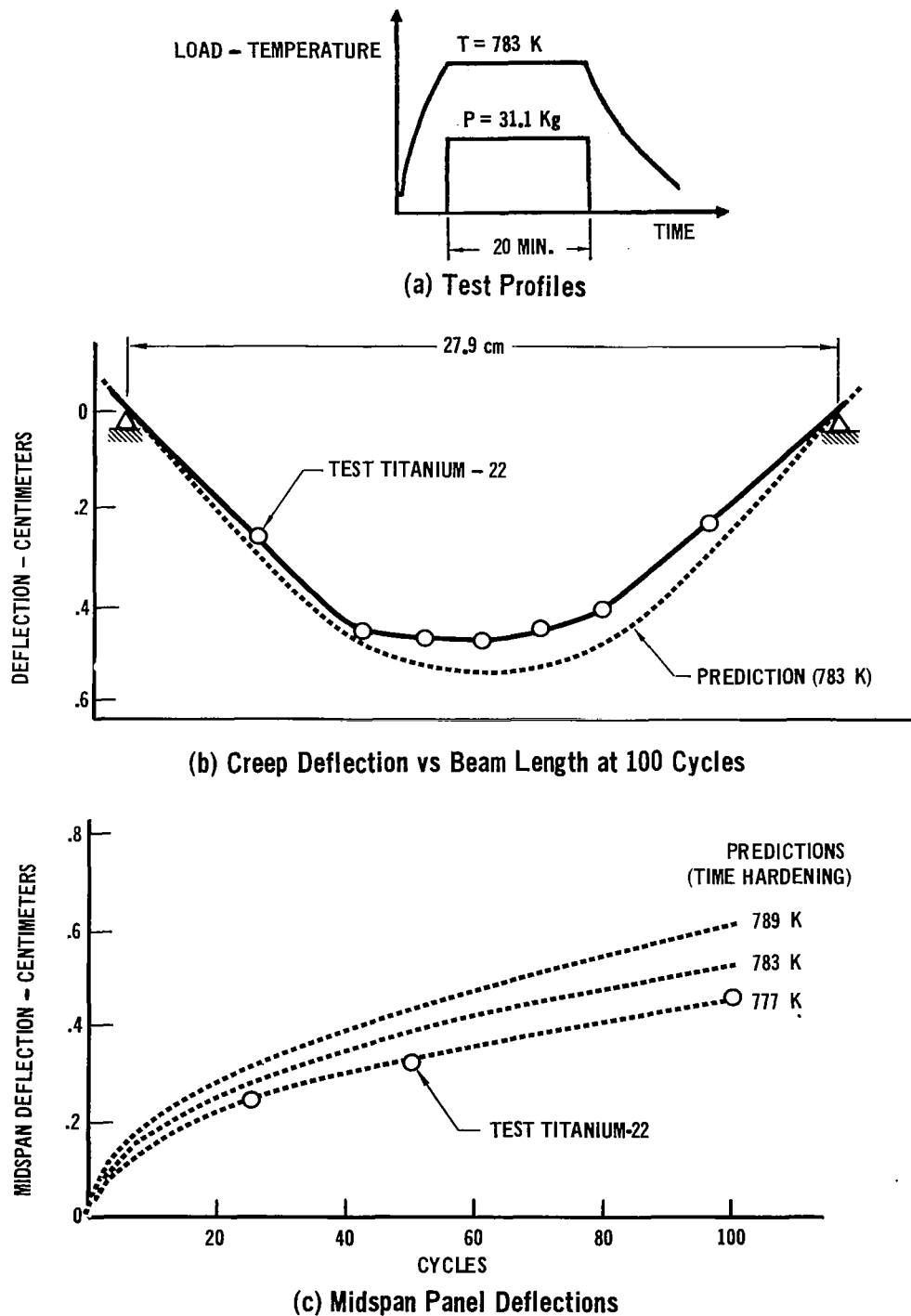
FIGURE 51 COMPARISON OF PREDICTED CREEP DEFLECTIONS WITH RESULTS
OF CORRUGATION STIFFENED PANEL TEST TITANIUM – 22.

61

In the analysis of subsize panel test Rene-22, studies were conducted on the effect of temperature level and distribution on predicted deflections. Results are shown in Figure 50(b) for the peak midspan temperature of 1111K and for +1% (+15°F ∿ +8°K) temperature variation based on furnace limitations. Each of these lines of predicted deflections is based on analysis using the measured panel temperature distributions along the panel length (Reference 2). The case of a constant 1111K temperature along the panel length was also analyzed. This resulted in a midspan 50 cycle creep deflection of .485 cm (.191 inch) as compared to the .424 cm (.167 inch) deflection when the panel temperature distribution was applied (Figure 50). This study demonstrates the sensitivity of Rene '41 panel creep deflections to temperature used in the predictions.

Ti-6Al-4V Subsize Panel Results

Four single skin corrugation and two rib-stiffened subsize Ti-6Al-4V panels were tested as outlined in Table 9. All panels were tested in positive bending (skin in compression).

TABLE 9 Ti-6Al-4V SUBSIZE PANEL TEST SUMMARY

| TEST | PANEL SPECIMEN | | | PEAK LOAD (P) | | PEAK TEMPERATURE | | CYCLES | FINAL MIDSPAN CREEP DEFLECTION (PREDICTION) | |
| | DESIGNATION | CONFIGURATION | PROFILES | | | | | | | |
				LBS.	Kg	°F	K		IN.	CM.
TITANIUM-21	T1	CORRUGATION	CONSTANT (FIG. 44a)	94.7	43.0	950.	783.	50	.2283 –	.5799 –
TITANIUM-22	T2	CORRUGATION	CONSTANT (FIG. 44a)	68.6	31.1	950.	783	100	.1856 (.21)	.4714 (.53)
TITANIUM-23	T3	CORRUGATION	PROFILE (FIG. 44b)	127.2	57.7	950.	783.	100	.1162 (.075)	.2951 (.19)
TITANIUM-24	T4	CORRUGATION	PROFILE (FIG. 44b)	126.9	57.6	950.	783.	50	.0922 (.06)	.2342 (.15)
TITANIUM-25	T7	RIB	PROFILE (FIG. 44b)	66.8	30.3	950.	783.	50	.0803 (.08)	.2040 (.20)
TITANIUM-26	T8	RIB	CONSTANT (FIG. 44a)	114.1	51.8	825.	714.	50	.1005 (.20)	.2563 (.52)

The first titanium panel tested (corrugation stiffened panel T1, Reference Table 9) was loaded to a calculated skin stress of approximately 69 MPa (10 ksi) which was 38% of the calculated skin crippling allowable stress. Wrinkles in the skin were noted after twenty-five test cycles and increased after fifty test cycles. Therefore, this test was suspended at the completion of fifty cycles. Because of this skin buckling, loads in subsequent tests of titanium panels were reduced and only a very slight skin waviness could be detected in titanium tests 22, 23 and 24. No apparent reason for the occurrence of the titanium panel skin waviness was found. However, investigation of the Phase I tensile creep data reveals the creep strain-stress relationship to be more linear than that obtained for L605. Therefore, the preliminary approach for

establishing test loads required was modified from that discussed earlier in this section to a more linear relationship between creep deflection and elastic deflections.

Analysis of Ti-6Al-4V panels was made using the time hardening theory of creep accumulation in conjunction with the titanium empirical creep strain equation (Table 5). Predictions based on the strain hardening theory of creep accumulation were significantly higher ($\sim$ 80%) than those based on time hardening The shape of predicted deflection curves as a function of time (or cycle) were in good agreement with the test data which is consistent with the prediction capability of the empirical equation. The resulting creep deflection variation of approximately 2% per °K again demonstrates the sensitivity of creep deflections to temperature. Oxide coatings were obtained on all of the titanium panels tested. These oxides ranged in color from purple-gold to a silvery blue for the individual specimens (Reference 2).

Titanium single skin corrugation stiffened panels T1 and T2 were tested to constant panel load and temperature profiles in tests Titanium-21 and Titanium-22, respectively. Applied loads were 43.0 kg (94.7 lbs) and 31.1 kg (68.6 lbs). The temperature was 783°K (950°F) for both tests over the twenty-minute cycle time. Because of the skin buckling which occurred in test Titanium-21 (Reference 2), no creep deflection analysis was conducted. Comparison of predicted creep deflections with data obtained in test Titanium-22 are, however, shown in Figure 51, based on time hardening. Also presented are the effects of applying $\pm 1\%$ ($\pm 10°F \sim 6°K$) temperature variation in the analysis, again demonstrating the sensitivity of creep deflections to temperature.

Titanium rib stiffened subsize panel T7 was also tested to mission load and temperature profiles, in test Titanium-25. Good agreement was obtained between test deflections and predictions based on time hardening. These deflections are presented in Figure 52.

Titanium rib-stiffened subsize panel T8 was tested to the constant load (51.8 kg) and temperature (714°K) profiles shown in Figure 53(a). Comparison of predicted and test deflections for this panel are presented in Figure 53(b) and (c). Predicted deflections as a function of cycle are shown for both time hardening and strain hardening theories of creep accumulation.

TDNiCr Subsize Panel Results

Two single skin corrugation TDNiCr subsize panels were tested as outlined in Table 10. Both panels were tested in positive bending (skin in compression).

A peak temperature of 1478°K (2200°F) was used in testing to agree with tensile creep tests conducted during Phase I. During Phase I it was noted that because TDNiCr exhibited very low creep strains before failure occurred, creep deflections should not be a designing criteria for thermal protection system panels fabricated of this material. Therefore, additional emphasis was placed on obtaining stress-temperature data where failures occurred. Test load levels for the subsize panels were therefore selected to be less than those at which panel failures would occur and very little panel creep deflection was expected.
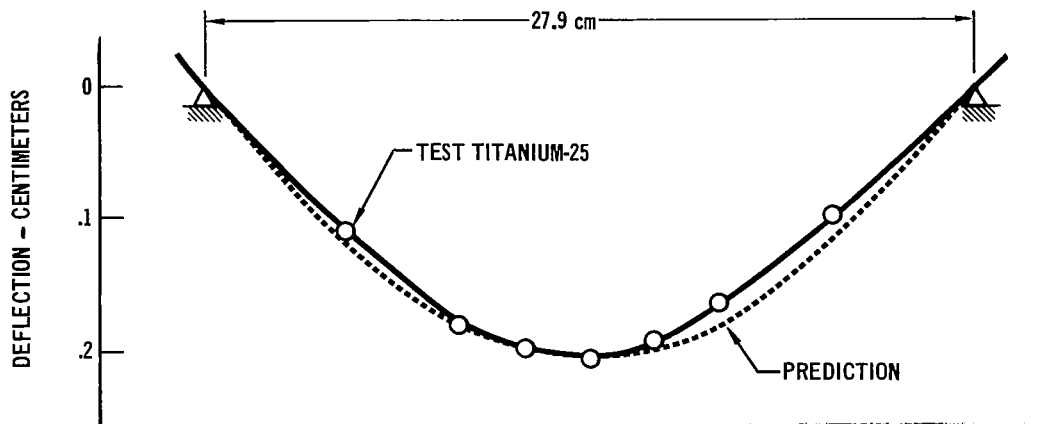
(a) Creep Deflection vs Beam Length at 50 Cycles
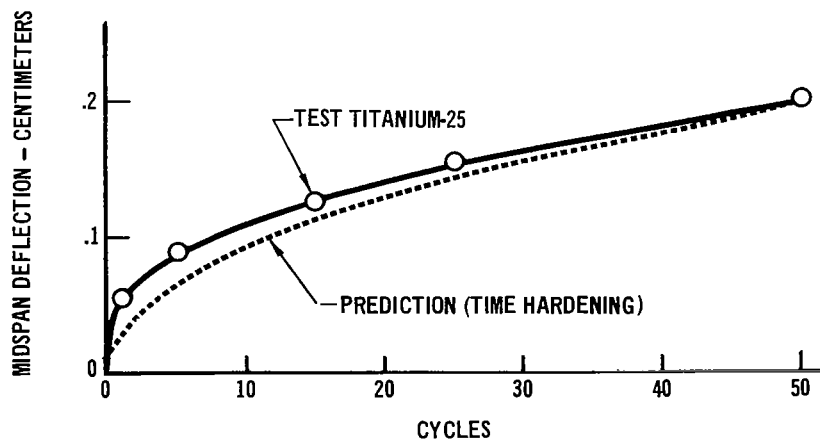
(b) Midspan Panel Deflections

FIGURE 52   COMPARISON OF PREDICTED CREEP DEFLECTIONS WITH
RESULTS OF RIB STIFFENED PANEL TEST TITANIUM-25
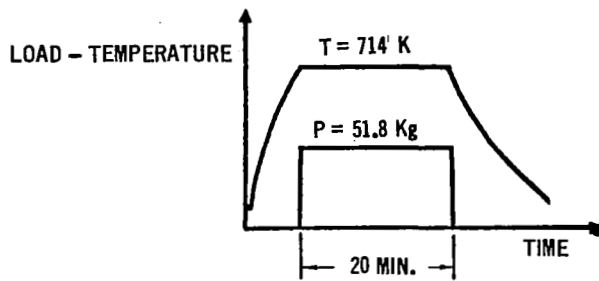
(a) Test Profiles
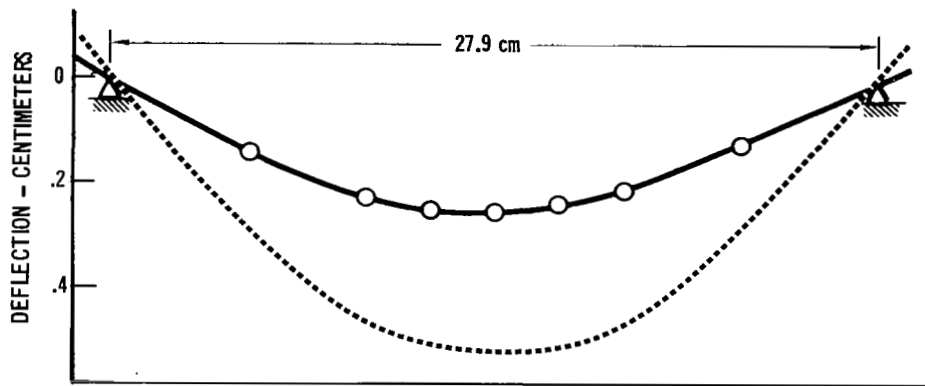
(b) Creep Deflection vs Beam Length at 50 Cycles
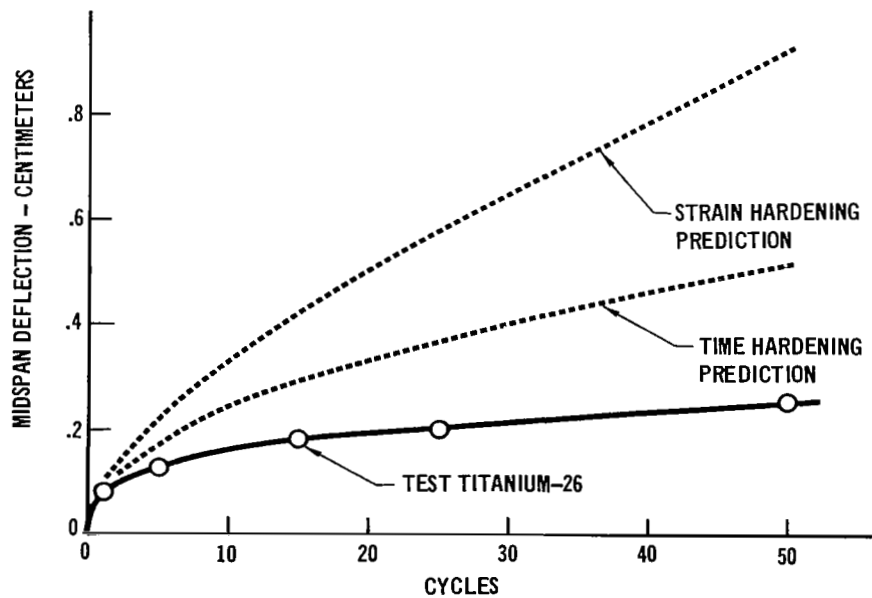
(c) Midspan Panel Deflections

FIGURE 53 COMPARISON OF PREDICTED CREEP DEFLECTIONS WITH RESULTS
OF RIB STIFFENED PANEL TEST TITANIUM-26

TABLE 10 TDNiCr SUBSIZE PANEL TEST SUMMARY

TEST	PANEL SPECIMEN		PROFILES	PEAK LOAD (P)		PEAK TEMPERATURE		CYCLES	FINAL MIDSPAN CREEP DEFLECTION (PREDICTION)	
	DESIGNATION	CONFIGURATION		LBS.	Kg	°F	K		IN.	CM.
TDNiCr-21	TD1	CORRUGATION	CONSTANT (FIG. 44a)	22.7	10.3	2200.	1478.	50	.0154 (.027)	.0391 (.069)
TDNiCr-22	TD2	CORRUGATION	MISSION (FIG. 44b)	26.3	11.9	2200.	1478.	100	.0225 (.010)	.0572 (.024)

Some inconsistency resulted in comparison of prediction with test deflections for the TDNiCr panels. The time hardening prediction obtained for the panel tested to a mission load and temperature profile was approximately 50% of the test value. This was consistent with results from the Phase I tensile tests. However, predictions for the constant load and temperature test panel were twice the test values.

Comparison of test and predicted deflections for TDNiCr-21 is shown in Figure 54. Also shown with the prediction for test TDNiCr-21 is the effect of a $\pm$1% (22°F $\sim$ 12°K) temperature variation. Predicted deflections using the strain hardening theory of creep accumulation were found to be approximately twice those based on time hardening. The time hardening prediction obtained for mission profile test TDNiCr-22 was approximately 50% of test values.

Phase II Conclusions

Many factors influence the creep deflections and predictions, including effects of thin gage sections and the degree to which material creep response can be characterized. It appears, however, that if tensile creep data are available to provide adequate definition of a material's creep response characteristics, then creep deflection predictions can be made in thin gage panel structures subjected to complex cyclic thermal and bending loads. The approach for creep deflection analysis incorporated in the TPSC computer program has been found to yield predicted panel cyclic creep deflections that are generally between half and twice the test deflections. Elastic deflections are predicted within expected numerical accuracy using only a few section elements and beam stations.

The time hardening theory of creep accumulation was generally found to be better than strain hardening in predicting the cyclic test data. However, caution must be used in its application. Much more work needs to be done toward defining material creep accumulation processes since it appears that this could be the most significant limitation to the analysis using the TPSC program.
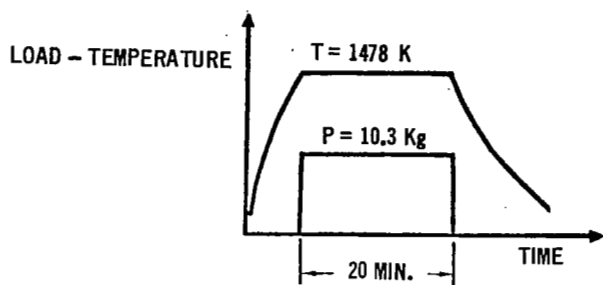
(a) Test Profiles
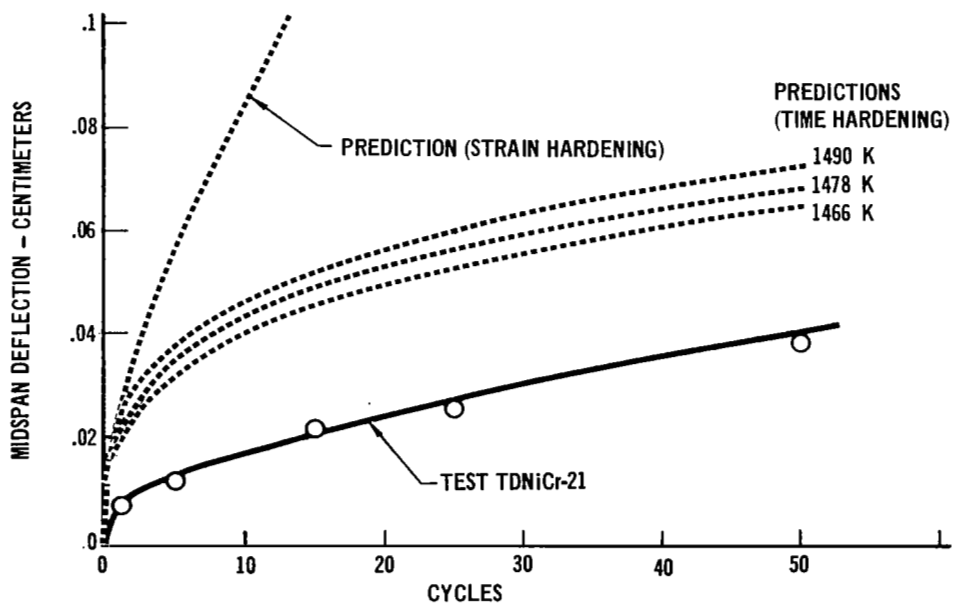
(b) Midspan Panel Deflection

FIGURE 54 COMPARISON OF PREDICTED CREEP DEFLECTIONS WITH RESULTS
OF CORRUGATION STIFFENED PANEL TEST TDNiCr–21

PHASE III - CORRELATION WITH FULL SIZE HEAT SHIELD DATA

In this phase, a comparison of predicted creep deflections with full size panel test deflections was made for L605, Rene' 41 and TDNiCr. Analysis was not performed on Ti-6Al-4V because no test information could be obtained from literature sources during this program.

Comparison of predicted creep deflections with test deflections were made for L605 and Rene' 41 full size panels (Reference 17). Each test assembly consisted of two test panels and smaller side panels to provide proper boundary conditions. The two primary test panels were each 50.8 cm x 50.8 cm. The panels were the same basic design; single faced, corrugation stiffened, with beaded face skins. These panels were fabricated using thin gage (approximately 0.025 cm) sheet material.

Testing (Reference 17) consisted of exposing the structures to repeated cycles of simulated mission environment consisting of ascent pressure, entry pressure and temperature, and cruise pressure. Blocks of these cycles were followed by blocks of acoustic test cycles.

Material cyclic creep response properties developed from the basic cyclic tests in Phase I (Reference 1) were used in the analyses and because the time hardening approach more consistently provided the best predictions of subsize panel data it was used for analysis of full size panel data. For these panels, the plate stiffness correction was negligible and, therefore, was not used. Edge stiffness was minimized in the full size panel tests to simulate as closely as possible actual entry vehicle panel conditions. Analysis of the panels was conducted for the reentry portion of the mission profile. Both pressure and temperature load inputs were based on idealization of the test profiles into discrete time steps.

Resulting predictions for the L605 and Rene' 41 panels, shown in Figure 55, provided a good correlation with test results. For both materials there was approximately a factor of two difference between test deflection results for two identical panels tested simultaneously. No explanation for this difference could be determined from the test data. Predictions for these panels were made at the center, where temperatures were highest. For the L605 panels the predicted center deflections were approximately 20% less than for the test panel which exhibited minimum deflection at the thirty cycle test completion. The prediction for L605 shown in Figure 55 is based on the maximum measured test temperature range at the panel center. Analysis conducted using the minimum value of the temperature range resulted in approximately a 10% lower creep deflection prediction. For the Rene' 41 panels the predicted deflection was very close to the higher of the test deflections at the panel center. Sensitivity of predicted deflections to variations in material gage and test temperature was also demonstrated for these panels. The two curves of highest predicted creep deflection are based on constant peak panel temperatures of 1144K, corresponding to the trajectory test profile temperature, and 1128K, minimum measured panel center temperature. These two analyses show the effect of this temperature variation (16 K) on the predicted creep deflections. Both of these predicted curves are based on skin and corrugation gages of 0.0216 cm and 0.0140 cm, respectively.
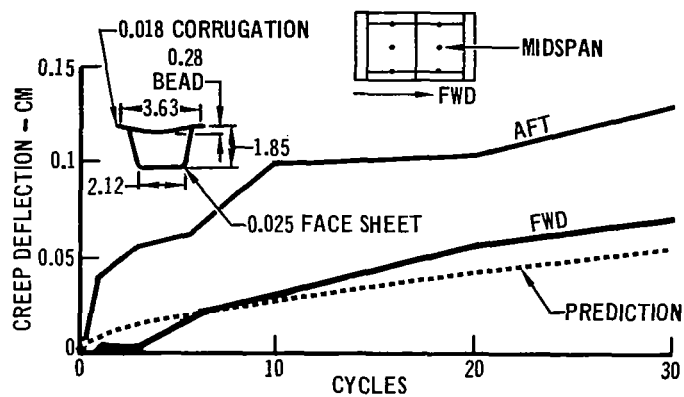
(a) L605 Panel Results
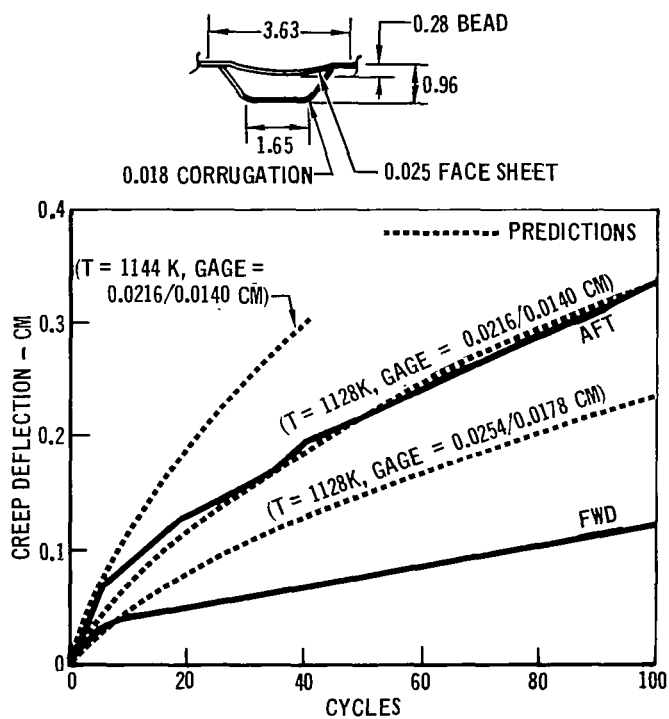
(b) Rene 41 Panel

FIGURE 55 COMPARISON OF FULLSIZE PANEL TEST AND
PREDICTED MIDSPAN CREEP DEFLECTIONS

To demonstrate the effect of gage used in the prediction, a third analysis was conducted using the skin and corrugation gages of 0.0254 cm and 0.0178 cm. A constant temperature of 1128K was applied, allowing comparison with the corresponding predicted deflections calculated for the thinner gages. This comparison was made because structural gage for analysis purpose was not exactly known due to oxidation of the metal and sheet tolerances.

A Haynes 25 (L605) panel, tested by Grumman Aerospace Corporation (References 18 and 19), was also analyzed. The panel tested, designated as panel No. 3 in the references, was segmented into four separate test panels. The cross section geometry was single face corrugation stiffened with a skin bead of approximately 0.25 cm depth. These panels were supported at the ends (simple support assumed for analysis) over an 16.8 inch span and subjected to a uniform pressure profile of 0.093 kg/cm (2.41 kPa) and temperature profiles having a peak of 1255K. Because temperature variations from cycle to cycle were noted to occur, analysis was conducted for two different temperatures based on the idealization shown in Figure 56 for each of the panels for which deflection data were shown in the references.

Comparison of resulting predictions with the Reference 18 experimental data, for the NE and SW panels in Figure 56(a) and 56(b) respectively, show that the experimental deflections are considerably higher than predicted. No explanation of this variation has been determined, although the depth of data reviewed was limited.

The TDNiCr panel data evaluated in this Phase were obtained from Reference 25. The TPS panel tested consisted of a corrugation stiffened TDNi-20 Cr metallic heat shield backed by a flexible fibrous quartz and radiative shield insulation system. The test article represented the intersection of two 50.8 cm square panels. Each panel consists of a beaded 0.025 cm skin and corrugation.

These panels were tested to 90 cycles of combined pressure and temperature loading, simulating critical heating and aerodynamic pressure environments expected during repeated missions of a reentry vehicle. Prior to these 90 cycles, the panels were subjected to 10 cycles of heating conditions only.

Analysis of the corrugation panel geometry under the idealized loads and temperature profiles was conducted using the analytical methods developed in Phase II (Reference 2). Analysis was based on a peak first step temperature of 1478K. Additional analysis conducted at 1489K showed only a 7% increase in predicted creep deflection. The empirical creep strain equation (Table 5) developed in Phase I, was used in the analysis to represent the material creep strain response and the time hardening theory of creep accumulation was applied.

Shown in Figure 57 are comparisons of the predicted creep deflections with measured permanent test deflections. The test deflections are plotted from initiation of the combined load and temperature cycles for four midspan locations. A significant variation is noted in these test data. In the Reference 20 report the variation was attributed to the slightly higher temperature observed at locations A and B. In addition it was noted that there was a significant increase in permanent deflection at locations A and B and a
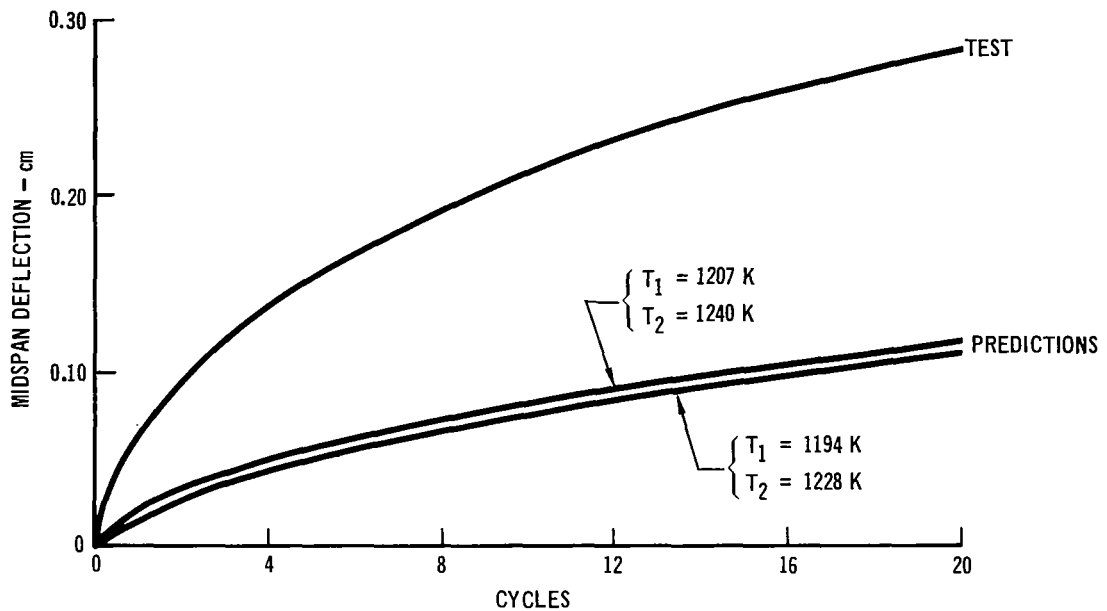
(a) NE Panel
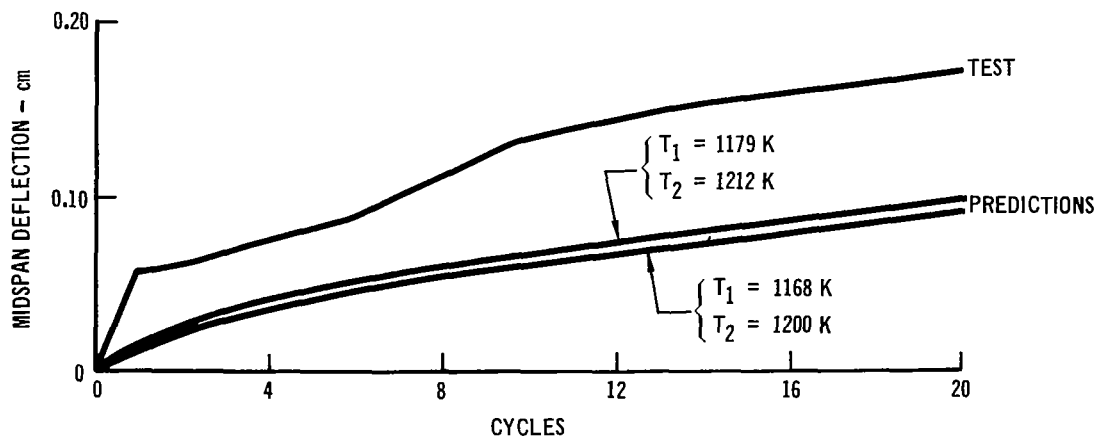
(b) SW Panel

FIGURE 56 COMPARISON OF L605 PANEL TEST RESULTS AND PREDICTIONS
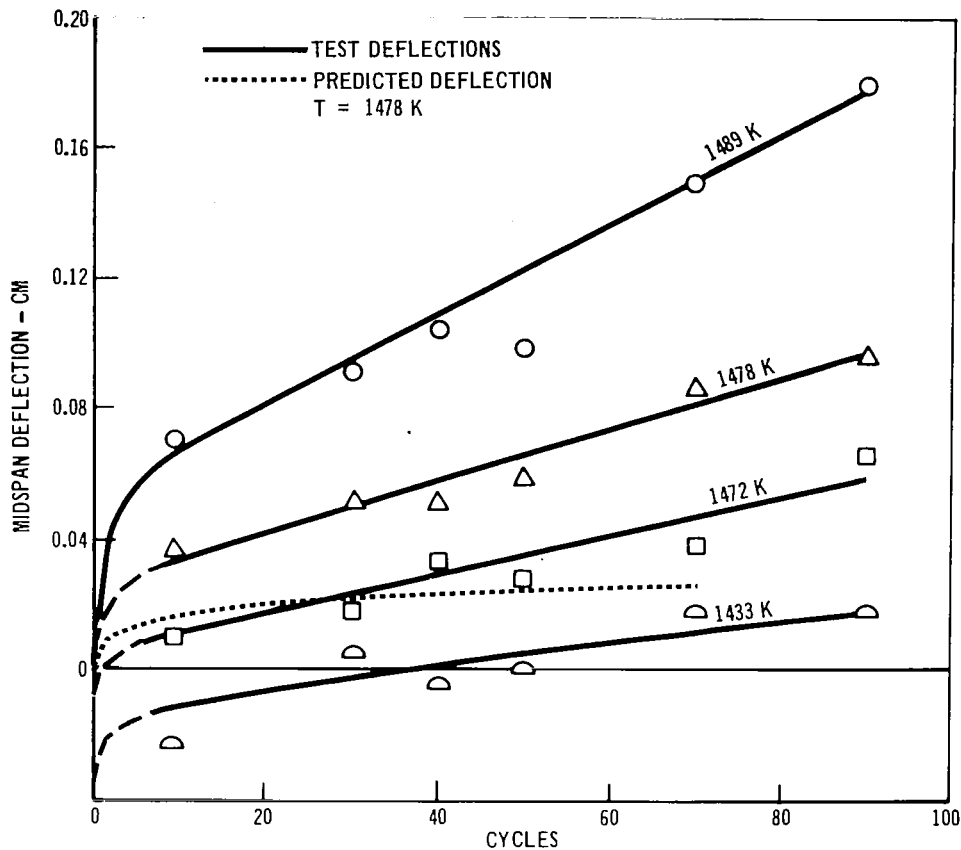
FIGURE 57 COMPARISON OF TDNiCr PANEL TEST DEFLECTIONS AND PREDICTIONS

rearrangement of permanent deflection at locations C and D between cycles 1 and 9. This was attributed to residual stresses, built into the panel during manufacture and assembly as well as thermally induced loads. Therefore, there remains some question as to the true amount of creep occurring between cycles 1 and 9.

The variation in creep behavior of the panel and the lower creep predicted (than was observed in subsize panel tests) is probably due to variations in material properties. Variations in creep data were observed in the literature survey data base.

Evaluation of Analytical Capability. - The approach for creep deflection analysis incorporated in the TPSC computer program was found to yield predicted panel cyclic creep deflections that are generally between half and twice the test deflections.

Several factors were identified (Reference 2) which can affect panel creep deflections. These include the applicability of empirical equations, the applicability of strain hardening or time hardening theories of creep accumulation, and the extent that stress distributions in thin gage elements vary

(Reference 21) from the uniform distributions assumed. In most cases the shape of the panel predicted deflection curves relative to test deflections could be correlated with the relative shape of tensile specimen creep curves.

The time hardening theory of creep accumulation was generally found to be better than strain hardening in predicting cyclic test creep. However, caution must be used in its application. Much more work needs to be done toward defining material creep accumulation processes since it appears that this could be the most significant limitation to the analysis in the TPSC program.

Review of subsize panel test results and associated predictions revealed two trends. The first of these was that for testing to similar cyclic profiles, the thinner gage corrugation stiffened panel exhibited greater deflections, relative to predictions, than the thicker gage rib stiffened panels. This is reasonable to expect since in the thinner gage panels less section area is effective in carrying the bending load (due to buckling of the skin between stiffeners) and therefore higher stresses, causing greater creep strain, may occur. The second trend was that panels tested under mission temperature and load profiles exhibited larger deflections, relative to predictions, than similar panels tested to constant temperature and load cycle profiles. The variation could not be attributed to the approaches for idealizing or modeling mission profiles into constant temperature and load steps since time steps where very low creep occurs were not included. It is recognized that including these low temperature and/or load steps when applying the time hardening theory of creep accumulation can affect predictions.

Based on comparison of predicted creep deflection with test deflections in full size thermal protection system panels, prediction capability for L605 and Rene' 41 appear to be reasonably good although there is much variation in the full size panel test data, even for panels tested simultaneously to the same temperature and load level. Resulting predictions of cyclic creep deflection have been shown to be sensitive to both stress level and temperature. Such factors as overshoot in temperature for only one cycle or a few cycles can significantly increase the total test deflections. In addition, the full size test panels were subjected to other environments such as high launch phase loading and acoustic environments, which could affect panel deflection.

Phase III Conclusions

Comparison of permanent cyclic creep deflections, obtained in testing of full size thermal protection system panels, with predicted values has met with varied degrees of success. Prediction capability for L605 and Rene' 41 appears to be reasonably good, although there is much variation in the test data, even for panels tested simultaneously to the same temperature and load level. Prediction capability for TDNiCr appears to be less accurate which is probably due to variation in material properties. These variations are well documented in the literature.

PHASE IV - THERMAL PROTECTION SYSTEM DESIGN CRITERIA

In the design of TPS panels several critical design conditions must be met. First, panels must be sized based on strength and stiffness considerations over the entire range of flight conditions. Material choice is dictated by the peak temperatures occurring during entry. Critical design conditions generally are found to be peak pressure loads and acoustic loadings occurring at room temperature during ascent or cruise conditions. Envelopes of panel strength and flight conditions such as that demonstrated in Figure 58 for a L605 panel, are helpful in visualizing the critical conditions for panels. This figure shows the panel to be critical during cruise where the peak pressure is applied at low temperatures. The panel strength then exceeds requirements throughout the remainder of the mission.

Once the flight envelope has been determined, panel deflections must be considered. These deflections include elastic deflections of the panel under applied differential pressure loads, thermal deflections which result from temperature gradients through the panel depth, and permanent creep deflections which accumulate throughout the life of the TPS panel. Various allowable deflections have been established such as those in References 14 and 22 which are shown in Equations (4) and (5) respectively.

$$\delta = .25 + .01L \text{ cm} \tag{4}$$

$$\delta = .25 + .04L \ [(B.S.-30.5)/280] \text{ cm} \tag{5}$$

These equations provide for maximum deflections of .75 cm and 2.25 cm [Body Station 310] respectively for a 50 cm (20 inch) long panel. Allowable total deflections must be established for each system based on the thermodynamic and aerodynamic requirements.

Knowing the maximum permissible deflection, the next step is to calculate the deflection of the structure during flight. This can be accomplished through the use of one of the cyclic equations presented in Table 5 and the computer program presented in Reference 3. The equations presented in Table 5 are only valid for the four materials studied. If another material is to be considered, then an equation will have to be developed using the approach presented in Reference 1. The calculated deflections can then be compared with the maximum allowable deflection and corresponding adjustments made in panel geometry.
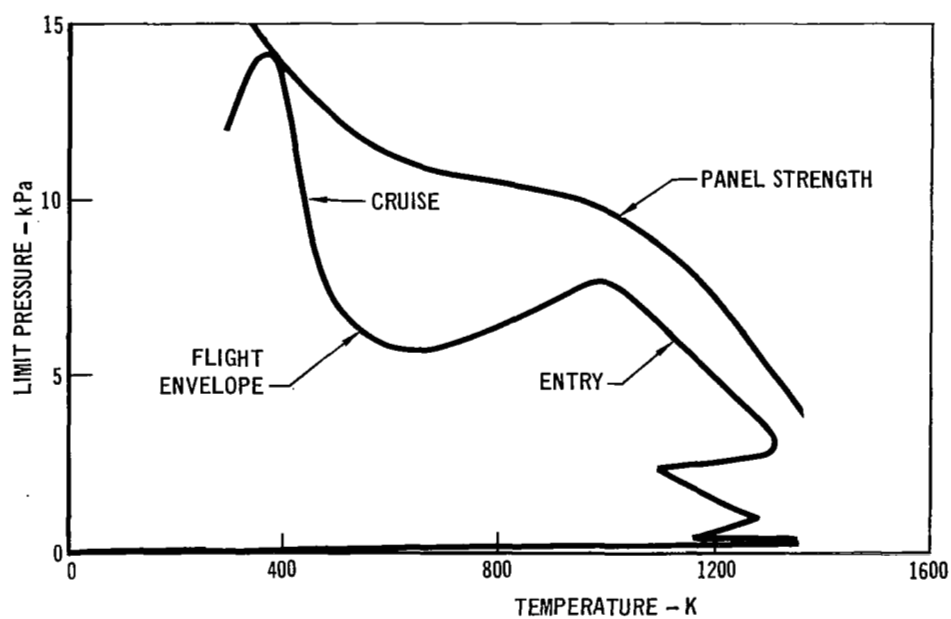
FIGURE 58 L 605 PANEL STRENGTH FOR FLIGHT ENVELOPE

CONCLUDING REMARKS

A method of analysis for predicting permanent deflections, due to creep, in stiffened panel structures has been developed. The resulting computer program, Thermal Protection System Creep (TPSC) uses iterative techniques and numerical integration to determine creep strains, deflections, and residual stresses. The TPSC computer program provides needed capability for prediction of permanent deflections, due to creep. Although developed for analysis of creep deflections in thermal protection system panels, the approach is applicable to creep analysis in any beam or stiffened plate structure subjected to bending loads. The approach for creep deflection analysis incorporated in the TPSC computer program has been found to yield predicted panel cyclic creep deflections that are generally between half and twice the test deflections.

Test results obtained on thin gage sheet specimens have demonstrated that there is no significant difference between cyclic and steady-state creep strains (for the same total time at load) for the alloys L605, Ti-6Al-4V, Rene' 41, and TDNiCr. Creep strain equations were developed for both steady-state and cyclic creep data using linear least squares analysis techniques. A single linear equation describing the combined steady-state and cyclic creep data, for each alloy, resulted in standard errors of estimate higher than obtained for the individual data sets.

The prediction of strains that are produced by complex trajectory and simulated mission tests (using equations based on simple cycles) was successfully accomplished. A computer program was specifically written for this analysis. This computer program is based on time and strain hardening theories of creep accumulation. For Ti-6Al-4V, and TDNiCr, the strain hardening theory of creep accumulation provided the best predictions while for Rene' 41 time hardening and for L605 a combination of strain and time hardening provided the best predictions.

The time hardening theory of creep accumulation was generally found to be better than strain hardening in predicting the subsize panel test data. However, caution must be used in its application, since including portions of the load and temperature profiles, where no creep is occurring, will extend the time for calculation in subsequent cycles. More work needs to be done toward defining material creep accumulation processes since it appears that this could be the most significant limitation to the analysis in the TPSC program.

Prediction of permanent cyclic creep deflections, based on documented test data for full size thermal protection system panels, has met with varied degrees of success. Prediction capability for L605 and Rene' 41 appears to be good, although there is variation in the test data, even for panels tested simultaneously to the same temperature and load level.

Resulting predictions of cyclic creep deflections were found to be sensitive to both stress level and temperature. Factors such as overshoot in temperature for only one cycle or a few cycles could significantly increase the total test deflections attained. In addition, the full size test panels were generally subjected to other environments such as high launch phase loading and

acoustic environments, which possible contribute to redistribution of panel relative displacement and variation in the data. Prediction capability for TDNiCr appears to be less accurate based on limited analysis conducted. This is probably due to variation in material properties. These variations are well documented in the literature.

In general, for the four alloys studied, no effects on creep strain due to variation of time per cycle (for the same total time) or atmospheric pressure were observed. A thickness effect on creep response was noted for all materials studied, although the effect was more pronounced in some cases than in others. For L605, thinner sheet crept faster than the thicker sheet, while in the case of Rene' 41, Ti-6Al-4V, and TDNiCr the reverse was true. An effect of material rolling direction on creep strains was observed in TDNiCr.

Significant data scatter was found to exist for both the literature survey and supplemental steady-state creep data bases of TDNiCr. For TDNiCr stress-rupture failures were obtained at creep strains of approximately 0.11% throughout the cyclic test temperature range.

APPENDIX A

CONVERSION OF U.S. CUSTOMARY UNITS TO SI UNITS

The International System of Units (designated SI) was adopted by the Eleventh General Conference on Weights and Measures in 1960. The units and conversion factors used in this report are taken from or based on NASA SP-7012, "The International System of Units, Physical Constants and Conversion Factors - Revised, 1973".

The following table expresses the definitions of miscellaneous units of measure as exact numerical multiples of coherent SI units, and provides multiplying factors for converting numbers and miscellaneous units to corresponding new numbers of SI units.

The first two digits of each numerical entry represent a power of 10. An asterisk follows each number that expresses an exact definition. For example, the entry "-02 2.54*" expresses the fact that 1 inch = 2.54 x 10^{-2} meter, exactly, by definition. Most of the definitions are extracted from National Bureau of Standards documents. Numbers not followed by an asterisk are only approximate representations of definitions, or are the results of physical measurements.

ALPHABETICAL LISTING

To convert from	to	multiply by
atmosphere (atm)	pascal (Pa)	+05 1.0133*
Fahrenheit (F)	kelvin (K)	$t_k = (5/9) (t_f + 459.67)$
foot (ft.)	meter (m)	-01 3.048*
inch (in.)	meter (m)	-02 2.54*
mil	meter (m)	-05 2.54*
millimeter of mercury (mm Hg)	pascal (Pa)	+02 1.333
nautical mile, U.S. (n.mi.)	meter (m)	+03 1.852*
pound force (lbf)	newton (N)	+00 4.448*
pound mass (lbm)	kilogram (kg)	-01 4.536*
torr (0°C)	pascal (Pa)	+02 1.333

PHYSICAL QUANTITY LISTING

Area

To convert from	to	multiply by
foot^2 (ft^2)	meter^2 (m^2)	-02 9.290*
inch^2 (in^2)	meter^2 (m^2)	-04 6.452*
inch^2 (in^2)	centimeter^2 (cm^2)	+00 6.452

PHYSICAL QUANTITY LISTING

Density

To convert from	to	multiply by	
pound mass/foot^3 (pcf, lbm/ft^3)	kilogram/meter^3 (kg/m^3)	+01	1.602
pound mass/inch^3 (lbm/in^3)	kilogram/meter^3 (kg/m^3)	+04	2.768
pound mass/inch^3 (lbm/in^3)	gram/centimeter^3 (g/cm^3)	+01	2.768

Force

kilogram force (kgf)	newton (N)	+00	9.807*
pound force (lbf)	newton (N)	+00	4.448*

Length

foot (ft)	meter (m)	-01	3.048*
inch (in.)	meter (m)	-02	2.54*
micron	meter (m)	-06	1.00*
mil	meter (m)	-05	2.54*
mile, U.S. nautical (n.mi.)	meter (m)	+03	1.852*

Mass

pound mass (lbm)	kilogram (kg)	-01	4.536*

Pressure

atmosphere (atm)	pascal (Pa)	+05	1.013*
millimeter of mercury (mm Hg)	pascal (Pa)	+02	1.333
newton/meter	pascal (Pa)	00	1.00*
pound/foot^2 (psf, lbf/ft^2)	pascal (Pa)	+01	4.788
pound/inch^2 (psi, lbf/in^2)	pascal (Pa)	+03	6.895

Temperature

Fahrenheit (F)	Kelvin (K)	$t_k = (5/9)(t_f + 459.67)$

Volume

foot^3 (ft^3)	meter^3 (m^3)	-02	2.832*
inch^3 (in^3)	meter^3 (m^3)	-05	1.639*
inch^3 (in^3)	centimeter^3 (cm^3, cc)	00	1.639

PREFIXES

The names of multiples and submultiples of SI units may be formed by application of the prefixes:

Multiple	Prefix
10^{-6}	micro (μ)
10^{-3}	milli (m)
10^{-2}	centi (c)
10^{-1}	deci (d)
10^{3}	kilo (k)
10^{6}	mega (M)
10^{9}	giga (G)

REFERENCES

1. Davis, J. W.; and Cramer, B. A: Prediction and Verification of Creep
    Behavior in Metallic Materials and Components for the Space Shuttle
    Thermal Protection System - Phase I - Cyclic Materials Creep Predictions.
    (NASA Contract NAS-1-11774.) NASA CR-132605-1, 1974.

2. Cramer, B. A.; and Davis, J. W.: Prediction and Verification of Creep
    Behavior in Metallic Materials and Components for the Space Shuttle Thermal
    Protection System - Phase II - Subsize Panel Cyclic Creep Predictions.
    (NASA Contract NAS-1-11774) NASA CR-132605-2, 1975.

3. Cramer, B. A.: Prediction and Verification of Creep Behavior in Metallic
    Materials nnd Components for the Space Shuttle Thermal Protection System -
    Phase III and IV. (NASA Contract NAS-1-11774.) NASA CR-132605-3, 1975.

4. Green, A.; et. al.: Research Investigation to Determine Mechanical Pro-
    perties of Nickel and Cobalt Base Alloys for Inclusion in Military Hand-
    book-5. AFML-TDR-116-Volume II, 1964.

5. Fritz, L. J.; et. al.: Characterization of the Mechanical and Physical
    Properties of TD-Ni-Cr ($Ni-20Cr-2ThO_2$) Alloy Sheet (NASA Contract NAS3-
    15558) NASA CR-121221, 1974.

6. Killpatrick, D. H.; and Hocker, R. G.: Stress-Rutpure and Creep in Disper-
    sion Strengthened Nickel-Chromium Alloys. DAC-62124. McDonnell Douglas
    Corporation, 1968.

7. Dixon, W. J.: Biomedical Computer Programs (BMD-02R). Automatic Computa-
    tion No. 2. University of California.

8. Dorn, J. E.: Mechanical Behavior of Materials at Elevated Temperature.
    McGraw Hill Book Company, 1961, pp 79-93 and 455-457.

9. Garafalo, F.: Fundamentals of Creep and Creep-Rupture in Metals.
    MacMillan Company, 1965, page 16.

10. Kennedy, A. J.: Processes of Creep and Fatigue in Metals. Olvier and Boyd,
    1962.

11. Cahn, R. W.: Physical Metallurgy. Second Edition, North Holland Publishing
    Company, 1965, pp 983-1009.

12. Lynch, J. H.: A Systematic Approach to Model Development by Comparison of
    Experimental and Analytical Regression Coefficients. NASA-TMX-1797, Lewis
    Research Center, NASA 1969.

13. Davies, O. L.: The Design and Analysis of Industrial Experiments. Second
    Edition, Hafner Publishing Company, 1956.

14. Andresson, T. L.: Space Shuttle: Aerodynamic Heating Tests of the MDAC Delta
    Wing Orbiter and Canard Booster (NASA Contract NAS-8-26016) NASA-CR-120007,
    1972.

REFERENCES (Continued)

15. Timeshenko, S.; and Woinowsky-Krieger, S.: Theory of Plates and Shells. McGraw-Hill Book Company, 1959, pp 214-218.

16. Lekhnitskii, S. G. (S. W. Tsai and T. Cheron, transl.): Anisotrophic Plates. Second Edition, Gordon and Breach Science Publishers, 1968, pp 329-333.

17. Anon.: Supplementary Structural Test Program (SSTP) - Large TPS Panel Tests. MDC-E0562, McDonnell Douglas Astronautics Company-East, 1972.

18. Harris, H. G.: Behavior of Full Size Metallic TPS panels under Cyclic Reentry Environment. Presented at the Information Exchange of Creep of Materials for Space Shuttle Protection Systems. NASA Langley Research Center, 2-3 December 1971.

19. Morman, K. N.: Correlation of Theoretical TPS Creep Deflections with Test Results. Presented at the Information Exchange of Creep of Materials for Space Shuttle Protection Systems. NASA Langley Research Center, 2-3 December 1971.

20. Eidinoff, H. L.; and Rose, L.: Thermal-Structural Evaluation of TDNi-20Cr Thermal Protection System Panels. (NASA Contract NAS-1-12277). NASA CR-132487, 1974.

21. Otto, O. R.: Integrated Structures 1972 Progress Report. MDC E0719, McDonnell Douglas Corporation, 1972.

22. Black, W. E.: Evaluation of Coated Columbium Alloy Heat Shields for Space Shuttle Thermal Protection System Application, Phase II - Subsize Heat Shield and Small Size TPS Evaluation. (NASA Contract NAS-1-9793). NASA CR-112119-2, 1973.